

DISSERTATION

THE ATMOSPHERIC CIRCULATION RESPONSE TO CLIMATE CHANGE-LIKE  
THERMAL FORCINGS IN A SIMPLE GENERAL CIRCULATION MODEL

Submitted by

Amy Hawes Butler

Department of Atmospheric Science

In partial fulfillment of the requirements

For the Degree of Doctor of Philosophy

Colorado State University

Fort Collins, Colorado

Fall 2009

UMI Number: 3401024

All rights reserved

**INFORMATION TO ALL USERS**

The quality of this reproduction is dependent upon the quality of the copy submitted.

In the unlikely event that the author did not send a complete manuscript and there are missing pages, these will be noted. Also, if material had to be removed, a note will indicate the deletion.



UMI 3401024

Copyright 2010 by ProQuest LLC.

All rights reserved. This edition of the work is protected against unauthorized copying under Title 17, United States Code.



ProQuest LLC  
789 East Eisenhower Parkway  
P.O. Box 1346  
Ann Arbor, MI 48106-1346

COLORADO STATE UNIVERSITY

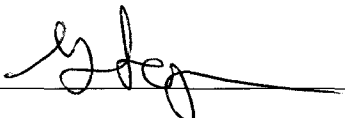
September 21, 2009

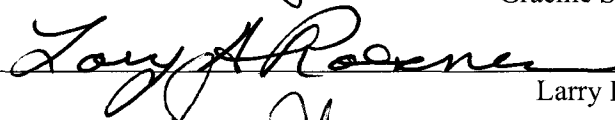
WE HEREBY RECOMMEND THAT THE DISSERTATION PREPARED UNDER OUR SUPERVISION BY AMY H. BUTLER ENTITLED "THE ATMOSPHERIC CIRCULATION RESPONSE TO CLIMATE CHANGE-LIKE THERMAL FORCINGS IN A SIMPLE GENERAL CIRCULATION MODEL" BE ACCEPTED AS FULLFILLING IN PART REQUIREMENTS FOR THE DEGREE OF DOCTOR OF PHILOSOPHY.

Committee on Graduate work

  
\_\_\_\_\_  
Scott Denning

  
\_\_\_\_\_  
Susan Solomon

  
\_\_\_\_\_  
Graeme Stephens

  
\_\_\_\_\_  
Larry Roesner

  
\_\_\_\_\_  
**Advisor** David W. J. Thompson

  
\_\_\_\_\_  
**Department Head** Richard Johnson

## ABSTRACT OF DISSERTATION

### THE ATMOSPHERIC CIRCULATION RESPONSE TO CLIMATE CHANGE-LIKE THERMAL FORCINGS IN A SIMPLE GENERAL CIRCULATION MODEL

Temperature changes due to increased greenhouse gases and depleted stratospheric ozone are associated with robust changes in the large-scale atmospheric circulation. In this thesis we explore how these anthropogenically-driven temperature changes affect the atmospheric circulation. Our approach is to force a simple dry dynamical general circulation model (GCM) with idealized thermal forcings that resemble three key effects of greenhouse gas increases and stratospheric ozone depletion: warming at the polar surface, warming of the tropical upper troposphere, and cooling of the polar stratosphere.

We examine the responses in both transient and steady state experiments. The key findings are: (1) heating in the upper tropical troposphere drives a robust poleward shift of the storm tracks as well as a weakening of the stratospheric Brewer-Dobson circulation and an expansion of the Hadley cell circulation; (2) cooling in the polar stratosphere also drives a poleward shift of the storm track, but the tropospheric response is very sensitive to the level and depth of the forcing; (3) warming at the polar surface drives an equatorward shift of the storm track. The equatorward shift due to polar warming opposes the poleward shift due to tropical upper tropospheric warming mostly in the NH, where polar surface warming is more pronounced. Lastly, (4) the combined

response to all three thermal forcings is quantitatively different from the sum of the responses to the individual forcings. Thus the response of the GCM to an individual thermal forcing is strongly dependent on the other thermal forcings applied to the model. The mechanisms of these responses are examined in transient simulations.

Amy Hawes Butler  
Department of Atmospheric Science  
Colorado State University  
Fort Collins, CO 80523  
Fall 2009

## **ACKNOWLEDGEMENTS**

This research was supported by the Environmental Protection Agency (EPA) Science to Achieve Results (STAR) graduate fellowship. It was also funded by the NSF Climate Dynamics Program. Much thanks to Dave Randall and Ross Heikes for use of the CSU dynamical core GCM and computing resources at NERSC.

## TABLE OF CONTENTS

<b>CHAPTER 1: INTRODUCTION.....</b>	<b>1</b>
1.1 Overview .....	1
1.2 A Review of the Atmospheric Circulation.....	2
1.3 Observed Changes in the Atmospheric Circulation.....	7
1.4 Simulated Changes in the Atmospheric Circulation.....	9
1.5 Proposed Mechanisms for Circulation Response to Thermal Forcings.....	10
1.6 Previous Studies using Simple GCMs.....	15
<b>CHAPTER 2: MODEL DESCRIPTION AND ANALYSIS</b>	
<b>TECHNIQUES .....</b>	<b>19</b>
2.1 Model Description .....	19
2.2 Control Climatology and Statistical Techniques .....	21
<b>CHAPTER 3: STEADY-STATE EXPERIMENTS .....</b>	<b>28</b>
3.1 Heating in the Tropical Upper Troposphere .....	30
3.2 Cooling in the Polar Stratosphere.....	38
3.3 Warming at the Polar Surface .....	43
3.4 Combined Response to all Three Thermal Forcings .....	44
3.5 Summary of Steady-State Experiment Results .....	48
<b>CHAPTER 4: TRANSIENT EXPERIMENTS.....</b>	<b>52</b>
4.1 Mechanisms and the Steady-State Experiments.....	52
4.2 Introduction to Transient Runs.....	61
4.3 Heating in the Tropical Upper Troposphere .....	63
4.4 Cooling in the Polar Stratosphere.....	69
4.5 Shallow Cooling in the Polar Stratosphere- Two Cases .....	74
4.6 Warming at the Polar Surface .....	78
4.7 Testing the Mechanisms.....	80
<b>CHAPTER 5: SUPPLEMENTAL CHAPTER ON LOWER</b>	
<b>STRATOSPHERIC TEMPERATURES AND OZONE.....</b>	<b>92</b>
5.1 Observed Trends in Lower-Stratospheric Temperatures .....	92
5.2 Observed Trends in Vertical Profiles of Ozone .....	105
5.3 Observed Relationships between MSU4 and Ozone .....	115
5.4 Summary and Future Work.....	118
<b>CHAPTER 6: CONCLUSIONS .....</b>	<b>121</b>
6.1 Summary of Key Findings .....	121
6.2 Remaining Questions and Future Work.....	127
<b>REFERENCES.....</b>	<b>129</b>

# CHAPTER 1: INTRODUCTION

## 1.1 Overview

The response of the global climate system to anthropogenic forcing will likely involve several robust temperature changes by the end of the 21<sup>st</sup> century, including (1) a warming troposphere and a cooling stratosphere due to the radiative effects of increasing greenhouse gases; (2) a maximum of tropospheric warming in the tropical upper troposphere as a consequence of increased latent heating by condensation of water vapor; (3) a maximum in surface temperature warming over Northern Hemisphere (NH) high-latitudes during winter due to ice/albedo feedbacks; (4) a minimum in surface temperature warming over the Southern Hemisphere mid-latitudes due to the high heat capacity of the Southern Ocean; and (5) strong polar stratospheric cooling in the spring/summer in the Southern Hemisphere (SH) due to ozone depletion, at least until ozone recovers in the latter half of the century [Fig 1.1, Intergovernmental Panel on Climate Change (IPCC) Fourth Assessment Report (AR4)].

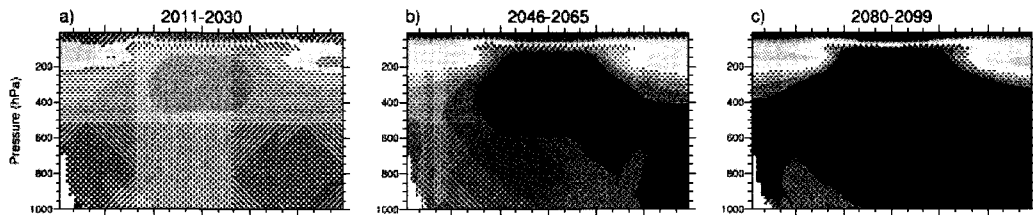


**Fig. 1.1.** From IPCC AR4 Chapter 10. Zonal-means of change in atmospheric temperatures ( $^{\circ}\text{C}$ ) as a function of pressure and latitude. “Values are the multi-model means for the A1B scenario for three periods (a-c). Stippling denotes regions where the multi-model ensemble mean divided by the multi-model standard deviation exceeds 1.0 (in magnitude). Anomalies are relative to the average of the period 1980-1999.”

These changes in temperature gradients are associated with changes in the atmospheric circulation, which may influence surface climate at least as much as the predicted warming. The broad purpose of this research is to understand how and why the circulation changes in relation to these predicted changes in temperature gradients using a simple general circulation model (GCM).

In this chapter, we introduce the observational and simulated evidence of changes in the atmospheric circulation due to anthropogenic forcing, and discuss potential mechanisms for how the forcing drives these changes. We then look at previous research in which simple GCMs have been used to explore circulation changes to a variety of different forcings, and discuss how our research is unique.

## **1.2 A Review of the Atmospheric Circulation**

The general circulation of the atmosphere is driven by differential heating of Earth by the sun and the rotation of the planet. If a hypothetical planet is rotating in space and a differential heating (with warming at the tropics and cooling at the poles) is instantaneously switched on, initially we would expect the warm air to rise at the tropics and sink at the poles, creating a thermally direct meridional circulation cell to maintain mass continuity (Fig. 1.2a). The Coriolis force would act on the poleward branch to create westerlies at upper levels and on the equatorward branch to create easterlies at lower levels.

Since the differential heating is still being applied, the westerlies at upper levels will continue to increase; however, friction at the surface will slow the easterlies at lower levels. Eventually, the vertical shear between upper and lower levels becomes unstable.

Somewhat analogous to ocean waves which break as the water nearest the sea floor slows, atmospheric waves (called baroclinic waves or eddies) will form in regions of instability in the atmosphere, which occur in the middle latitudes (Fig. 1.2b). These waves propagate vertically and transport heat poleward, thus acting against the differential solar heating. The vertical component of baroclinic waves is termed the “eddy heat flux”.

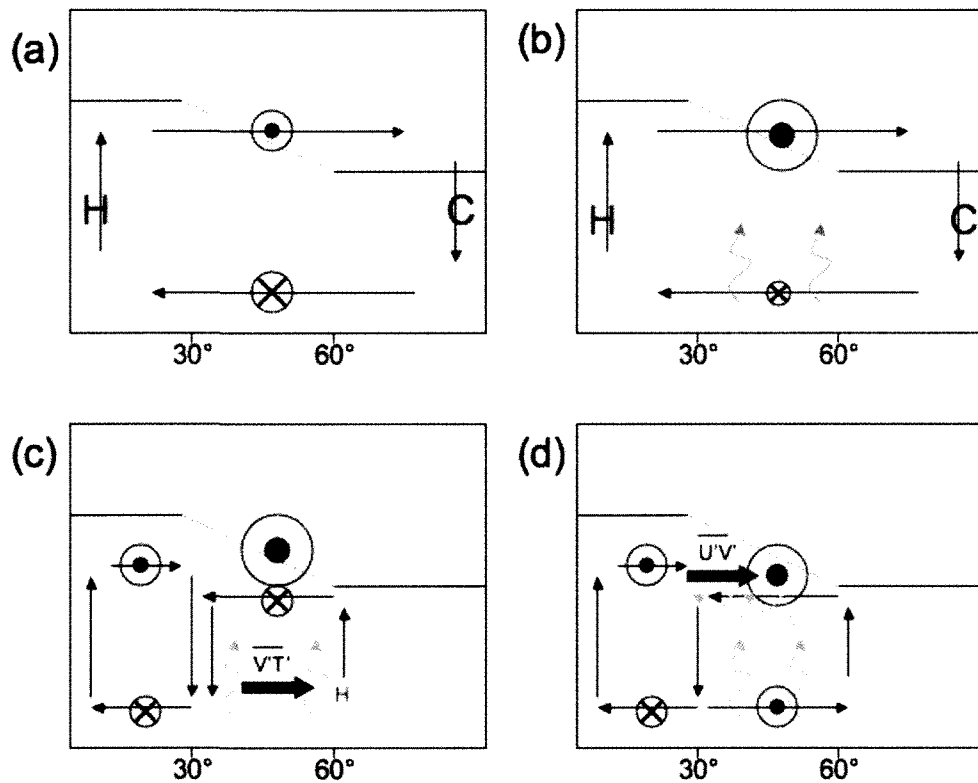


**Fig 1.2.** A latitude versus height schematic depicting the events that occur when a differential heating from equator to pole (representative of solar heating) is applied to a rotating planet. Only one hemisphere is shown. Circles with crosses represent easterly winds; with black circles, westerly winds. Black arrows mark meridional circulations. Yellow arrows represent baroclinic waves. The solid/dashed/solid line in each plot is the tropopause height. See text for details.

The warm air brought poleward by the eddy heat fluxes drive an anomalous meridional circulation with rising motion near 60° latitude and sinking near 30° latitude

(Fig. 1.2c). The original thermally direct meridional circulation cell is limited to latitudes equatorward of  $30^\circ$  and is termed the Hadley cell circulation. The new thermally “indirect” circulation driven by the eddies is termed the Ferrell cell circulation. The Coriolis force acts on the equatorward upper branch of the Ferrell cell to exert an easterly force, opposing the westerlies there.

The waves propagate into the upper troposphere and then turn equatorward, where they break at some critical latitude (waves can't propagate in easterlies or if their phase speeds exceed the background flow speed). The horizontal component of the waves is termed the “eddy momentum flux”. The eddy momentum and heat fluxes are found as  $\overline{u'v'}$  and  $\overline{v'T'}$ , respectively, where here the overbars denote the zonal-mean and the primes denote departures from the zonal-mean. Equatorward-propagating waves transport westerly momentum from the subtropics to the middle latitudes (Fig. 1.2d). The eddy momentum fluxes converge westerly momentum into the upper levels of the mid-latitudes, which is acted on by the Coriolis force and drives the counter-clockwise Ferrell cell circulation. The Coriolis force acting on the poleward lower branch of the Ferrell cell means that westerlies occur at the surface in the middle latitudes.

Angular momentum is also conserved. Westerly angular momentum is transferred from Earth to the atmosphere in the tropics, where the atmosphere rotates more slowly than the Earth's surface. This westerly momentum is then transported upward and poleward by the Hadley cell, and then eddies remove this angular momentum from the upper-level subtropics and transport the momentum poleward and downward to the mid-latitude surface, where the atmosphere is rotating faster than Earth's surface and momentum is returned to Earth's surface.

The extension of westerlies at middle latitudes from the surface to upper levels is called the mid-latitude jet or the storm track, as this eddy-driven jet is where baroclinic disturbances or storms occur. The dominant patterns of large-scale atmospheric climate variability in the extratropics, the so-called “annular modes”, are characterized by north-south vacillations in the latitudinal position of the mid-latitude jets. The annular modes emerge as the leading empirical orthogonal function (EOF) of extratropical sea level pressure, zonal wind, or geopotential height fields [Thompson and Wallace 2000]. By convention, the positive polarity of the annular modes is defined as periods when the extratropical jet and storm track are anomalously poleward of their climatological positions.

The annular modes have refolding timescales of ~10-20 days, but have substantial variance at lower frequencies [Hartmann and Lo 1998]. The annular modes are thought to persist in the atmosphere due to a positive feedback between eddy momentum flux anomalies and the zonal flow [Robinson 2000; Lorentz and Hartmann 2001, 2003]. An initial perturbation of the latitudinal position of the jet, matched by a perturbation in the meridional temperature gradient to maintain thermal wind, will shift the region of eddy generation. As these waves grow and propagate vertically and then equatorward in the atmosphere, they transfer westerly momentum into the latitude of baroclinic eddy generation, thereby creating enhanced upper tropospheric westerly wind anomalies on the poleward flank of the climatological mid-latitude jet and anomalous easterly wind anomalies on the equatorward flank. The Coriolis force acting on the anomalous wind anomalies induces an anomalous mean meridional circulation (MMC) that enhances lower tropospheric baroclinicity in the middle latitudes, and thus successive baroclinic

eddies tend to form along the same latitude band as the original waves and maintain the initial jet shift. This positive feedback is thought to account for the selection of the annular modes as the leading patterns of variability in their respective hemispheres.

The annular modes are associated with variability in extratropical surface temperature and precipitation. For example, the positive polarity of the Northern annular mode (NAM) is associated with warmer than normal surface temperatures over the high-latitudes of Eurasia and North America, and colder than normal surface temperatures over eastern Canada and the Middle East [Hurrell 1995, 1996; Cohen and Entekhabi 1999; Terray and Cassou 2000; Ambaum et al. 2001; Marshall et al. 2001; Thompson and Wallace 2001; Quadrelli et al. 2001; Higgins et al. 2002; Scaife et al. 2005]. A positive NAM is also associated with higher than normal precipitation over northern Europe and western Canada, and lower than normal precipitation over Southern Europe, the western United States, and eastern Canada. Likewise, the positive polarity of the Southern annular mode (SAM) is associated with colder than normal surface temperatures over most of Antarctica and warmer than normal temperatures over the Antarctic Peninsula, where enhanced westerlies increase the advection of warm oceanic air over cold land [Thompson and Wallace 2000; Renwick 2002; Thompson and Solomon 2002; Schneider et al. 2004; Marshall et al. 2006; Gillett et al. 2006].

In this section, we have examined why the atmospheric general circulation has more than one meridional circulation cell, why baroclinic eddies form, and why mid-latitude surface westerlies are present. We also described the dominant pattern of natural atmospheric variability in the extratropics. In the next section, we look at how the

atmospheric circulation is changing and is expected to change in the future due to anthropogenic forcing.

### **1.3 Observed Changes in the Atmospheric Circulation**

Significant changes in the extratropical atmospheric circulation in both hemispheres have been observed in recent decades. For example, between the 1960s and late 1990s, the sea level pressure decreased over both polar caps, the tropospheric mid-latitude westerlies increased, the stratospheric polar vortex strengthened, and the storm tracks shifted polewards [Hurrell 1995; Thompson et al. 2000; Ostermeier and Wallace 2003; Lu et al. 2004; Liu et al. 2007]. These observed atmospheric circulation changes are consistent with robust positive trends in the annular modes [Thompson and Wallace 2000]. Because the annular modes explain a significant fraction of the variability in surface climate, trends in the annular modes could have important implications on surface climate.

Indeed, a large fraction of observed climate trends in the Northern and Southern Hemispheres are linearly congruent with the observed trends in the NAM and SAM, respectively. For the ~30 years between 1969-1997, ~50% of the observed January/February/March (JFM) warming over Eurasia, nearly all of the JFM cooling over Greenland, and ~30% of the JFM warming over the NH poleward of 20°N were linearly congruent with the positive trend in the NAM [Thompson et al. 2000]. From 1969-2000, ~50% of the observed warming over the Antarctic Peninsula, ~90% of the cooling over eastern Antarctica, and much of the changes in SH westerlies were linearly congruent

with the positive trend in the SAM [Thompson and Solomon 2002]. Nonetheless, recent observations suggest that while the positive trend in the SAM has remained robust to present day, the trend in the NAM has relaxed since the late 1990s, although present day index values are still consistently more positive than values in the 1950s-1960s [Fig. 1.3; e.g., Overland and Wang 2005].

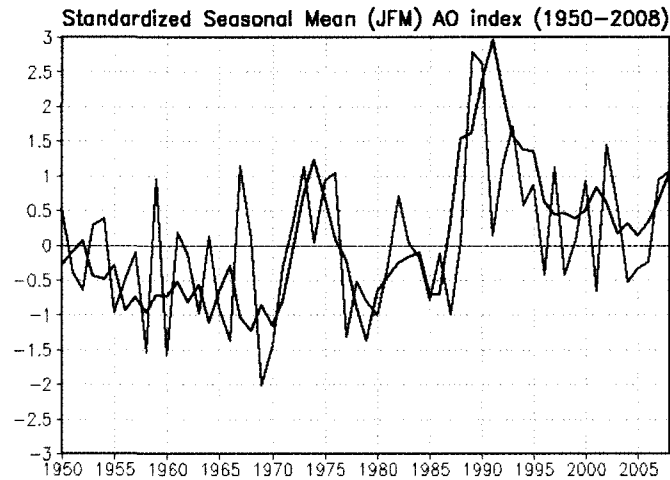


**Fig 1.3.** The standardized JFM mean of the NAM index from 1950-2008 (from the NOAA/NCEP Climate Prediction Center).

Outside of the extratropics, observed changes in large-scale circulation patterns involve poleward shifts of the subtropical jets and an expansion of the Hadley cell circulation since 1979 [Seidel et al. 2008]. Several independent datasets, including total column ozone, satellite-based temperatures, tropopause height, and outgoing longwave radiation, suggest that the tropical belt (determined by the width of the Hadley cell circulation) has expanded  $2^{\circ}$  to  $4.8^{\circ}$  latitude in the last 25 years [Hudson et al. 2006; Fu et al. 2006; Seidel and Randel 2007; Hu and Fu 2007]. The Hadley cell width determines the latitude of the subtropical dry regions where atmospheric subsidence occurs and precipitation is minimal. A poleward extension of the Hadley cell could thus have

important implications for surface climate as well as water resources in populated areas near the subtropics.

#### **1.4 Simulated Changes in the Atmospheric Circulation**

Robust changes in the atmospheric circulation have also been found in climate change scenarios run on complex general circulation models. The most robust responses are found in the SH. Simulations forced with the observed ozone depletion of the past few decades suggest that the observed poleward shift in the SH storm track is largely consistent with forcing by stratospheric ozone depletion [Sexton 2001; Kindem and Christiansen 2001; Gillett and Thompson 2003; Miller et al. 2006], while simulations forced by future ozone recovery reveal SH trends in the opposite sense [Son et al. 2008]. Simulations forced with past increases in greenhouse gases do not reveal a robust poleward shift in the SH storm track, but those forced with future projections of CO<sub>2</sub> do [Shindell et al. 1999; Fyfe et al. 1999; Kushner et al. 2001; Cai et al. 2003; Shindell and Schmidt 2004; Brandefelt and Kallen 2004; Yin 2005; Arblaster and Meehl 2006; Lu et al. 2008]. In fact, the predicted poleward shift in the SH stormtrack is one of the most robust climate change responses in the IPCC AR4 model simulations [Miller et al. 2006; Sigmond et al. 2007].

In contrast to the SH, the simulated response of the NH circulation to anthropogenic forcing is less robust. Most simulations do not reveal a robust trend in the NAM in response to past increases in greenhouse gases [Gillett et al. 2000], and those that do are strongly model dependent [Shindell et al. 1999]. Some studies suggest that

only models with a well-resolved stratosphere can accurately simulate the observed trends in the NH storm track position [Shindell et al. 1999; Shindell et al. 2001; Eichelberger and Holton 2002], but others studies find no difference in trends for models lacking stratospheric resolution [Gillett et al. 2002; Gillett et al. 2003]. The IPCC AR4 simulations predict only a weak poleward shift in the NH storm track in response to future increases in greenhouse gases [Miller et al. 2006].

In the tropics, models forced with both past increases in greenhouse gases and stratospheric ozone depletion show a widening of the Hadley cell circulation that is substantially smaller than observed [Johanson and Fu 2008]. This discrepancy suggests that models are not currently capturing other factors responsible for the  $\sim 2\text{-}5^\circ$  latitude Hadley cell expansion from 1979-2005. The simulated Hadley cell circulation response to future increases in greenhouse gases also involves a robust weakening and poleward expansion of the Hadley cell circulation. The future widening of this circulation predicted by models is on the order of  $\sim 0.6^\circ$  latitude per degree warming, which is again much smaller expansion than that seen in observations for a similar change in temperature [Lu et al. 2007].

### **1.5 Proposed Mechanisms for Circulation Response to Thermal Forcings**

Understanding the atmospheric circulation response to ozone and greenhouse gas forcing is clearly important not only for understanding recent observed changes in the circulation but also predicted future changes. Presumably, the atmospheric circulation is sensitive to spatial gradients in the temperature field induced by stratospheric ozone

depletion and increasing greenhouse gases. For example, because increasing greenhouse gases tend to warm the troposphere and cool the stratosphere, and because the height of the tropopause is greater near the equator than at the pole, enhanced greenhouse gases act to increase the meridional temperature gradient ( $dT/dy$ ) near the tropopause level [Kushner et al. 2001; Eichelberger and Holton 2002]. Stratospheric ozone depletion acts similarly by decreasing the amount of ultraviolet sunlight absorbed in the polar stratosphere in the springtime, cooling the polar cap and enhancing the meridional temperature gradient across the extratropical lower stratosphere. In addition, the tropical upper troposphere is expected to warm more than the rest of the troposphere because convective air parcels will follow the moist adiabatic lapse rate [Xu and Emanuel 1989], which decreases as the temperature warms [Hartmann 1994; Frierson 2008]. This effect may also enhance the meridional temperature gradient at tropopause levels. The changes in the upper-level meridional temperature gradient must drive changes in the zonal wind by the thermal wind relationship. However, the total zonal wind response to climate change is not merely a vertical increase of westerly winds with height, but includes a barotropic component that extends to the surface and involves a poleward shift of the tropospheric mid-latitude jet that projects onto the annular mode pattern [e.g., Kushner et al. 2001].

What incites this eddy-driven component is unclear, although zonal wind changes in the lower stratosphere are thought to be key to the coupling with the tropospheric circulation [Baldwin and Dunkerton 2001; Polvani and Kushner 2002; Haigh et al. 2005; Christiansen 2005]. Figure 1.4 schematically depicts one major theory proposed by Chen and Held [2007] and Chen et al. [2007]. In the climatology (Fig. 1.4, top), as discussed

in Section 1.2, baroclinic waves propagate poleward and equatorward. When they break in the subtropics, they deposit easterly momentum there (gray hatching) and transfer westerly momentum (gray dots) to the latitude of the mid-latitude jet in order to balance the Coriolis force acting on the upper equatorward branch of the Ferrell cell. Chen and Held [2007] and Chen et al. [2007] propose that when the upper level meridional temperature gradient is increased, then 1) enhanced westerly zonal flow in the vicinity of the tropopause/lower stratosphere increases eastward eddy phase speeds there (Fig. 1.4, bottom left, red wavy arrows); and 2) the enhanced eastward eddy phase speeds are

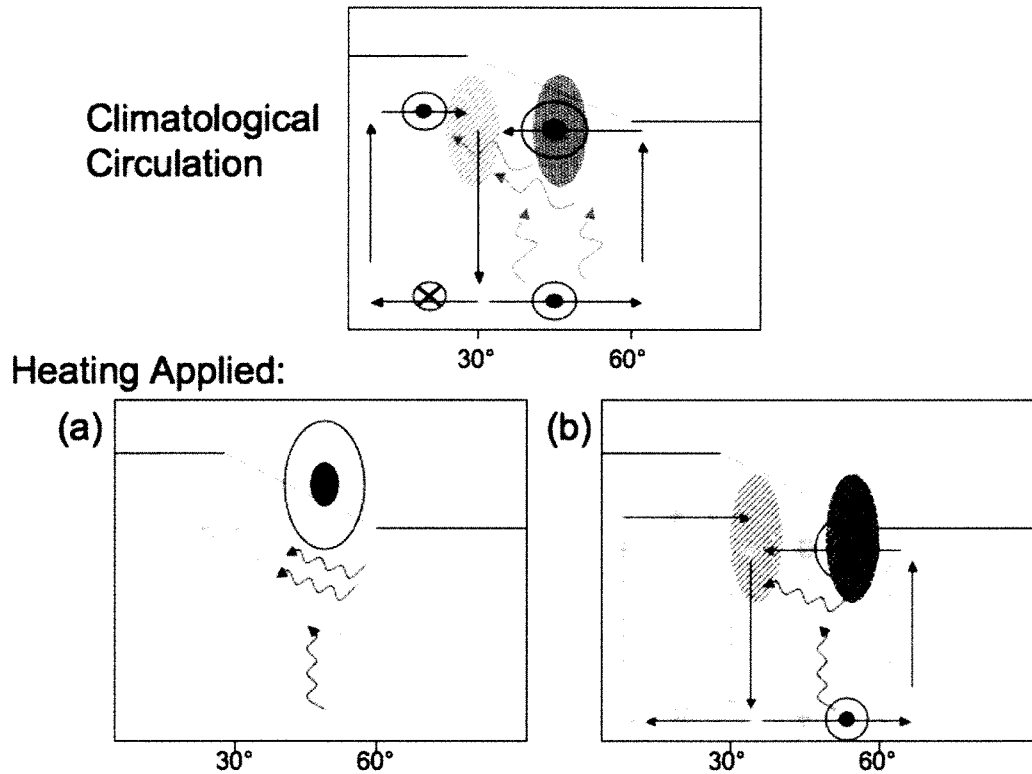


**Fig 1.4.** A latitude versus height schematic depicting (top) the climatological atmospheric circulation and (bottom) the circulation changes expected according to the eddy phase speed theory of Chen and Held [2007] when the upper level winds are enhanced (panel *a*). Red items correspond to the circulation after the forcing, gray items to the climatology. Only one hemisphere is shown. See text and Fig. 1.2 for more details.

associated with a poleward shift in the latitude of maximum wave breaking - and thus easterly momentum deposition - in the subtropics (Fig. 1.4, bottom right, red hatching). The shift in the wave breaking occurs because transient waves cannot propagate through a mean background flow that is slower than their phase speeds, so if the eddy phase speeds increase (assuming a constant mean background flow), then the waves can't propagate as far equatorward where the background flow is slower than in the mid-latitudes.

The poleward shift in the easterly momentum deposition in the subtropical upper troposphere increases lower tropospheric baroclinicity in the middle latitudes via an anomalous thermally damped meridional circulation cell, shifting baroclinic wave generation poleward [Robinson 2000, 2006]. The resulting baroclinic wave fluxes reinforce the original poleward shift in the easterly momentum deposition in the subtropical upper troposphere and the westerly momentum deposition that maintains the new location of the mid-latitude jet.

Besides changing meridional temperature gradients at upper levels, strong warming of the Arctic associated with ice-albedo feedbacks could affect the atmospheric circulation by reducing the surface meridional temperature gradient, and thus the strength and location of the region of maximum baroclinicity where eddies form. Thus polar surface warming could mitigate changes caused by a stronger temperature gradient at upper levels [Yin 2005; Lorenz and DeWeaver 2007; Kodama and Iwasaki 2009].

Ozone and greenhouse gas forcing also drive changes in vertical temperature gradients ( $dT/dz$ ). Changing the vertical temperature gradient can cause significant changes in the static stability of the atmosphere. Increases in tropospheric static stability

are predicted under global warming conditions [Xu and Emanuel 1989; Frierson 2006]. Due to the moist adiabatic temperature structure in the tropics, as warming occurs the upper tropical troposphere warms more than the lower troposphere, leading to more dry static stability in the tropics. In the mid-latitudes the static stability also increases due to increases in moisture content that accompany an overall warming of the earth [Frierson 2006; Frierson 2008]. As depicted schematically in Figure 1.5, these changes in static stability, which is inversely proportional to Eady growth rate, may reduce baroclinic eddy

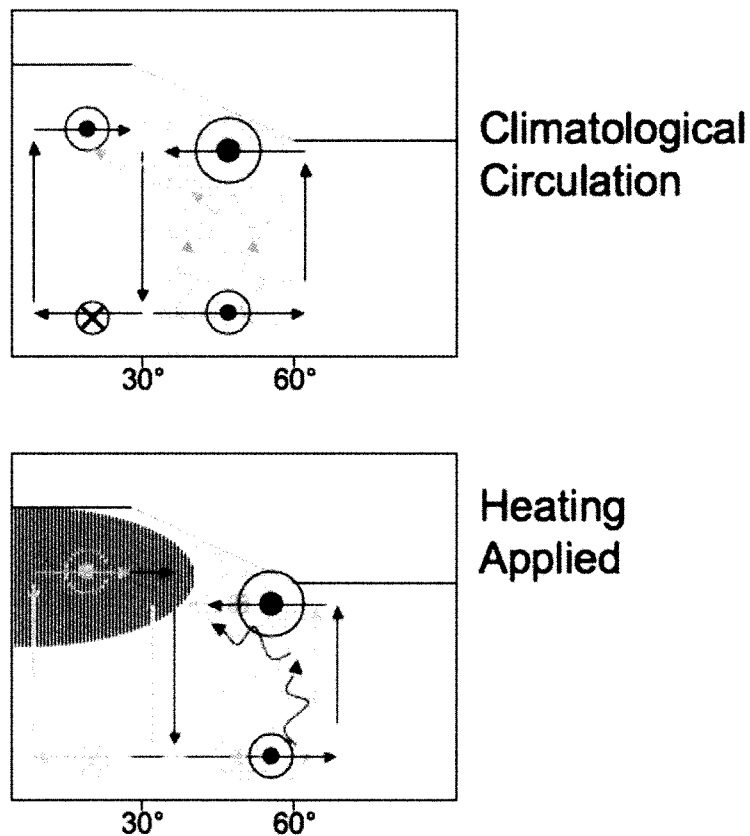


**Fig 1.5.** A latitude versus height schematic depicting (top) the climatological atmospheric circulation and (bottom) the circulation changes expected according to static stability theory of Frierson [2008] when an upper tropical tropospheric heating is applied (red hatching). Red items correspond to the circulation after the forcing, gray items to the climatology. The blue hatching represents the region of maximum baroclinicity. Only one hemisphere is shown. See text for details.

growth on the equatorward side of the storm tracks and thus shift the eddy activity poleward [Frierson 2008; Lu et al., 2008]. Note that in the schematic, we ignore upper level wind changes due to warming in the upper tropical troposphere for clarity, but most likely the theories discussed in Fig. 1.4 and 1.5 are both relevant. However, it seems as though this theory may be less relevant in the case of stratospheric cooling, where the static stability in the mid-latitude troposphere may not be strongly affected.

Finally, Yin [2005] and Lorenz and DeWeaver [2007] suggest that the atmospheric circulation can be changed by raising or lowering the altitude where the vertical temperature gradient changes sign (i.e. the tropopause height), even if the static stability is kept the same. The idea is that a higher tropopause height could allow for a deeper baroclinic zone in the troposphere, which offers more available potential energy to be used by baroclinic waves. A higher tropopause in the mid-latitudes, where the tropopause is sloped, could lead to both an upward and poleward shift in the regions of baroclinicity and an associated shift in the tropospheric circulation.

It is difficult to assess which dynamical mechanisms are driving the circulation response to climate change in observations and fully-coupled GCMs, because of many other processes and feedbacks that may complicate the interpretation of the atmospheric circulation response to a forcing. In this study we use a simple dry dynamical general circulation model in order to test the atmospheric circulation response and its sensitivity to idealized thermal forcings designed to mimic greenhouse gas and ozone forcing.

## **1.6 Previous Studies using Simple GCMs**

Simple general circulation models have been used in the past to better understand the atmospheric circulation response to imposed forcings, but surprisingly few studies have examined the response of the circulation to thermal forcing in an idealized context. Some notable research is discussed here.

Polvani and Kushner [2002] and Kushner and Polvani [2004] explored the annular mode response to thermal forcing in the polar stratosphere. By applying a cooling in the polar stratosphere of a simple atmospheric GCM, they simulated a strengthening of the stratospheric polar vortex accompanied by a poleward shift in the tropospheric jet. They find eddy forcing in the stratosphere does drive some changes in the troposphere but that eddy feedbacks in the troposphere are necessary to account for the full response. Eddies, which are generated in the region of maximum baroclinicity at the surface, are thought to maintain an initial shift in the jet by converging westerly momentum into the shifted jet location at upper levels, driving a residual meridional circulation through the Coriolis force which acts to reinforce the initial shift in baroclinicity at the surface [Lorenz and Hartmann 2001]. Gerber and Polvani [2009] and Chan and Plumb [2009] highlight the sensitivity of the results in Polvani and Kushner [2002] to the presence of topography and the tropospheric equilibrium temperature profile, respectively.

Ring and Plumb [2008] applied tropospheric thermal forcings in order to explore the response of the atmospheric circulation. They find that the projection of the atmospheric circulation response onto the annular modes depends strongly on where in space the forcing is applied. In particular, the response projects better onto the annular modes if the temperature gradient changes are confined poleward of  $45^\circ$  latitude and do

not extend into the tropics. They also note that feedback between the mean flow and the eddies is essential to simulating an annular mode-like response.

Son and Lee [2005, 2006] imposed tropical heating and high-latitude cooling to understand changes in the jet structure in response to changes in temperature gradient. They find that depending on the strength of the imposed thermal forcing, the circulation response will vary between a one or two jet regime. Eichelberger and Hartmann [2005] find that heating in the tropical troposphere enhances the strength of the stratospheric Brewer-Dobson circulation. They attribute the stratospheric changes to changes in the tropospheric midlatitude baroclinicity and a subsequent increase in vertical wave propagation. Haigh et al. [2005] and Simpson et al. [2009] examined the changes in the tropospheric circulation associated with the solar cycle heating in the lower stratosphere. They find that during a solar maximum there is a poleward shift of the mid-latitude jet compared to during a solar minimum. They also find that in agreement with Kushner and Polvani [2004], the feedbacks between the tropospheric wind and eddies are necessary to generate the full response of the tropospheric circulation. Finally, Lorenz and DeWeaver [2007] consider the effect of anthropogenically-induced changes in tropopause height on the extratropical circulation, and as discussed above, find a poleward shift of the jet as their model tropopause is raised.

While the above studies are the first to examine the atmospheric circulation response to thermal forcing in an idealized context, numerous aspects of the annular mode response to thermal forcing remain to be addressed, particularly with regard to the response to anthropogenic forcing. For example: the experiments in Polvani and Kushner [2002] are relevant for understanding the annular mode response to Antarctic ozone

depletion, but the sensitivity of their results to changes in the altitude and shape of the polar stratospheric cooling is unknown. The tropical heating profile in Son and Lee [2005] is much narrower than the expected response to increasing greenhouse gases, and their analysis is focused largely on the effects of tropical and polar heating on the number of jets in the extratropical circulation. Eichelberger and Hartmann [2005] do not consider the response of the tropospheric flow to the imposed tropical tropospheric heating and do not test the sensitivity of their results to changes in the shape of the forcing. Haigh et al. [2005] and Simpson et al. [2009] focus on the thermal effects of the solar cycle in the tropical stratosphere. Lorenz and DeWeaver [2007] focus on the height of the tropopause, rather than the thermal forcing itself, as the key forcing mechanism.

In this study, we provide new insight into the atmospheric circulation response to thermal forcing in a simple GCM. We focus on the three principal heatings most commonly associated with anthropogenic forcing: (1) enhanced warming in the tropical troposphere, which mimics stronger latent heating in the tropical troposphere; (2) enhanced cooling in the polar stratosphere, which mimics the cooling associated with polar ozone depletion; and (3) enhanced warming at the surface over the polar regions, which mimics the heating associated with the ice/albedo feedback in the Arctic. Chapter 2 describes the simple GCM as well as the analysis techniques used in this study. We describe the results from steady-state experiments in Chapter 3, and transient simulations in Chapter 4. Chapter 5 supplements the model research with observational analysis exploring variability and trends in observed vertical profiles of ozone in relation to lower-stratospheric temperatures. Chapter 6 includes a summary of the findings.

## CHAPTER 2: MODEL DESCRIPTION AND ANALYSIS TECHNIQUES

### 2.1 Model Description

We use the simple dry dynamical core of the Colorado State University general circulation model [Ringler et al. 2000]. The model uses a hybrid sigma-isentropic vertical coordinate that smoothly transitions from the sigma coordinate ( $\sigma=p/p_s$ ) near the surface to the isentropic coordinate in the free troposphere and stratosphere, giving the benefits of terrain-following sigma coordinates near the earth's surface but quasi-Lagrangian isentropic coordinates aloft [Konor and Arakawa 1997]. The model is discretized in the horizontal using a geodesic grid [Fig. 2.1; Heikes and Randall 1995]. The geodesic grid is constructed from an icosahedron through recursive division of each triangular face. The advantages of the geodesic grid are that it has no singularity at the

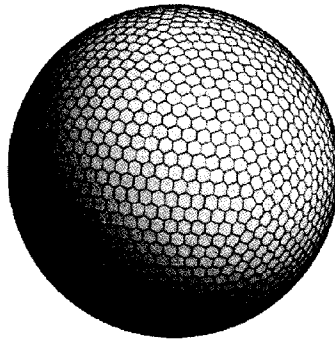
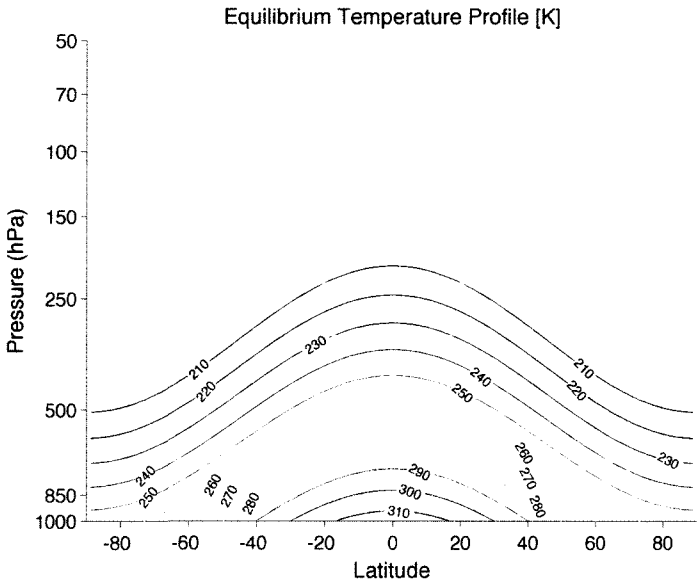


Fig 2.1. The model's geodesic grid.

poles and has approximately homogeneous and isotropic resolution throughout the globe [Heikes and Randall 1995].

The equations and parameters used in the control run are identical to those specified in Held and Suarez [1994]. All experiments are run with no topography and under equinoctial conditions. The circulation in the model is driven by Newtonian cooling of the temperature field towards a prescribed zonally- and hemispherically-symmetric “radiative equilibrium” temperature profile (Figure 2.2). Rayleigh damping of low-level winds is included to represent surface friction. There are 10,242 geodesic grid cells resulting in a horizontal resolution of  $\sim 250$  km or  $2.25^\circ$ , and 25 vertical layers



**Fig 2.2.** The Held-Suarez radiative equilibrium temperature profile [K].

(interpolated to 39 pressure levels at 25 mb intervals) with the model top at 1 mb. Since there is no topography, results are shown only for zonal-mean quantities.

The steady-state experiments (Chapter 3) are integrated for 2160 days with a model time step of 80 seconds (output is recorded once daily). The first 360 days of all runs are discarded to account for initial spin-up, which leaves 1800 days for the analysis of each run (the zonal-mean wind and temperature fields both reach their long-term mean values within ~200 days).

The transient simulations (Chapter 4) are started from 12 different initial conditions generated from the equilibrium control run and separated by 50 days, so the initial conditions are independent from one another. The thermal forcing is turned on after 10 days, and each run lasts 150 days. Ensemble-mean runs are created by averaging the output from the 12 transient simulations. An equivalent ensemble-mean control run is also created using the same initial conditions. Output is recorded every 6 hours.

## 2.2 Control Climatology and Statistical Techniques

The long-term mean control climatology of the model is shown in Figure 2.3. The top panel shows the climatological-mean, zonal-mean zonal wind and eddy momentum fluxes; the middle panel shows the climatological-mean, zonal-mean temperature and eddy heat fluxes. In both panels, the dark black lines indicate the height of the tropopause, which is estimated as the pressure level where the lapse rate ( $dT/dz$ ) changes sign. The eddy momentum and heat fluxes are found as  $\overline{u'v'}$  and  $\overline{v'T'}$ , respectively, where here the overbars denote the zonal-mean and the primes denote departures from the zonal-mean. The eddy fluxes are calculated on daily time scales before being averaged over all days in the integration.

Consistent with Held and Suarez [1994], the zonal-mean zonal wind is westerly throughout the upper troposphere poleward of  $\sim 10^\circ$  latitude and peaks around 30 m/s near 250 hPa and  $45^\circ$  latitude. The largest eddy momentum fluxes are found near  $\sim 250$

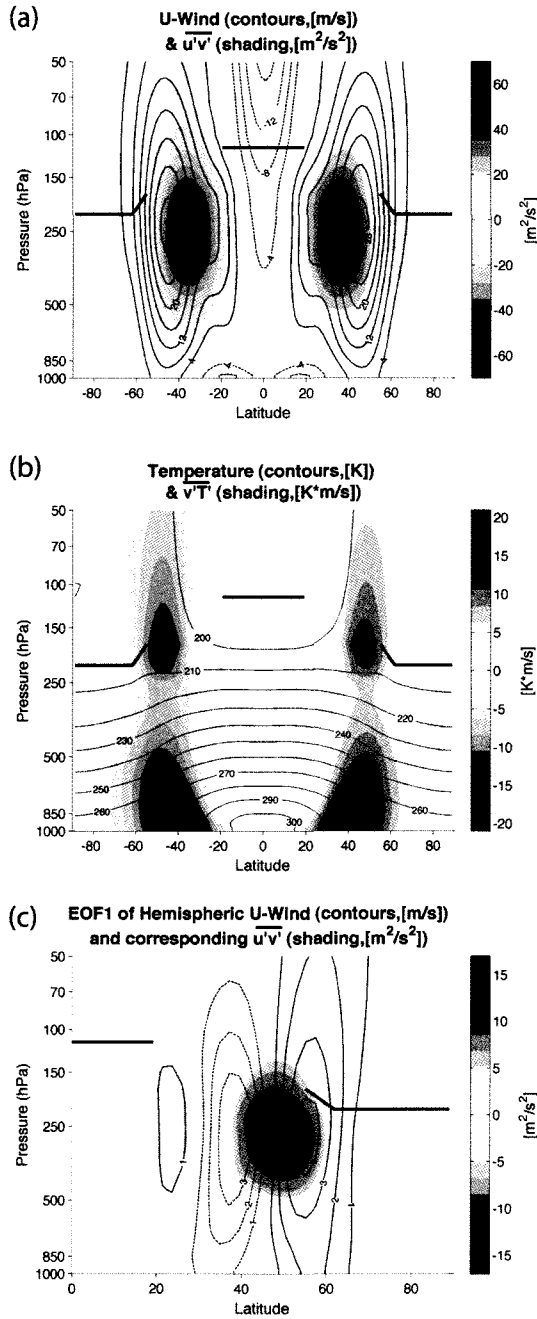


**Fig 2.3.** The model control climatology. Bold black lines in all plots represent the control run tropopause height. (a) Contours: Zonal-mean zonal wind [m/s]. Shading: eddy momentum flux [m<sup>2</sup>/s<sup>2</sup>]. (b) Contours: Zonal-mean temperature [K]. Shading: eddy heat flux [K m/s]. (c) Contours: Leading EOF of the zonal-mean zonal wind poleward of  $20^\circ$  latitude. Units are m/s per standard deviation of the PC time series. Shading: Eddy momentum flux anomalies regressed onto the PC time series of the zonal-mean zonal wind [m<sup>2</sup>/s<sup>2</sup> per standard deviation of the PC time series].

hPa between  $\sim 30\text{-}40^\circ$  latitude, and hence the surface flow is noticeably westerly poleward of  $\sim 40^\circ$  but easterly equatorward of  $\sim 30^\circ$  latitude. The eddy heat fluxes exhibit two distinct maxima: one near the surface at  $\sim 40^\circ$  latitude; the other near 200 hPa at  $\sim 45^\circ$  latitude. The former lies along the largest gradient in surface temperature and reflects the generation of baroclinic waves in the lower troposphere; the latter reflects the flux of wave activity into the model stratosphere and thus the driving of the model Brewer-Dobson circulation. The tropopause height is  $\sim 210$  hPa at the poles and  $\sim 110$  hPa at the tropics (the tropopause height is highly variable across the axis of the model jet, and is thus not shown in the subtropics).

The leading pattern of variability in the model wind field is shown in Fig. 2.3c (note that the top panels are shown from pole to pole, but that the bottom panel is shown for only one hemisphere). Here the leading pattern of variability is defined as the first empirical orthogonal function (EOF) of the zonal-mean zonal-wind field, and is found by: 1) removing the long-term mean from the zonal-mean wind field; 2) weighting the zonal-mean zonal wind field by the square root of the cosine of latitude; and 3) eigenanalyzing the covariance matrix for the region poleward of  $20^\circ$  latitude from 1000 hPa to the model top. The EOF and its associated momentum fluxes are found by regressing the zonal wind and momentum flux fields onto standardized values of the resulting leading principal component time series (Fig. 2.3c). The leading EOF of the zonal flow is reminiscent of those found in other simple GCMs [e.g., Yu and Hartmann 1993; Robinson 1994, 1996; Ring and Plumb 2007; Gerber et al. 2008], and is characterized by out-of-phase fluctuations in the zonal-mean zonal wind field with centers of action located near  $35^\circ$  and  $55^\circ$  latitude, and by anomalously poleward

momentum fluxes near 250 hPa and 45° latitude. The pattern in Fig. 2.3c is hereafter referred to as the model annular mode, and its positive polarity is defined as periods when the momentum fluxes are anomalously poleward across 45° latitude.

The timescale of the model annular mode is important since the amplitude of its response to external forcing is directly related to the model decorrelation timescale [Ring and Plumb 2008; Gerber et al. 2008]. The “decorrelation” timescale  $\tau$  is calculated from the autocorrelation function:

$$(1) \quad r(t) = \exp\left(-\frac{t}{\tau}\right)$$

where  $t$  is the lag in days and  $\tau$  is termed the “efolding” timescale when  $r(t)=1/e \sim 0.37$ . The decorrelation timescale in the control run climatology, based on the leading EOF of zonal-mean zonal winds as a function of pressure and latitude polewards of 20° latitude, is about 26 days (+/- 4.4 days). Here the uncertainty of the decorrelation timescale is roughly estimated using this equation derived in Gerber et al. [2008]:

$$(2) \quad std(\tau_N) \approx k\tau^{3/2}(2N)^{-1/2}$$

where  $k = e(1 - 3 * e^{-2})^{1/2} \sim 2$ , and N is 1800 days. In this case, we assume that the hemispheres are statistically the same in the model, so we can average the autocorrelation functions from both hemispheres in order to reduce the uncertainty.

The observed decorrelation timescale for the annular modes is 10-20 days, but Held Suarez-type models with zonally symmetric boundary conditions generally have

difficulty reproducing these timescales [Gerber et al. 2007; Gerber and Vallis 2007], so 26 days is a very reasonable value and is close to the benchmark range proposed by Gerber et al. [2008]. As noted in Gerber et al. [2008] and Chan and Plumb [2009], experiments with very long model annular mode timescales (e.g., as in Kushner and Polvani 2004) are thought to have unrealistically large responses to external forcing. The timescale of the annular mode can be improved by increasing the spatial resolution of the model, adding zonal asymmetries such as topography, or adjusting model parameters such as the momentum and thermal damping [Gerber and Vallis 2007].

In some cases, we consider the component of the model response that projects onto the model annular mode. Where this is done, the annular mode fit is found by 1) regressing the surface zonal wind response onto the surface component of the annular mode shown in Fig. 2.3c; and 2) multiplying the full annular mode pattern in Fig. 2.3c by the resulting regression coefficient [e.g., Kushner et al. 2001].

Statistical significance is assessed using the t-statistic for the difference in means:

$$(3) \quad t = \frac{\bar{x}_1 - \bar{x}_2}{\sigma \sqrt{\frac{1}{N_1} + \frac{1}{N_2}}} \quad \text{where } \sigma^2 = \frac{N_1 s_1^2 + N_2 s_2^2}{N_1 + N_2 - 2}$$

where  $\sigma^2$  is the pooled variance,  $N_1$  ( $N_2$ ) is the sample size of sample 1 (2), and  $s_1$  ( $s_2$ ) is the sample standard deviation of samples 1 (2). In this case the difference in means is the difference between the long-term mean forced run and the long-term mean control run, or what we call the “response”. The persistence in the data is taken into account in the above equation by using the “effective” sample size for each sample as defined by Bretherton et al. [1999]:

$$(4) \quad N_{eff} \sim N * \frac{1 - a_1 a_2}{1 + a_1 a_2}$$

where  $N$  is the number of data points, “ $a_1$ ” is the lag-one autocorrelation of the first time series, and “ $a_2$ ” is the lag-one autocorrelation of the second time series. As persistence increases, the effective sample size decreases.

In cases where we show streamfunction  $\varphi$ , it is calculated as:

$$(5) \quad \bar{v} * 2\pi a * \cos \phi = g \frac{d\varphi}{dp}$$

where the integration is calculated using the boundary conditions of  $\varphi=0$  at the surface;  $a$  is the radius of the earth,  $\bar{v}$  represents the zonal-mean of the meridional wind component, and  $\phi$  is latitude.

In cases where eddy phase speeds are calculated, we follow Hayashi [1971], Randel and Held [1991], and Chen et al. [2007]. The  $u$  and  $v$  components at a given pressure level (as functions of time, latitude, and longitude), from the model control run and heating run output, are first subdivided into periods of 150 days. A Hanning window is applied to the each subdivided time dimension. The  $u$  and  $v$  fields are then decomposed into spatial harmonics via Fourier analysis, yielding coefficients for the sine and cosine parts for each variable; and then each of these coefficients (4 total:  $C_u$ ,  $S_u$ ,  $C_v$ ,  $S_v$ ) are further decomposed into temporal harmonics, so that there are now 8 total coefficients ( $C_u \rightarrow A_u, B_u$ ;  $S_u \rightarrow a_u, b_u$ ;  $C_v \rightarrow A_v, B_v$ ;  $S_v \rightarrow a_v, b_v$ ). According to Hayashi [1971], these coefficients can be combined to determine the spectra  $P_{\pm\omega}$  of westward (+ $\omega$ ) and eastward (- $\omega$ ) propagating waves using the following equations:

$$(6) \quad \begin{aligned} 4R_{k,\pm\omega}^2 &= (Au \mp bu) * (Av \mp bv) + (\mp Bu - au) * (\mp Bv - av) \\ P_{\pm\omega} &= \frac{1}{2} R_{k,\pm\omega}^2 \end{aligned}$$

The spectra of eddy momentum flux convergence per day is then calculated as:

$$(7) \quad -\frac{d}{a * t * \cos^2 \phi * d\phi} * (\cos^2 \phi * P_{\pm\omega})$$

where  $a$  is the radius of the earth,  $t$  is one day (in seconds),  $\phi$  is latitude, and  $P_{\pm\omega}$  is the spectra of eastward and westward propagating waves as defined in equation (6).

These spectra are smoothed using a Gaussian window, and then averaged over all subdivisions of 150 days. The wavenumber/frequency spectra at each latitude ( $P_{n,w}$ ) are then transformed into wavenumber/angular phase speed spectra ( $P_{n,c}$ ) by constructing a phase speed grid and interpolating the spectral density at each phase speed from the two closest frequency estimates of  $P_{n,w}$ . The equation relating this transformation is equation (3b) from Randel and Held [1991]:

$$(8) \quad P_{n,c} = P_{n,w} * \left(\frac{n}{a \cos \phi}\right)$$

These new spectra are then summed over all wavenumbers, so the plotted result is phase speed spectra for westward and eastward propagating waves as a function of latitude.

## CHAPTER 3: STEADY-STATE EXPERIMENTS

In this chapter we explore and document the steady-state response of the CSU GCM to three thermal forcings designed to qualitatively mimic the spatially-varying heatings associated with anthropogenic forcing: 1) enhanced warming in the tropical upper troposphere (which mimics the heating associated with stronger latent heat release in the tropics); 2) enhanced cooling in the polar stratosphere (which mimics the effects of Antarctic ozone depletion); and 3) enhanced warming at the surface over polar regions (which mimics the heating associated with the ice/albedo feedback).

The analytic functions for all thermal forcings are summarized in Table 3.1. The forcings are all applied as an external forcing  $Q$  in the thermodynamic equation:

$$(9) \quad \frac{dT}{dt} = \dots - k_T(\phi, \sigma)[T - T_{eq}(\phi, p)] + Q$$

Here  $k_T$  is a damping coefficient and is a function of latitude and height, with largest values near the surface and in the tropics. Applying the forcing in this manner is mathematically equivalent to relaxing the temperature profile to a new equilibrium profile equal to  $Q/k_T$ .

The thermal forcings have the same maximum amplitude (0.5 K/day); hence variations in the responses are due solely to variations in the structure and location of the forcings, not their amplitudes. The maximum amplitude (0.5 K/day) is approximate, but

**Table 3.1.** Description of Heating Runs.

Heat run	Description of heating	Equation for forcing x=lat (radians), y=sigma level	Values for $\sigma_x$ , $\sigma_y$ , $x_o$ , $y_o$	Center of heating +/- half-depth (lat)	Center of heating +/- half-depth (press)
Fig 3.1a	Heating in Tropical Upper Troposphere	$q_o * \exp[-(\frac{(x - x_o)^2}{2\sigma_x^2} + \frac{(y - y_o)^2}{2\sigma_y^2})]$	$\sigma_x=0.40$ $x_o=0$ $\sigma_y=0.11$ $y_o=0.3$	$0^\circ +/- 27^\circ$	300 +/- 125 mb
Fig 3.1b	Shallow Heating in Tropical Upper Troposphere	Same as 3.1a	$\sigma_x=0.40$ $x_o=0$ $\sigma_y=0.07$ $y_o=0.3$	$0^\circ +/- 27^\circ$	300 +/- 75 mb
Fig 3.1c	Narrow Heating in Tropical Upper Troposphere	Same as 3.1a	$\sigma_x=0.21$ $x_o=0$ $\sigma_y=0.11$ $y_o=0.3$	$0^\circ +/- 13.5^\circ$	300 +/- 125 mb
Fig 3.1d	Heating in Tropical Middle Troposphere	Same as 3.1a	$\sigma_x=0.40$ $x_o=0$ $\sigma_y=0.11$ $y_o=0.5$	$0^\circ +/- 27^\circ$	500 +/- 125 mb
Fig 3.4a	Cooling in Lower Polar Stratosphere	$q_o * \exp[-2 * (\frac{(x - x_o)^2}{2\sigma_x^2} + \frac{(y - y_o)^2}{2\sigma_y^2})]$	$\sigma_x=0.40$ $x_o=1.57$ $\sigma_y=0.14$ $y_o=0.1$	$90^\circ - 18^\circ$	100 +/- 115 mb
Fig 3.4b	Cooling in Mid Polar Stratosphere	Same as 3.4a	$\sigma_x=0.40$ $x_o=1.57$ $\sigma_y=0.10$ $y_o=0.075$	$90^\circ - 18^\circ$	75 +/- 80 mb
Fig 3.4c	Cooling in Upper Polar Stratosphere	Same as 3.4a	$\sigma_x=0.31$ $x_o=1.57$ $\sigma_y=0.03$ $y_o=0.05$	$90^\circ - 13.5^\circ$	50 +/- 25mb
Fig 3.5a	Shallow Cooling in Lower Stratosphere	$q_o * \exp[-(\frac{(x - x_o)^2}{2\sigma_x^2} + \frac{(-7000 * \ln y + 7000 * \ln y_o)^2}{2\sigma_y^2})]$	$\sigma_x=0.28$ $x_o=1.57$ $\sigma_y=2100$ $y_o=0.2$	$90^\circ - 18^\circ$	200 mb +/- 2.5 km
Fig 3.5b		Same as 3.5a	$\sigma_x=0.28$ $x_o=1.57$ $\sigma_y=2100$ $y_o=0.175$	$90^\circ - 18^\circ$	175 mb +/- 2.5 km
Fig 3.5c		Same as 3.5a	$\sigma_x=0.28$ $x_o=1.57$ $\sigma_y=2100$ $y_o=0.15$	$90^\circ - 18^\circ$	150 mb +/- 2.5 km
Fig 3.6	Heating at Polar Surface	for $x > 0$ , $q_o * (\cos(x - x_o))^{15} * e^{6*(y-y_o)}$ for $x < 0$ , 0	$x_o=1.57$ $y_o=1$	$90^\circ - 16^\circ$	1000 - 125 mb
Fig 3.7	Combination of Figs. 3.1a, 3.4a, 3.6	Sum of 3.1a, 3.4a, and 3.6			

provides physically reasonable changes in temperature. For example, 0.5 K/day heating produces a steady-state warming of about 5K at the polar surface. This value approximates the temperature changes simulated at the Northern Hemisphere polar surface in climate change scenario SRES A1B [IPCC AR4, Chapter 10]. Similarly, 0.5 K/day cooling produces an 8K cooling in the polar stratosphere, comparable to observed temperature changes due to ozone depletion since 1969 [Randel and Wu 1999; Thompson and Solomon 2002]. The 0.5 K/day heating produces a temperature change in the tropical troposphere that is approximately double (~10K) that seen in climate change scenarios (~5K) [IPCC AR4, Chapter 10].

In all results, the “response” to a given heating is defined as the difference between the long-term means of the perturbed and control simulations. The significance of key features is documented in Tables 3.2-3.4 using a two-tailed test of the  $t$ -statistic for the difference of means. Table 3.2 documents the significance of the polar stratospheric cooling in Fig. 3.1; Table 3.3 the significance of the tropical stratospheric temperature changes in Figs. 3.4 and 3.5; Table 3.4 documents the significance of the changes in the surface winds, and in the eddy heat and momentum fluxes found in all figures.

### **3.1 Heating in the Tropical Upper Troposphere**

In the first set of experiments, we examine the model response to zonally-symmetric thermal forcing in the tropical troposphere. We consider first the forcing and responses shown in row (a) of Figure 3.1. The left panel shows the thermal forcing; the

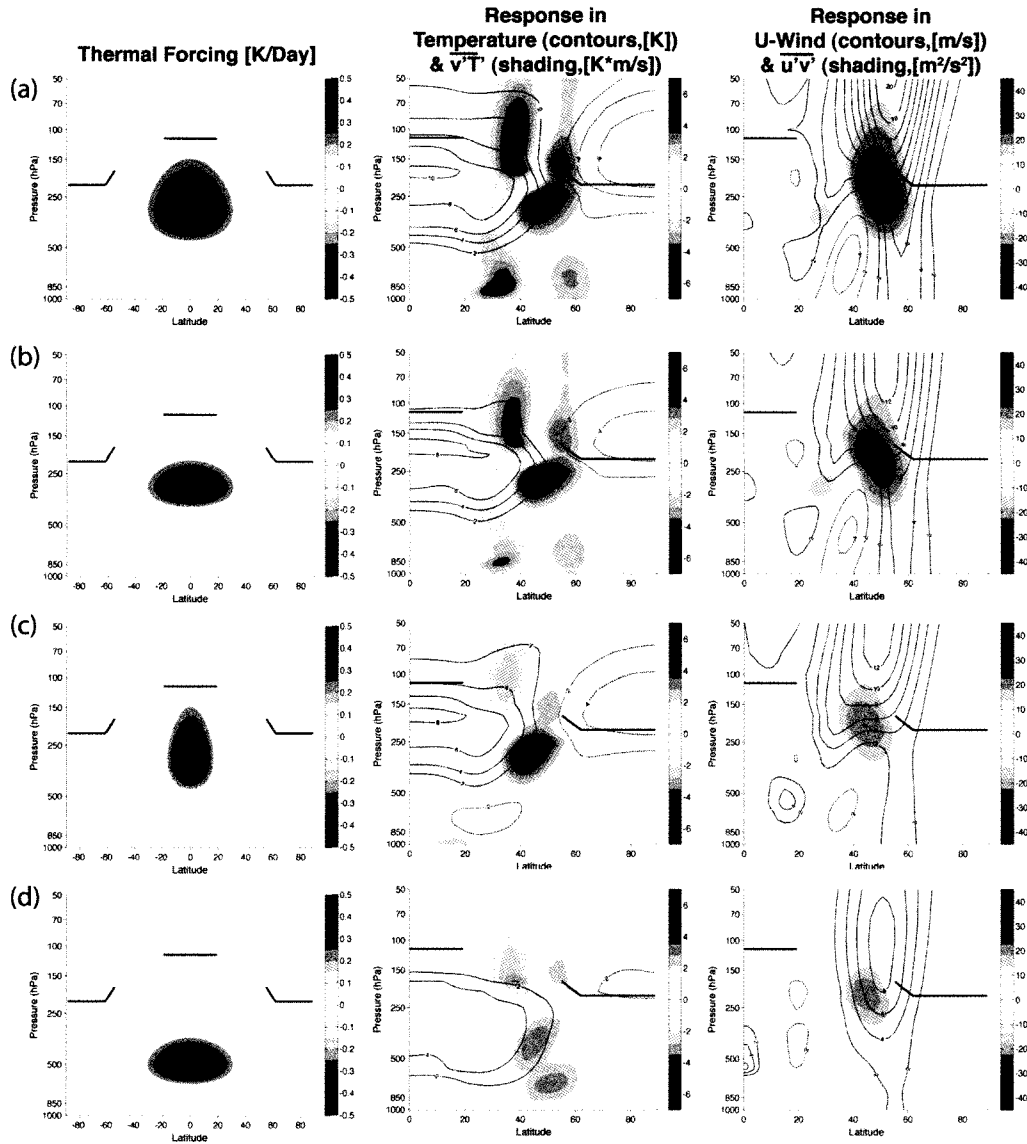


**Fig 3.1.** The zonal-mean response to tropical tropospheric heating. Bold black lines in all plots represent the control run tropopause height. Left plots show the thermal forcing [K/day]. Middle plots show (shading) the total eddy heat flux response [K\*m/s] and (contours) the temperature response [K]. Right plots show (shading) the total eddy momentum flux response [ $m^2/s^2$ ] and (contours) the zonal-mean zonal wind response [m/s]. Row (a) shows results for tropical upper tropospheric heating; row (b) results for shallow tropical upper tropospheric heating; row (c) results for narrow tropical upper tropospheric heating; and row (c) results for tropical heating centered at 500 hPa. Note the forcings are shown pole-pole but the responses are shown for only one hemisphere. The thermal forcings are detailed in Table 3.1.

middle panel the responses in the zonal-mean temperature field and the eddy heat flux; and the right panel the responses in the zonal-mean wind field and the eddy momentum flux. The forcing is centered at 300 hPa and the equator, and amplitudes greater than 0.25 K/day are limited to the region bounded by 175 hPa, 425 hPa, and 27° latitude (Table 3.1). Although most of the heating falls below the model tropopause (bold black line), there is weak heating (less than 0.1 K/day) in the lower tropical stratosphere; however, as demonstrated in the sensitivity experiments below, this feature has little bearing on the response. Since the forcing is symmetric about the equator, we show the response in only one hemisphere.

The response to the thermal forcing includes several pronounced features. In the temperature field and the eddy heat fluxes, these include (row a, middle): 1) warming in the tropical troposphere that extends to  $\sim 45^\circ$  latitude, with a maximum amplitude of  $\sim 10\text{K}$ ; 2) cooling in the polar stratosphere with a maximum amplitude  $\sim 6\text{K}$ ; 3) increased poleward heat fluxes north of  $50^\circ$  juxtaposed against reduced poleward heat fluxes south of  $50^\circ$  latitude at most levels; and 4) a maximum in anomalous poleward heat fluxes in the upper troposphere near  $\sim 50^\circ$  latitude and 300 hPa. In the wind field and the eddy momentum fluxes, the most pronounced features include (row a, right): 1) westerly anomalies that amplify with height between about  $30\text{-}70^\circ$  latitude above 250 hPa; 2) anomalous westerly surface winds centered near  $55^\circ$  and anomalous easterly surface winds centered near  $35^\circ$  latitude consistent with a poleward shift in the model mid-latitude jet; and 3) anomalous poleward momentum fluxes centered near 200 hPa and  $45^\circ$  latitude.

The warming in the tropical troposphere and the westerly vertical shear of the extratropical zonal-flow above  $\sim 500$  hPa are expected on the basis of the thermal wind response to the heating. But the other aspects of the response are eddy-driven and are not readily predicted by linear theory. In the troposphere, the pronounced changes in the eddy fluxes of heat and momentum are consistent with a poleward shift in the model

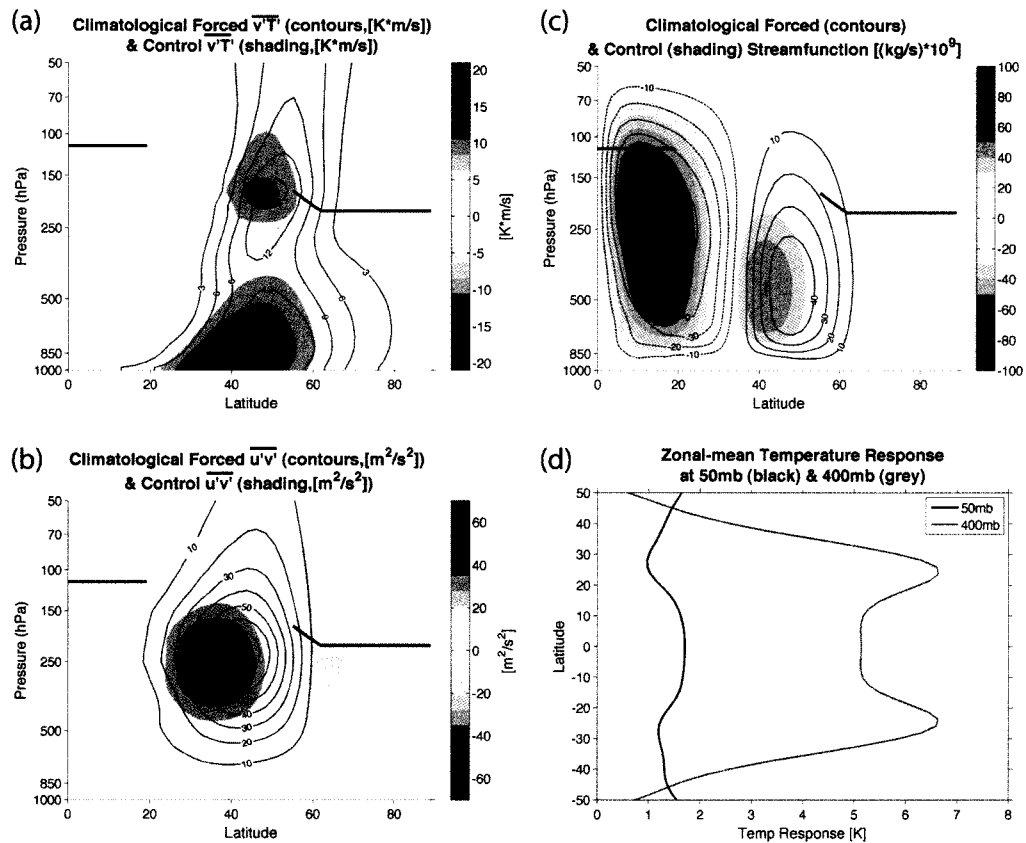


**Fig 3.2.** Additional results from the forcing considered in Fig. 3.1a. (a) Long-term means of the total eddy heat fluxes from the forced (contours) and control (shading) runs  $[K \cdot m/s]$ . (b) Long-term means of the total eddy momentum fluxes from the forced (contours) and control (shading) runs  $[m^2/s^2]$ . (c) Long-term means of the meridional streamfunction from the forced (contours) and control (shading) runs  $[(kg/s) \cdot 10^9]$ . Blue shading and dashed contours correspond to clockwise circulation; red shading and solid contours correspond to counterclockwise circulation. (d) The responses in zonal-mean temperatures from Fig. 3.1a highlighted at 50 mb (black) and 400 mb (grey)  $[K]$ .

storm track (the long-term mean eddy fluxes from the control and perturbed runs are superposed in Figures 3.2a and 3.2b). Accordingly, the tropospheric circulation response to the heating in Fig. 3.1a projects strongly onto the positive polarity of the model annular mode, as quantified in Fig. 3.3 (left column).

The poleward contraction of the mid-latitude storm tracks is accompanied by a poleward extension of the model Hadley cell circulation in the tropics (Fig. 3.2c): in the control run (shading), the Hadley circulation is associated with rising motion at the equator and subsidence at  $\sim 25^\circ$  latitude. The eddy-driven Ferrell cell has a circulation in the opposite sense and extends to  $\sim 50^\circ$  latitude in each hemisphere. When we apply the

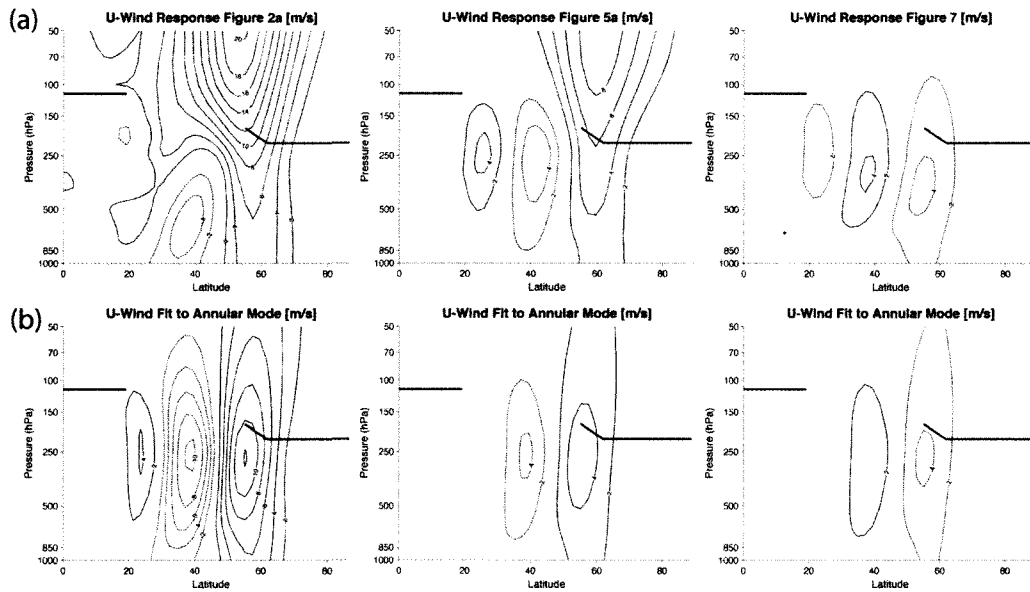


**Figure 3.3.** (a) From left to right: the zonal-mean zonal wind responses [m/s] duplicated from Figures 3.1a, 3.4a and 3.6. (b) The linear fits of the responses to the model annular mode [m/s]. See text for details.

heating to the upper tropical troposphere, we see a considerable widening of the Hadley cell circulation (black contours), as well as a weakening. The regions of subsidence are

now located  $\sim 35^\circ$  latitude in each hemisphere. In addition, the Ferrell cell has shifted substantially poleward, as we may anticipate from the poleward shift of the eddies in Figure 3.2a and 3.2b. These changes in the Hadley cell circulation are also noted in observations and numerical simulations [Fu et al. 2006; Seidel and Randel 2007; Frierson et al. 2007; Lu et al. 2007, 2008; Seidel et al. 2008].

In the stratosphere, the out-of-phase temperature anomalies between polar and tropical latitudes are accompanied by negative hemispherically-averaged eddy heat fluxes at 100 hPa (i.e., at 100 hPa, the anomalously negative heat fluxes equatorward of  $40^\circ$  are larger than the anomalously positive heat fluxes poleward of  $45^\circ$  latitude). The polar stratospheric cooling is statistically significant (Table 3.2), and both the meridional dipole in stratospheric temperatures and the decreased flux of wave activity at 100 hPa are indicative of a weakening of the model Brewer-Dobson circulation. The weakened Brewer-Dobson circulation may also be enhancing the heating in the tropics due to adiabatic compression, potentially creating a positive feedback whereby the initial heating weakens the Brewer-Dobson circulation, which then enhances the initial heating. An additional intriguing feature is that the lower stratospheric and upper tropospheric

Heat run	Mean temperature response 100mb, 60-90° (Difference [K], significance)
Fig 3.1a	-4.85, >99%
Fig 3.1b	-2.61, >99%
Fig 3.1c	-3.05, >99%
Fig 3.1d	-0.27, NS

**Table 3.2.** Mean temperature response at 100 mb, cosine-weighted and averaged from 60-90° for the specified tropical tropospheric heating run [K]; and the significance given by the 2-tailed *t*-test for the difference between means. NS= not significant (<90% significance).

temperature anomalies exhibit minima and maxima, respectively, at subtropical latitudes that are reminiscent of those found in the observed temperature trends at those levels [Fig. 3.2d, Fu et al. 2006].

The results in row (a) of Figure 3.1 thus reveal three robust changes of the model circulation to tropical tropospheric heating: 1) a poleward contraction in the model storm track and hence a shift towards the positive polarity of the model annular mode; 2) a poleward expansion of the model Hadley cell circulation; and 3) a weakening of the model Brewer-Dobson circulation. The poleward shift in the storm track and the expansion of the Hadley cell circulation are qualitatively in agreement with circulation changes simulated in climate change scenarios of more complex IPCC AR4 models, and recent studies have argued that tropical heating may drive the simulated trends in coupled climate change simulations [e.g., Chen and Held 2007; Lu et al. 2007, 2008; Chen et al. 2007]. But as far as we know, the results in row (a) are the first to demonstrate that this is, in fact, the case in a simple GCM.

However, the inferred weakening of the model Brewer-Dobson circulation is in the opposite sense of that found in experiments run on both simple [Eichelberger and Hartmann 2005] and complex [e.g., Rind et al. 1998; Butchart and Scaife 2001; Li et al. 2008] climate models. One possible reason for this difference is that our model is set to equinoctial conditions, while other studies frequently use NH winter conditions, including a stratospheric polar night jet. The different background flows in the stratosphere could mean quite different responses in the stratospheric overturning circulation; research is in progress to determine the response to solsticial conditions, as discussed in the Conclusions section.

How robust are the key responses found in the top row of Figure 3.1? In rows (b-d) of Figure 3.1 we examine the sensitivity of the model response to changes in the shape and altitude of the tropical heating. The results in rows (b-d) are derived from forcings similar to that used in row (a), except that the forcing is compressed in the vertical (row b); compressed meridionally (row c); and compressed in the vertical and lowered so that it is centered at 500 hPa (row d). The analytic expressions for all heating profiles are again summarized in Table 3.1.

Compressing the heating in the vertical (row b) weakens slightly the extratropical wind and temperature responses, but overall has no effect on the key features of the response. The model jet and eddy fluxes are still shifted poleward, the model annular mode is still biased towards its positive polarity, and the model Brewer-Dobson circulation is still weakened. Compressing the heating in the meridional direction (row c) only slightly weakens the amplitude of the stratospheric response and has a more pronounced effect on the amplitude of the extratropical tropospheric response. But even in this case, the tropospheric wind and eddy momentum fluxes are still shifted poleward, the eddy heat fluxes still exhibit a distinct maximum in the upper troposphere at  $\sim 40^\circ$  latitude, and the surface eddy heat fluxes are still anomalously poleward at  $\sim 55^\circ$  latitude. Interestingly, the meridional scale of the tropical tropospheric warming is unchanged between rows (a) and (c), despite the fact that the imposed heating has been compressed substantially in the meridional direction. This is likely due to weak equatorial rotation which tends to minimize temperature gradients in the tropics.

When the heating is compressed vertically and limited to the middle troposphere (row d), the sign of the responses in the wind and temperature fields remain unchanged,

but the amplitudes of the responses are diminished considerably, particularly in the polar stratosphere (note that the cooling over the polar stratosphere is no longer significant, Table 3.2). Nonetheless, the changes in the eddy heat and momentum fluxes are significant (Table 3.4).

### **3.2 Cooling in the Polar Stratosphere**

In the second set of experiments, we apply a zonally-symmetric thermal forcing in the polar stratosphere, i.e., in the region most strongly affected by Antarctic ozone depletion. We first consider the forcing shown in row (a) of Figure 3.4. Here the cooling is centered at 100 hPa and damps to 0.25 K/day by 215 hPa and 72° latitude (Table 3.1). The cooling is analogous but not identical to that used in Polvani and Kushner [2002] and Kushner and Polvani [2004].

As expected from the linear zonal-mean response, the thermal forcing is associated with cooling in the polar stratosphere (Fig. 3.4, row a, middle) and anomalous westerly shear in the extratropical stratosphere (Fig. 3.4, row a, right). But as is the case for tropical heating, the response to polar stratospheric cooling also includes a pronounced eddy-driven component. The eddy driven component is for the most part consistent with that found in Polvani and Kushner [2002]. Cooling in the polar stratosphere drives increased poleward momentum fluxes across ~50° latitude and thus equivalent barotropic westerlies that extend from the surface to the lower stratosphere. As is the case for tropical heating, the changes in the zonal flow reflect a poleward shift in

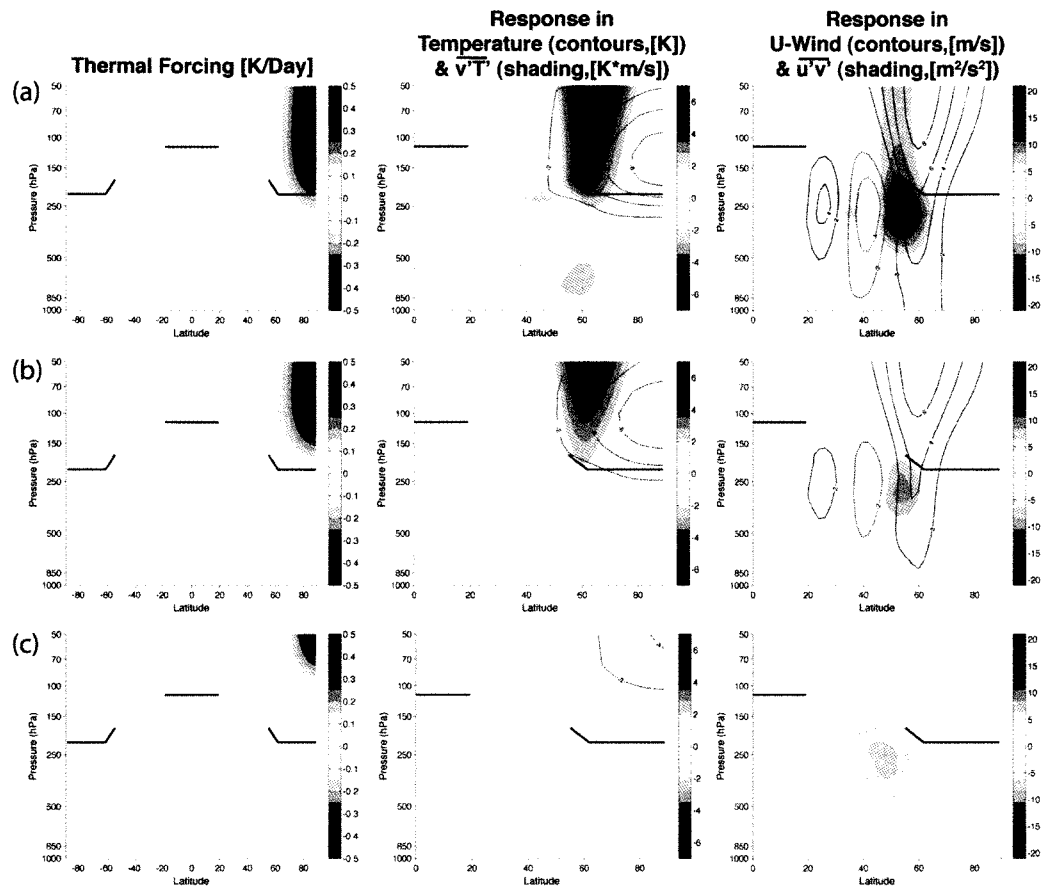


**Figure 3.4.** As in Fig. 3.1, but for the responses to the polar stratospheric thermal forcings shown in the left column. The forcings are documented in Table 3.1 and are centered at 100 hPa (a), 75 hPa (b) and 50 hPa (c). Note the shading scaling in the right panels is about half that for Fig. 3.1.

the model extratropical jet, and the barotropic component of the response projects strongly onto the positive polarity in the model annular mode (Fig. 3.3, middle column).

In contrast to the case for tropical heating, the response to polar stratospheric cooling is also marked by large increases in eddy heat fluxes in the polar stratosphere (Fig. 3.4, row a, middle). The stratospheric heat fluxes are highly significant (Table 3.4, column 3) but are in the opposite sense of those found in Kushner and Polvani [2004]. The poleward heat fluxes act to oppose the effects of the polar diabatic cooling, and since

the hemispherically-averaged heat fluxes along 100 hPa are anomalously poleward (Table 3.4), they act to increase the net wave driving in the model stratosphere. We note that while the increase in wave driving must drive anomalous cooling in middle or tropical latitudes of the tropical stratosphere due to an enhanced model Brewer-Dobson circulation, we do not see significant cooling in this region (Table 3.3); it's possible stronger cooling is occurring above 50 hPa, the highest resolved layer in the model. We do see weak cooling  $\sim 0.2\text{-}0.3$  K at 50 hPa from the equator to  $30^\circ\text{N}$  that is likely due to the enhanced rising branch of the stratospheric circulation.

Hence, the extratropical stratospheric response to polar stratospheric cooling (Fig. 3.4a) differs considerably from the response to tropical tropospheric heating (Fig. 3.1a), despite the fact both responses are associated with temperature falls in the polar stratosphere. In the case of Fig. 3.4a, the polar cooling is driven by the thermal forcing but is damped by increased stratospheric wave driving; in the case of Fig. 3.1a, the polar cooling is driven by the decreased stratospheric wave driving. Thus polar stratospheric cooling is associated with an increase in stratospheric wave drag (and thus an enhanced

Heat run	Mean temperature response 100mb, 0-30° (Difference [K], significance)
Fig 5a	-0.17, NS
Fig 5b	-0.04, NS
Fig 5c	0.04, NS
Fig 6a	0.20, NS
Fig 6b	-0.49, >95%
Fig 6c	0.04, NS

**Table 3.3.** Mean temperature response at 100mb, cosine-weighted and averaged from 0-30° for the specified stratospheric cooling run [K]; and the significance given by the 2-tailed *t*-test for the difference between means. NS= not significant (<90% significance).

model Brewer-Dobson circulation) and tropical tropospheric heating is associated with a decrease in stratospheric wave drag (and thus a weakened Brewer-Dobson circulation).

How sensitive is the eddy-driven response to the shape and location of the stratospheric cooling? In rows (b-c) of Figure 3.4 we examine the effect of lifting the lower bound of the cooling while continuing to allow the upper bound of the cooling to extend through the top of the stratosphere. When the center of the heating is lifted by 25 hPa (row b), the amplitude of the response is damped by ~50%, but the structure of the response is unchanged and the key features remain significant: the heat fluxes are still anomalously positive in the polar stratosphere, the upper tropospheric momentum fluxes are still anomalously poleward across 50° latitude, and the surface zonal flow is still anomalously easterly along ~40° and westerly along ~60° latitude (see also Table 3.4). However, when the center of the heating is lifted by 50 hPa (row c), the barotropic component of the response largely vanishes.

The results in Fig. 3.4 therefore suggest that the tropospheric eddy-driven response is a strong function of the amplitude of the cooling in the lowermost stratosphere. This implies that the tropospheric eddy-driven response is robust only when the zonal wind anomalies associated with the direct (zonal-mean balanced) response project onto the tropospheric momentum fluxes. Thus the results in Fig. 3.4 provide a measure of support for the hypothesis outlined in Chen and Held [2007], i.e., that the phase speeds of the eddy fluxes at the tropopause level are directly affected by the strength of the zonal-flow there. We will discuss the implications of the results in Fig. 3.4 for stratosphere/troposphere coupling in more detail in Section 3.5.

The sensitivity of the tropospheric response to polar stratospheric cooling is investigated further in Figure 3.5. We again examine the effect of lifting the cooling, but in this case the depth of the cooling is only  $\sim 100$  hPa. Row (a) shows results for shallow cooling centered at 200 hPa. The structure of the response is largely unchanged from that shown in the top of Figure 3.4, albeit the amplitude of the response is weaker. Note that the increased heat fluxes in the polar stratosphere are confined to the levels where cooling

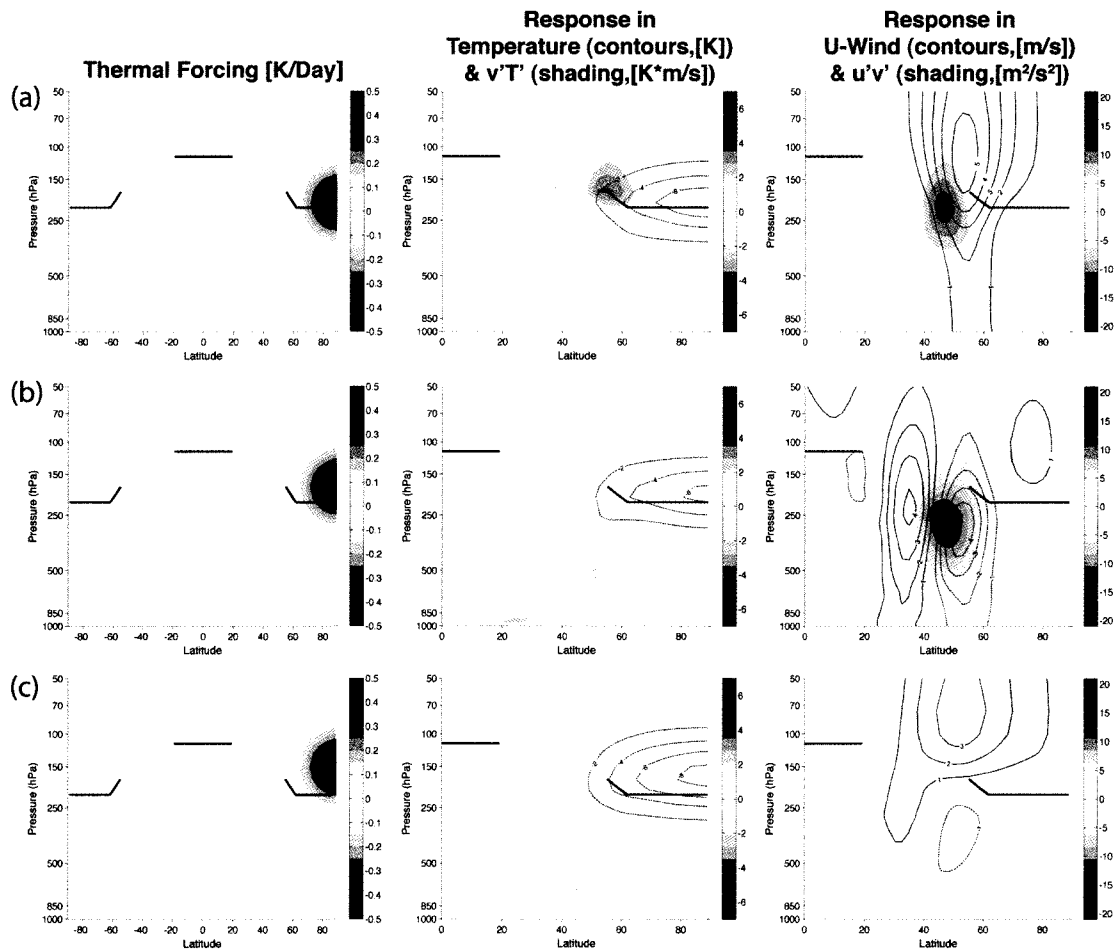


**Figure 3.5.** As in Fig. 3.4, but for the responses to the polar stratospheric thermal forcings shown in the left column. The forcings are documented in Table 3.1 and are centered at 200 hPa (a), 175 hPa (b) and 150 hPa (c).

is occurring (row a, middle panel). Rows (b) and (c) show results for the same shallow cooling, but in these cases the cooling has been lifted by 25 hPa (row b) and 50 hPa (row c). Lifting the cooling has little effect on the changes in polar stratospheric temperatures (middle column), but has a dramatic effect on the changes in the tropospheric circulation (right column). When the cooling is lifted by 25 hPa to 175 hPa (row b), the tropospheric response changes sign: the momentum fluxes are anomalously equatorward and the model jet is shifted equatorward (the equatorward momentum fluxes are statistically significant; Table 3.4). When the cooling is lifted by 50 hPa to 150 hPa (row c), the tropospheric response is negligible. Note that in all cases, the vertical shear of the zonal flow is westerly in the upper troposphere along  $60^\circ$  latitude (as required by thermal wind): in rows (a) and (c) the shear is associated with increasing westerly anomalies with height; in row (b) it is associated with weakening easterly anomalies with height.

### **3.3 Warming at the Polar Surface**

The third forcing we examine is zonally-symmetric heating at the surface over the pole, i.e., the region predicted to warm most dramatically over the next century due to the ice/albedo feedback over the Arctic. The heating is detailed in Table 3.1, and the structure of the heating and the corresponding responses are shown in Figure 3.6. A temperature increase of  $\sim 4\text{K}$  occurs at the polar surface (middle column). The tropospheric circulation response (right column) is dominated by anomalously equatorward momentum fluxes across  $\sim 40^\circ$  latitude, anomalously weak eddy heat fluxes at  $\sim 50^\circ$  latitude, and marked significant barotropic wind anomalies at  $\sim 55^\circ$  latitude and

~35° latitude. The changes in the momentum fluxes and zonal flow are statistically significant (Table 3.4) and project strongly onto the negative polarity of the model annular mode (Figure 3.3, right column). Hence the GCM response to shallow polar warming is consistent with an equatorward shift in the model jet, and is reminiscent of the midwinter response of the annular mode to predicted sea-ice trends in fully coupled GCMs [Deser et al. 2009].

The annular mode response to polar warming is thus in the opposite sense of the response to tropical tropospheric warming. The shallow polar heating does not directly perturb the flow in the upper troposphere, but likely does so by shifting the region of largest baroclinicity (and thus wave generation) in the lower troposphere equatorward. The mechanisms that likely underlie the response are discussed in section 4.5 and the Conclusions.

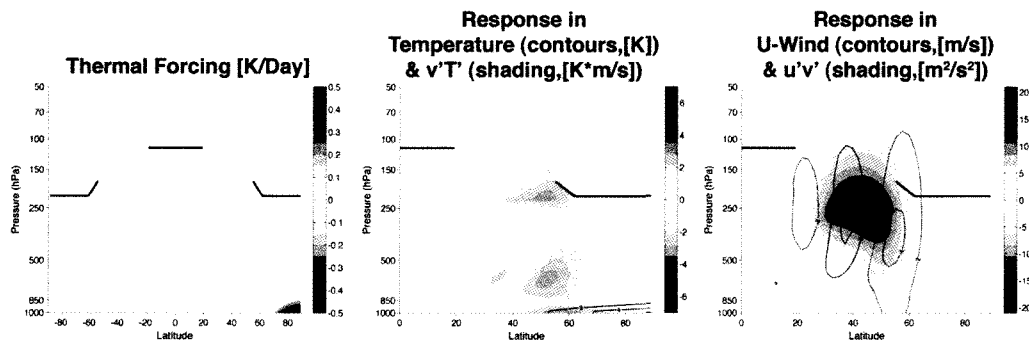


**Figure 3.6.** As in Fig. 3.1, but for the responses to the polar surface thermal forcing shown in the left panel.

### 3.4 Combined Response to all Three Thermal Forcings

In this experiment we examine the combined response to multiple forcings, and then compare the results with the sum of the responses to the individual forcings. We

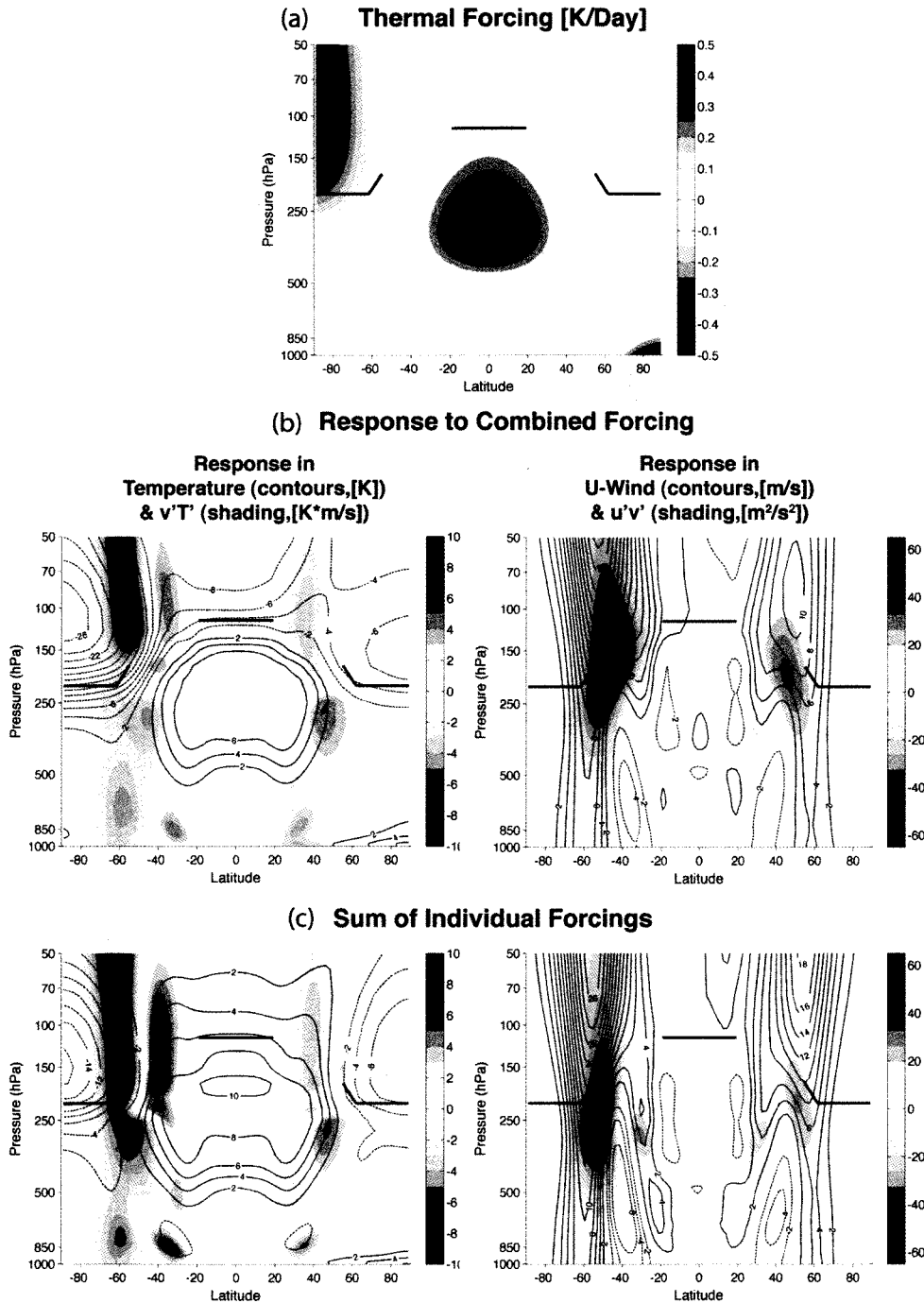


**Figure 3.7.** (a) The combined forcing. (b) The responses to the combined forcing (results are organized as in the middle and right panels of Fig. 3.1). (c) The linear sum of the responses from Figures 3.1a, 3.4a, and 3.6, where the responses in Fig. 3.4a are applied only to the Southern Hemisphere and the responses in Fig. 3.6 are applied only to the Northern Hemisphere. See text for details. Note that the shading scale is greater than that in Figure 3.1a.

consider three principal thermal forcings: the tropical tropospheric heating from Fig. 3.1a; the polar stratospheric cooling from Fig. 3.4a; and the polar surface warming from Fig. 3.6. The stratospheric cooling is limited to the SH to represent hemispheric asymmetries in ozone depletion; the polar surface warming is limited to the NH to represent hemispheric asymmetries in polar climate change. The combined forcing is shown in the top panel in Fig. 3.7; the responses to the combined forcing are shown in row (b); and the sums of the individual responses to the three forcings are shown in row (c); note that row (c) shows the sums of the response from Fig. 3.1a, Fig. 3.4a (applied to the SH), and Fig. 3.6 (applied to the NH).

The results in Fig. 3.7 confirm that the effects on the annular modes of tropical

Heat run	Eddy momentum flux response 250mb, 45-55° (Difference [m <sup>2</sup> /s <sup>2</sup> ], significance)	Surface U response, 55-65° (Difference [m/s], significance)	Eddy heat flux response, 100mb, 0-90° (Difference [K m/s], significance)
Fig 3.1a	33.2, >99%	4.98, >99%	-0.87, >99%
Fig 3.1b	26.7, >99%	3.96, >99%	-0.65, >99%
Fig 3.1c	17.2, >99%	2.39, >99%	-0.49, >99%
Fig 3.1d	16.3, >99%	1.76, >99%	-0.22, >95%
Fig 3.4a	12.8, >99%	2.67, >99%	0.43, >99%
Fig 3.4b	7.71, >99%	1.68, >99%	0.35, >99%
Fig 3.4c	-5.55, >99%	-0.83, >99%	0.02, NS
Fig 3.5a	10.0, >99%	1.28, >99%	-0.03, NS
Fig 3.5b	-10.5, >99%	-1.25, >99%	0.32, >99%
Fig 3.5c	-0.38, NS	0.02, NS	-0.01, NS
Fig 3.6	-13.7, >99%	-1.83, >99%	-0.01, NS
Fig 3.7	NH: 27.1, >99% SH: -41.8, >99%	NH: 3.96, >99% SH: 6.90, >99%	NH: -0.78, >99% SH: -0.64, >99%

**Table 3.4.** Mean eddy momentum flux response [m<sup>2</sup>/s<sup>2</sup>], zonal wind response [m/s], and eddy heat flux response [K m/s] at given levels and latitude bands for the specified heating run; and the significance given by the 2-tailed *t*-test for the difference between means. NS= not significant (<90% significance).

tropospheric and polar surface warming are in the opposite sense. Thus the simulated response of the annular mode to tropical tropospheric warming is mitigated in the Northern Hemisphere by Arctic warming, and this mitigation may provide an explanation for the relatively weak NH annular mode trends found in several climate change simulations [e.g., Miller et al. 2006]. More surprisingly, the results in Fig. 3.7 highlight an unexpected degree of nonlinearity in the response to multiple thermal forcings. The response to the combined forcings (Fig. 3.7 row b) is structurally similar but has very different amplitude than the sum of the individual responses (Fig. 3.7 row c), particularly in the SH. The most pronounced differences between the combined responses (row b) and the sum of the individual responses (row c) include larger cooling in the SH and tropical stratosphere in the combined response (compare the left panels in rows b and c), but larger momentum flux and thus barotropic westerly wind anomalies in the summed responses (compare the right panels in rows b and c). Thus the response to thermal forcing is highly nonlinear, and the response to a single forcing depends critically on the other forcings in the system.

We performed one additional experiment to test the effect of land-sea contrasts. IPCC-class simulations suggest that larger surface warming will occur over land regions than ocean regions due to the greater heat capacity of the oceans, and little research has been done to see how these land-sea contrasts in heating might affect the atmospheric circulation response. Greater land-sea contrasts should drive stronger planetary wave forcing. We impose a wave number 2 thermal forcing centered at  $50^\circ$  latitude at the surface with alternating heating and cooling every  $90^\circ$  longitude in order to roughly simulate the effects of land-sea temperature contrasts. The zonal-mean thermal forcing is

zero at every latitude. The response of the zonal-mean zonal winds, as well as the change in eddy momentum flux, is negligible (not shown). While this forcing should enable stationary planetary wave forcing, the effect is evidently small.

### **3.5 Summary of Steady-State Experiment Results**

In this study we examined the structure and robustness of the simple GCM response to three thermal forcings commonly associated with anthropogenic climate change: warming in the tropical troposphere; enhanced cooling in the polar stratosphere; and enhanced warming at the polar surface. We also documented the nonlinearity of the response to the forcings imposed concurrently and separately. The results highlight several novel aspects of the GCM response to thermal forcing.

First, the results reveal that heating in the tropical troposphere drives a robust poleward contraction of the extratropical storm track that projects strongly onto the positive polarity of the model annular mode. Similar changes in the annular modes are found in fully coupled climate models forced by increasing CO<sub>2</sub> [Fyfe et al. 1999; Kushner et al. 2001; Yin 2005; Miller et al. 2006; Arblaster and Meehl 2006; Lu et al. 2008], and Chen and Held [2007] and Lu et al. [2008] have argued that the tropical warming found in such simulations plays a key role in driving the storm tracks poleward. But as far as we know, the results shown here are the first to explicitly demonstrate a direct relationship between tropical heating and the annular modes in the dry dynamical core of a GCM. The results suggest that tropical heating plays a central role in driving

the simulated trends in the annular modes in IPCC-class climate change simulations [e.g., Miller et al. 2006; Hegerl, Zwiers et al. 2007].

Second, the results suggest that heating in the tropical troposphere is also associated with a decreased flux of wave activity into the model stratosphere and hence a weakening of the model Brewer-Dobson circulation. The weakening is evidenced as changes in both the temperature field and the hemispherically-averaged poleward heat flux in the model stratosphere, and is robust to changes in the shape of the forcing. The changes in the Brewer-Dobson circulation associated with tropical heating are surprising since they are in the opposite sense of those found in previous climate change simulations; for example, Rind et al. [1998], Butchart and Scaife [2001], and Li et al. [2008] note a strengthening of the Brewer-Dobson circulation in response to increasing greenhouse gases, and Eichelberger and Hartmann [2005] reveal a strengthening of the Brewer-Dobson circulation in response to prescribed tropical tropospheric heating.

Third, the results confirm previous findings that diabatic cooling in the polar stratosphere is associated with a positive bias in the model annular mode, as noted previously in Polvani and Kushner [2002] and Kushner and Polvani [2004]. But the results shown here also highlight the sensitivity of the tropospheric response to the scale and level of the forcing. When the cooling extends throughout the depth of the polar stratosphere, the amplitude of the tropospheric response decreases as the lower limit of the cooling is lifted upwards. However, when the cooling is limited to a relatively shallow layer ( $\sim 100$  hPa), the tropospheric response changes dramatically as the cooling is lifted vertically: when the cooling is centered at 200 hPa, the annular mode is shifted towards its positive polarity; when the cooling is centered at 175 hPa, the annular mode is

shifted towards its negative polarity; when the cooling is lifted to 150 hPa, the tropospheric response is negligible.

Fourth, cooling in the polar stratosphere is also associated with a marked increase in heat fluxes in the polar stratosphere, and a hemispherically-averaged increase in wave activity across 100 hPa. Thus polar cooling increases the wave drag in the extratropical stratosphere. Similar increases in stratospheric wave drag have been inferred from observations of stratospheric temperatures and ozone [Thompson and Solomon 2009], and the inferred increases in observed wave driving appear to peak in the SH in association with the Antarctic ozone hole [Fu et al., submitted to J. Climate, 2009].

Fifth, the results reveal that warming at the surface over polar regions is associated with an equatorward contraction of the storm track that also projects onto the model annular mode. The changes in the model annular mode are the same sign as those found during midwinter in coupled climate simulations forced with predicted decreases in Arctic sea-ice [Deser et al., submitted to J. Climate, 2009]. The annular mode response to surface polar warming is in the opposite sense of the annular mode response to tropical tropospheric heating. The results thus suggest that the simulated response of the annular modes to greenhouse warming is likely to be weaker on average in the NH where polar warming is largest.

Finally, the response to the sum of the forcings is structurally similar but quantitatively very different than the sum of the responses to the individual forcings. The nonlinearity of the response to multiple forcings complicates predictions of the circulation response to a given thermal forcing, as the response to a single thermal forcing is a function of the other forcings applied to the system. More generally, the

nonlinearity reveals that the response to a given thermal forcing is a strong function of the configuration of the atmospheric flow.

In the next chapter, we conduct a series of “switch-on” heating experiments that allow us to test in more detail the mechanisms that drive both the stratospheric and tropospheric components of the response.

## CHAPTER 4: TRANSIENT EXPERIMENTS

### 4.1 Mechanisms and the Steady-State Experiments

In Chapter 3, we investigated the steady-state atmospheric circulation response to diabatic heatings designed to mimic three important aspects of the expected climate response to anthropogenic forcing. The principal findings were the following:

1) Under equinoctial conditions, warming in the tropical troposphere drives two robust responses in the extratropical circulation: a poleward shift of the storm tracks congruent with a bias towards the positive polarity of the annular modes, and a weakening of the stratospheric Brewer-Dobson circulation. The former result suggests heating in the tropical troposphere plays a fundamental role in the poleward contraction of the storm tracks found in IPCC-class climate simulations; the latter result is in the opposite sense of that found in most previous climate change experiments.

2) Cooling in the polar stratosphere also shifts the storm tracks poleward, as noted in previous studies. But the tropospheric response is shown to be very sensitive to the level of the forcing: when the cooling is largest below the model tropopause, the annular mode is shifted towards its positive polarity; when the cooling is largest just above the tropopause, the annular mode is shifted in the opposite sense; when the cooling is lifted  $\sim 50$  hPa above the tropopause, the tropospheric response is negligible.

3) Warming at the polar surface is associated with an equatorward shift in the storm tracks. The tropospheric circulation response to polar warming is in the opposite sense of the response to tropical tropospheric heating, so the results suggest that the net tropospheric circulation response to future climate change may be weaker in the Northern Hemisphere because polar warming is largest there.

4) The combined response to all three thermal forcings is quantitatively different from the sum of the responses to the individual forcings. Thus the response of the GCM to a given thermal forcing is a function of the other thermal forcings applied to the model.

What physical processes drive the steady-state responses found in this study? In this chapter we will examine the mechanisms behind two of the major circulation responses to thermal forcings: the shift in the tropospheric storm track and the changes in the stratospheric Brewer-Dobson circulation. As discussed in Chapter 1.5 and 1.6, several mechanisms have been proposed as relevant for understanding the tropospheric storm track response to climate change, and can be organized into two broad categories:

- a. The atmospheric circulation response is driven predominantly by changes in the meridional temperature gradient. Major mechanisms include:
  - An increase in the upper-level temperature gradient enhances the eastward lower-stratospheric winds, which increases the eastward phase speeds of the eddies. Waves with faster phase speeds break further poleward, shifting the eddy fluxes and thus the storm tracks poleward and ultimately changing the location of eddy generation [Chen and Held 2007, Chen et al. 2007].
  - An increase of the lower tropospheric temperature gradient reduces baroclinicity at the surface, weakening and/or shifting the location of eddy

generation and thus the storm track equatorward [Yin 2005; Lorenz and DeWeaver 2007].

- b. The atmospheric circulation response is driven predominantly by changes in the vertical temperature gradient. Major mechanisms include:
- An increase in tropical and mid-latitude static stability in the troposphere reduces baroclinic eddy generation on the equatorward side of the storm tracks and thus shifts the eddy activity poleward [Frierson 2008; Lu et al., 2008].
  - A raised tropopause height drives a deeper baroclinic zone in the troposphere, which offers more available potential energy to be used by baroclinic waves. Where the tropopause is sloped, a higher tropopause height could drive an upward and poleward shift in the baroclinicity and an associated shift in the tropospheric circulation [Lorenz and DeWeaver 2007; Yin 2005].

All these mechanisms may prove relevant to some degree. But the mechanism described by Chen and Held [2007] and Chen et al. [2007] provides in our view the simplest and most consistent explanation for the changes in the model troposphere simulated in the steady-state experiments.

As discussed in Chapter 1.5 and summarized in Fig. 1.4, the hypothesis suggests the following causal linkages between heating in the tropical troposphere and the extratropical storm track: 1) the zonal-mean balanced response to the tropical heating induces westerly flow in the vicinity of the wave fluxes in the upper troposphere; 2) the enhanced westerly flow increases the eastward phase speeds of the wave fluxes; 3) the increased phase speeds draw the latitude of maximum wave breaking poleward in the

subtropics; 4) the anomalously poleward wave breaking drives thermally damped meridional circulation anomalies that enhance the lower tropospheric baroclinicity in middle latitudes; and 5) the enhanced lower tropospheric baroclinicity draws the region of largest wave generation and hence heat fluxes poleward. That the response of the extratropical storm track is reduced when the tropical heating is confined to the deep tropics is consistent with the above reasoning, i.e., the direct response to the narrower heating is associated with weaker westerly wind anomalies in the upper troposphere at middle latitudes.

Further support for this theory is found in Figure 4.1, in which we show the control climatology (shading) and the response (contours) of the 250 hPa eddy momentum flux convergence as a function of phase speed for the tropical heating run, as well as the time-mean zonal wind for the control (black line) and the forced (red line) runs (as in Chen and Held [2007]; this calculation is described in Chapter 2.2). In the control run (shading), eddy momentum flux convergence occurs from  $\sim 40\text{-}60^\circ$  latitude in each hemisphere, while divergence occurs from  $\sim 20\text{-}40^\circ$  latitude. Most of the eddies converging/diverging at this level have phase speeds of  $\sim 5\text{-}10$  m/s. The time-averaged zonal-mean zonal wind (black line) is representative of the latitude beyond which eddies cannot propagate in the subtropics.

The response to the tropical heating run (contours) includes a poleward shift of the eddy momentum flux convergence, as we have seen in Chapter 3, but also a shift toward faster eastward-propagating eddies with phase speeds  $\sim 10\text{-}15$  m/s. Note that the critical latitude in the subtropics, as represented by the forced zonal-mean zonal wind (red line), does not change much between the control run and the heating run. Most of

the zonal wind increases at this level occur on the poleward side of the mid-latitude jets. Thus, the poleward shift in the eddy momentum fluxes cannot be attributed to a shift in the subtropical critical latitude but rather to an inability of the faster eddies to propagate as far equatorward. This agrees well with changes seen in both observations and complex models [Chen and Held 2007; Lu et al. 2008].

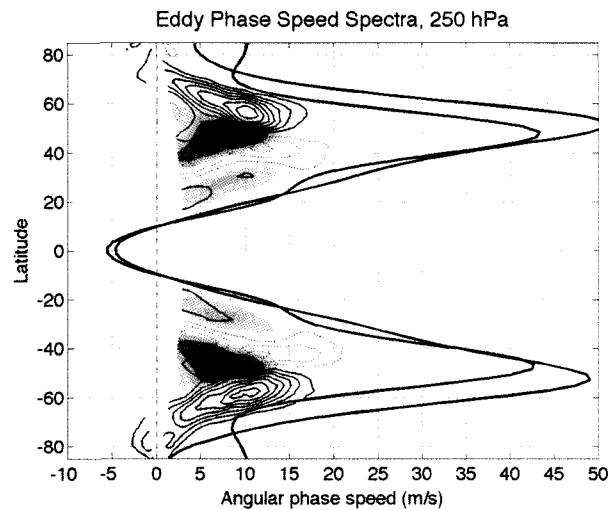


**Figure 4.1.** The long-term mean control run (shaded) and response (contours) of the eddy momentum flux convergence (red, solid) and divergence (blue, dashed) at 250 hPa as a function of latitude and angular phase speed for the tropical heating run. Positive angular phase speeds represent eastward-propagating waves; negative speeds represent westward-propagating waves. The long-term mean of the zonally-averaged zonal wind at 250 hPa divided by  $\cos \theta$  for the control run (black) and the forced run (red) is also shown. Contour levels are 0.02 m/s/day.

A similar response is expected on the basis of polar stratospheric cooling, since the direct response to the polar cooling also includes enhanced westerly flow in mid- to high latitudes at the tropopause level. Thus as noted in Chen and Held [2007], their mechanism holds - at least qualitatively - for the response to both tropical heating and stratosphere/troposphere coupling. How about the case where the tropospheric response

changes sign as the polar heating is lifted from just below to just above the tropopause (as in Fig. 3.5)? Lorenz and DeWeaver [2007] argue that the height of the tropopause plays a key role in determining the storm track response to thermal forcing. But the implied anomalies in tropopause height in Fig. 3.5 are seemingly inconsistent with forcing of the troposphere by lifting the tropopause. That is, as the cooling is lifted above the tropopause in Fig. 3.5, the tropopause must be pulled upwards. If Lorenz and DeWeaver [2007] are correct, the resulting lifting of the tropopause should induce westerly - not easterly as found - zonal wind anomalies in the troposphere [e.g., Ambaum et al. 2001].

Again, the mechanism outlined in Chen and Held [2007] appears to provide a qualitative explanation for the results. The instantaneous response to the polar cooling is presumably associated with sinking motion over the cooling. The sinking motion drives meridional circulation anomalies that, in turn, drive easterly flow below and equatorward

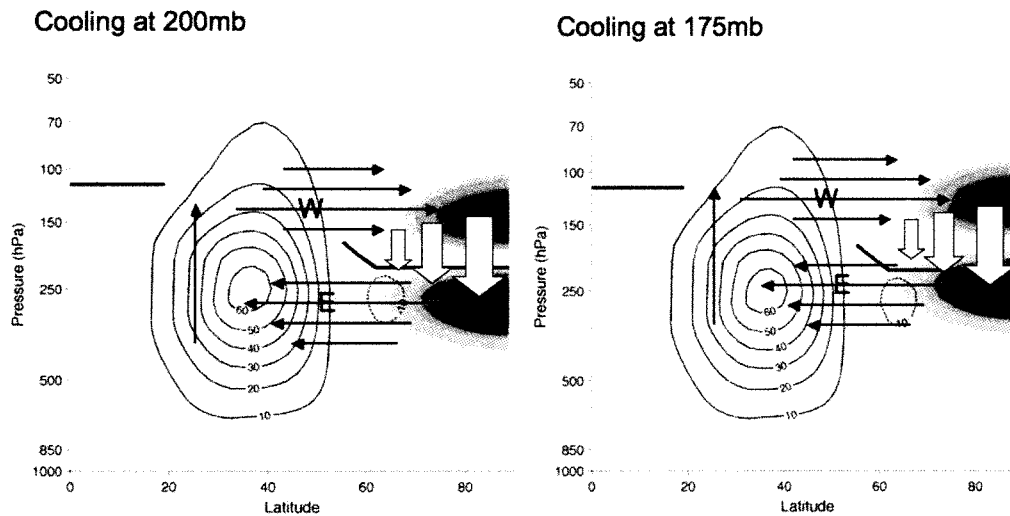


**Figure 4.2.** Schematic of the change in thermal forcing with height ( $dQ/dz$ ) in shading and the climatological eddy momentum fluxes in contours for stratospheric cooling imposed at (left) 200 mb and (right) 175 mb (as in Fig. 3.5 rows (a) and (b)). The white arrows represent the initial sinking motion associated with a cooling, which then drives a meridional circulation shown by the black arrows.

of the cooling maximum and westerly flow above and equatorward of the cooling maximum (i.e., anticyclonic vorticity anomalies below the maximum cooling and cyclonic above; see the schematic in Fig. 4.2). The largest accelerations of the zonal flow should occur at levels where the convergence of the sinking motion is largest. Thus the largest easterly accelerations should occur where the change in the thermal forcing with height ( $dQ/dz$ ) is most negative and the largest westerly accelerations should occur where  $dQ/dz$  is most positive (Fig. 4.2).

Figure 4.3, which shows the vertical profile of the control climatological eddy momentum fluxes and  $dQ/dz$  averaged from 40-90°N for these two cooling experiments, suggests that the sign of the tropospheric response is, indeed, consistent with the overlap between the vertical gradient of the heating (which determines the level where the

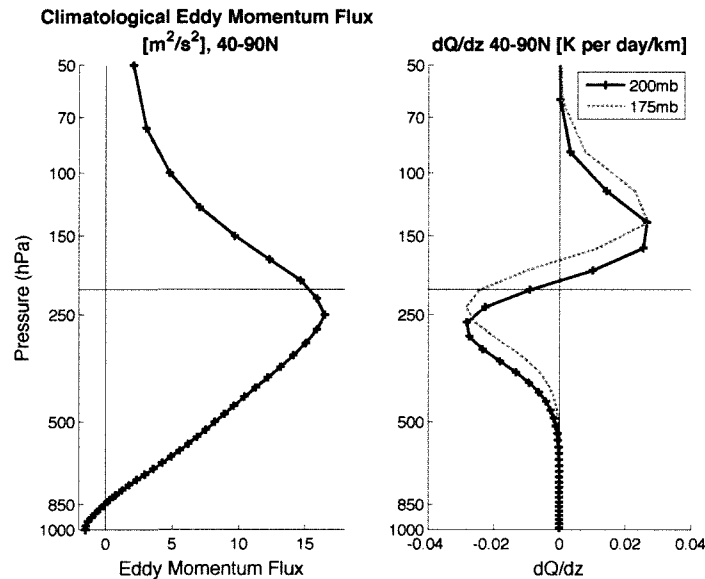


**Figure 4.3.** (left) The control climatological eddy momentum flux averaged from 40-90°N. (right) The change in thermal forcing with height ( $dQ/dz$ ) averaged from 40-90°N for the cooling from Fig. 3.5 centered at 200 mb (solid line) and 175 mb (dashed). The horizontal line in each plot is the polar tropopause height.

instantaneous westerly and easterly accelerations are largest) and the region of largest climatological eddy fluxes. If the largest eddy momentum fluxes are overlain by easterly anomalies, then the tropospheric storm track is shifted equatorwards; if the largest eddy momentum fluxes are overlain by westerly anomalies, then the tropospheric storm track is shifted polewards. The transient simulations can be used to see whether such a mechanism occurs when the thermal forcing is first turned on; in practice, the sinking that follows the cooling may overshoot the ideal location for projection onto the eddy momentum fluxes [Thompson et al. 2006].

Finally, in regards to the polar heating runs, the results are seemingly consistent with moving the largest surface meridional temperature gradient, and hence the latitude of largest eddy generation, poleward. In this case, there is no need to invoke interactions between the mean flow and the momentum fluxes in the free troposphere.

Next we discuss possible mechanisms for the changes in the stratospheric Brewer-Dobson circulation. The weakening of the Brewer-Dobson circulation in our tropical tropospheric heating experiment is associated with reduced heat fluxes in the lowermost subtropical stratosphere and thus reduced vertical wave propagation there (Fig. 3.1; note the weak increases in vertical wave propagation along  $\sim 60^\circ$  latitude are not large enough to overwhelm the subtropical decreases). In contrast, in the polar stratospheric cooling experiment there is a strengthening of the Brewer-Dobson circulation associated with strong increases in the heat fluxes in the mid-latitude stratosphere and thus increases in the vertical wave propagation (Fig. 3.4).

Although most complex general circulation models show an increase in the Brewer-Dobson circulation in response to a doubling of  $\text{CO}_2$ , there is no consensus on

why this increase occurs [Rind et al. 2001; Sigmond et al. 2004; Butchart et al. 2006].

The two most widely cited theories are:

- a. A change in mid-latitude baroclinicity due to tropical tropospheric warming and/or polar stratospheric cooling changes the *generation* of synoptic and planetary wave propagation from the troposphere into the stratosphere, ultimately changing the stratospheric wave drag and thus the Brewer-Dobson circulation [Butchart and Scaife 2001; Rind et al. 2001; Eichelberger and Hartmann 2005].
- b. A change in the lower stratospheric background flow changes the *propagation* of synoptic and planetary waves into the stratosphere, either by refracting waves or allowing them to propagate further [Garcia and Randel 2008; Sigmond and Scinocca 2009].

In our tropical tropospheric warming experiment, we did not find an increase in the Brewer-Dobson circulation but rather a decrease. There are strong increases in tropospheric vertical wave propagation at  $\sim 45^\circ$  latitude and  $\sim 250$  hPa, but these increases only extend weakly into the stratosphere (refer to Fig. 3.1), and at 100 hPa the hemispherically-averaged stratospheric wave drag is reduced overall. Thus although an increase in tropospheric wave propagation seems to occur for certain latitude bands as per theory (*a*), ultimately this theory does not explain the hemispherically-averaged decrease in wave propagation into the stratosphere and thus the reduced Brewer-Dobson circulation in our tropical heating runs. Theory (*a*) may explain the strengthened Brewer-Dobson circulation we observe in the polar stratospheric cooling experiment, although it's not clear if the enhanced stratospheric heat fluxes are a result of greater generation of vertically propagating waves from the troposphere (Fig. 3.4).

In general, theory (*b*) seems more in agreement with our steady-state results. For example, in the polar stratospheric cooling experiments, the region of strongest heat fluxes in the stratosphere tends to follow the region of enhanced westerlies at upper levels, suggesting that more waves can propagate and break in the stratosphere when the westerly winds are enhanced. In the tropical tropospheric warming experiment, it may be that the lower stratospheric winds become strong enough to limit further propagation [e.g., Charney and Drazin 1961], and thus any increases in tropospheric wave generation that occur in the mid-latitudes are reduced in the stratosphere, ultimately weakening the Brewer-Dobson circulation.

## **4.2 Introduction to Transient Runs**

In the rest of the chapter we examine the mechanisms underlying the responses documented in the steady-state experiments of Chapter 3, and focus on testing the theories outlined above. To look at the evolution of how thermal forcings drive changes in the circulation, we must look at the time-dependent or “transient” response to a heating that is turned on instantaneously. In this chapter we focus on the temporal evolution of five of the thermal forcings described in Chapter 3: (1) heating in the tropical upper troposphere (Fig 3.1a), (2) cooling in the lower polar stratosphere (Fig. 3.4a), (3) shallow polar cooling at 200 hPa (Fig. 3.5a), (4) shallow polar cooling at 175 hPa (Fig. 3.5b), and (5) heating at the Arctic surface (Fig. 3.6).

As discussed in Chapter 2, the transient simulations are started from 12 different initial conditions generated from the equilibrium control run. The thermal forcing is

turned on after 10 days, and each run continues for 150 days with output recorded every 6 hours. Ensemble-mean runs are created by averaging the output from the 12 transient simulations. An equivalent ensemble-mean control run is also created using the same initial conditions. This ensemble-mean control run averaged over the 150-day experiment looks nearly identical to the equilibrium control run shown in Figure 2.3.

The number of transient simulations needs to be large enough that the “noise” in each individual simulation is damped sufficiently after averaging with the other simulations to reveal the “signal” in the ensemble-mean. We choose to use 12 transient simulations here partly due to computational constraints, but also because this number appears to be great enough to create an ensemble-mean run with substantially damped variability relative to each individual run. Figure 4.4 shows time series of zonal-mean temperature, zonal wind, eddy momentum flux, and eddy heat flux at specified locations in latitude and pressure for the control run, where the ensemble-mean (heavy line) is the average of the individual simulations (thin lines). The equatorial temperature (Fig. 4.4a) has relatively high signal-to-noise in individual simulations, while the eddy momentum and heat flux time series (c,d) have relatively low signal-to-noise in individual simulations. The variance is greatly reduced in the ensemble-mean, although the variability is not completely damped. For example, the eddy heat flux individual simulation variances range from 13-20  $\text{K}^2\text{m}^2/\text{s}^2$ , but the ensemble mean variance is 1.3  $\text{K}^2\text{m}^2/\text{s}^2$ .

Our goal in sections 4.3-4.6 is to document the transient changes that occur in the

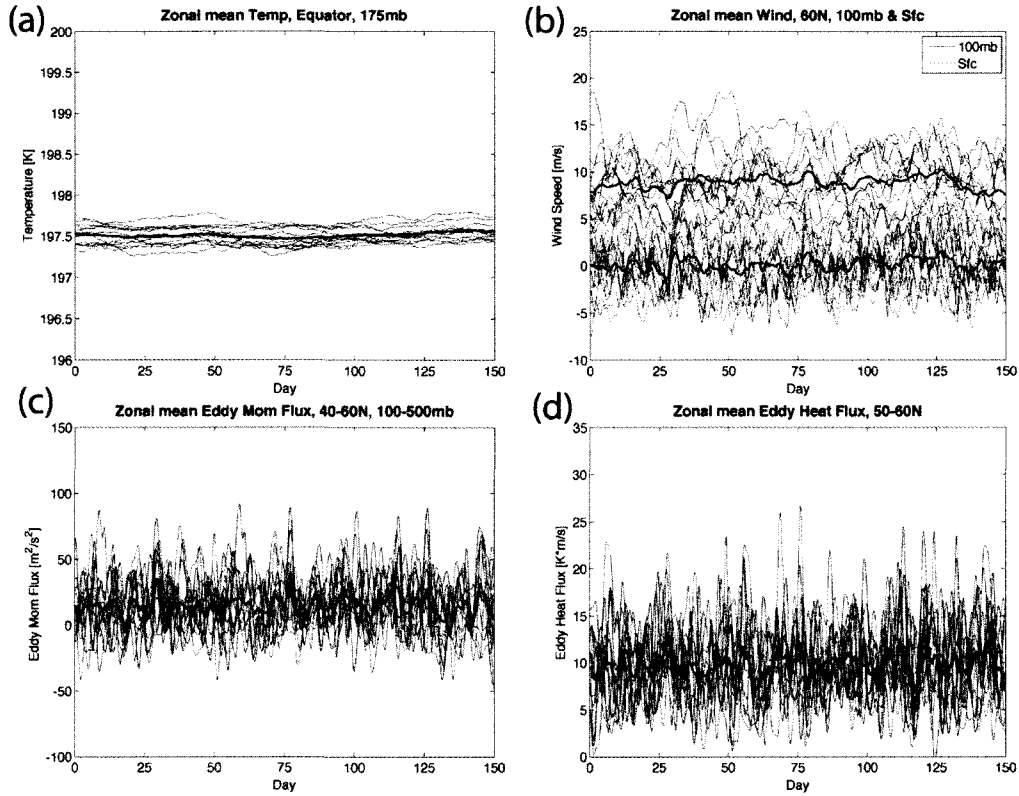


**Figure 4.4.** Time series from the control transient simulation. 12 individual runs shown in thin lines, ensemble-mean run shown in heavy line. (a) Zonal-mean temperature [K] at the equator and 175 hPa. (b) Zonal-mean zonal wind [m/s] at 60°N and 100 hPa (blue) and the surface (red). (c) Zonal-mean eddy momentum flux [ $\text{m}^2/\text{s}^2$ ] cosine-weighted from 40-60°N and 100-500 hPa. (d) Zonal-mean eddy heat flux [ $\text{K}\cdot\text{m}/\text{s}$ ] cosine-weighted from 50-60°N and the whole column.

atmospheric circulation when the key thermal forcings examined in Chapter 3 are turned on, and in section 4.7 to examine the evolution of the changes in the tropical tropospheric heating run in the context of the theories discussed above.

### 4.3 Heating in the Tropical Upper Troposphere

In the first transient experiment we impose the tropical upper tropospheric heating described in Figure 3.1a and Table 3.1. To show how these forced transient simulations

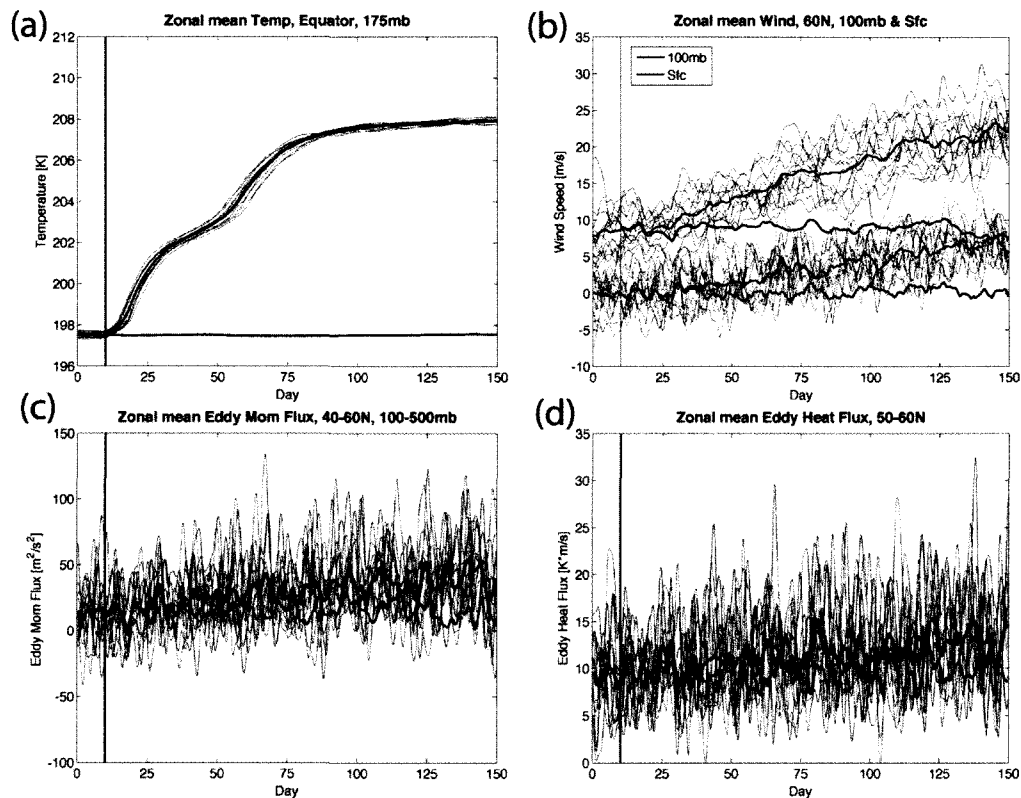


**Figure 4.5.** Time series from the tropical heating transient simulation. 12 individual forced runs shown in thin lines, ensemble-mean run shown in heavy line for both the control and the forced run (the control run stays relatively flat over time). (a) Zonal-mean temperature [K] at the equator and 175 hPa. (b) Zonal-mean zonal wind [m/s] at 60°N and 100 hPa (blue) and the surface (red). (c) Zonal-mean eddy momentum flux [m<sup>2</sup>/s<sup>2</sup>] cosine-weighted from 40-60°N and 100-500 hPa. (d) Zonal-mean eddy heat flux [K\*m/s] cosine-weighted from 50-60°N and the whole column.

compare with the natural variability of the control transient simulations, Figure 4.5 shows the same fields as Fig. 4.4 for the runs forced with tropical heating. One of the most interesting initial observations is that in every forced transient simulation, the temperature at the equator and 175 hPa (Fig. 4.5a) rapidly increases initially, slows down from ~day 30-50, and then rapidly increases again. The temperature essentially stops increasing around day 80, when a new equilibrium is reached. We hypothesize that this secondary

increase in temperature occurs once the forcing drives a weakened Brewer-Dobson circulation, which would enhance the initial perturbation in the tropics. In accordance with this hypothesis, the polar lower stratospheric temperatures decrease from ~day 30-50 (see Fig. 4.19) as the tropical temperature increase flattens, suggesting that the Brewer-Dobson circulation has weakened at that point, further enhancing tropical temperatures until a new equilibrium is reached ~day 80.

---

The zonal winds at 60°N and 100 hPa (Fig. 4.5b, blue lines) quickly rise above the natural variability of the control run ensemble-mean at the same location, and start increasing ~5 days before the zonal wind starts increasing at the surface (Fig. 4.5b, red lines). The eddy momentum fluxes from 40-60°N and 100-500 hPa start increasing at the same time as the zonal winds at 100 hPa, ~day 20 (Fig. 4.5c). Although it is difficult to see in this plot, the eddy heat fluxes from 50-60°N (Fig. 4.5d) start increasing ~1.5-2 days before the eddy momentum fluxes.

We can also look at the response to the forcing (defined as the ensemble-mean forced run minus the ensemble-mean control run) as a function of latitude and time for a given pressure (Figure 4.6). At 100 hPa (Fig. 4.6a), the temperature increases are strongest at subtropical latitudes (which may be due to either adiabatic warming from the anomalous downwelling by the Brewer-Dobson circulation in these regions, or from the shift in the tropospheric jet, as discussed in Chapter 3 [Fu et al. 2006]). By day 80, the temperature at the poles has started to significantly decrease, suggesting that a weakening of the hemispheric-scale Brewer-Dobson circulation has occurred by this point; though weak decreases initially occur ~day 30-50 as mentioned above. The poleward eddy heat

flux response is reduced (suggesting reduced stratospheric wave drag) at subtropical latitudes and enhanced (suggesting enhanced stratospheric wave drag) at mid-latitudes.

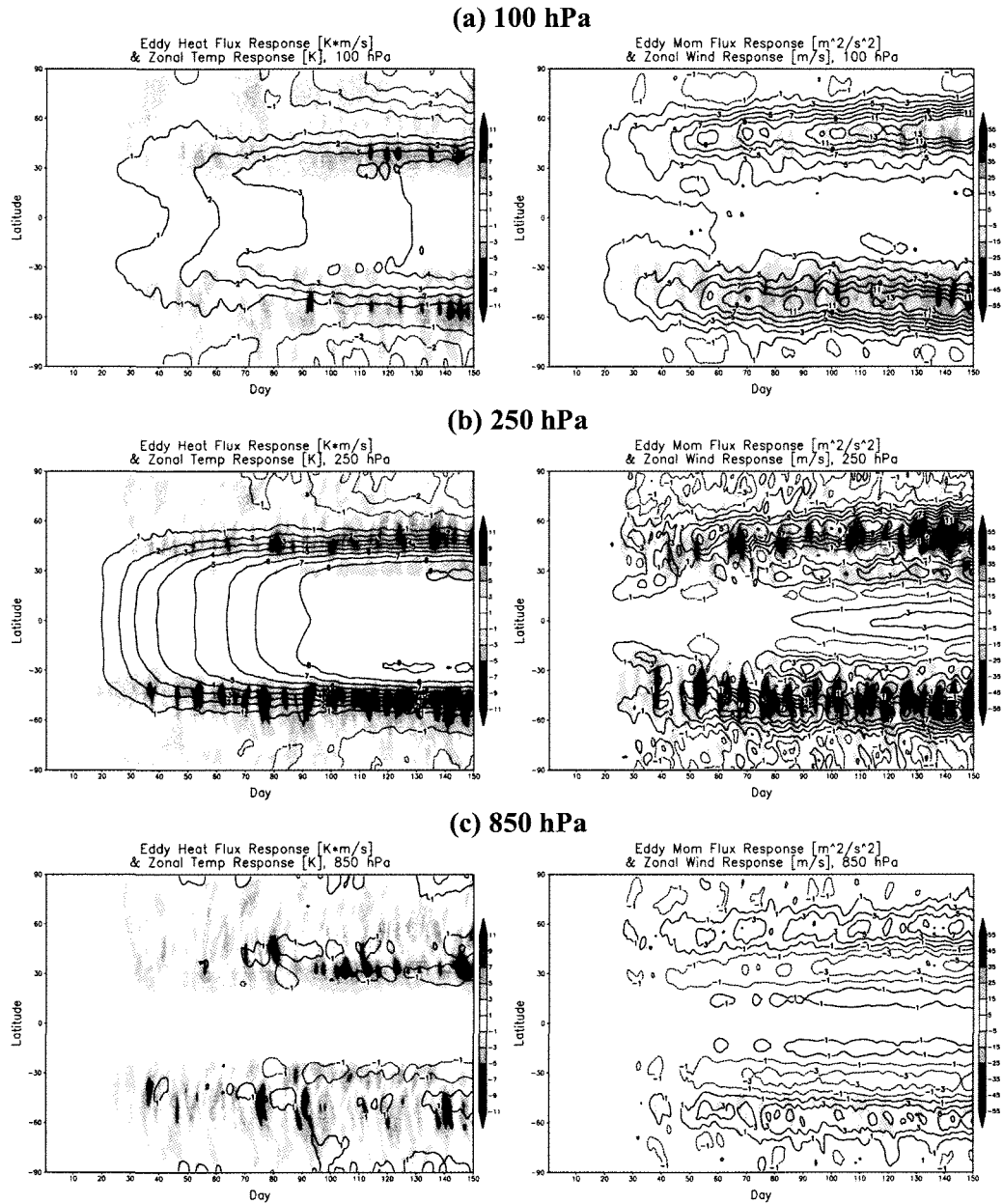


**Figure 4.6.** Time versus latitude contour plots of the response (ensemble forced run minus ensemble control run) for the (left panels) eddy heat flux (shading, [ $\text{K}\cdot\text{m/s}$ ]) and temperature (contours, [K]); and (right panels) eddy momentum flux (shading, [ $\text{m}^2/\text{s}^2$ ]) and zonal wind (contours, [m/s]). 3 different pressure levels are shown: (a) 100 hPa, (b) 250 hPa, and (c) 850 hPa.

Meanwhile, the zonal winds become stronger and the latitude of maximum wind strength moves poleward over time. The wind changes at this level follow the region of greatest temperature gradient, as demanded by thermal wind requirements. The eddy momentum fluxes also increase and move poleward over time, in line with changes in the zonal wind. This collocation suggests that the eddy momentum fluxes are a response, rather than a driver, of changes in the zonal wind in the lower stratosphere, in contrast to the mid-troposphere where the eddies are driving the tropospheric circulation response.

At 250 hPa (Fig. 4.6b), the temperature changes are stronger and more uniform throughout the tropics. Some weak cooling of the polar latitudes at this pressure level can also be seen. The poleward eddy heat fluxes are enhanced in the mid-latitudes, where the temperature gradient changes are the largest, although a thin band of anomalously equatorward eddy heat fluxes forms around day 80 at  $\sim 30^\circ$  latitude. The zonal winds become more westerly in the mid-latitudes, and higher frequency variations in the winds are clearly associated with variations in the eddy momentum flux response (namely, variations in the convergence of eddy momentum flux lead variations in the mid-latitude winds). There is an interesting response in the tropics: anomalous westerlies start forming  $\sim$ day 90 at the equator, flanked by anomalous easterlies at  $\sim 15^\circ$  latitude. Although the tropical westerlies are weak compared to changes in the mid-latitudes, it's possible they represent the equatorial superrotation common in idealized models forced in hemispherically symmetric (equinoctial) conditions [Kraucunas and Hartmann 2005].

In the lower troposphere at 850 hPa (Fig. 4.6c), the temperature changes are small, but the poleward eddy heat fluxes show increases in the mid-latitudes and decreases in the subtropics, suggesting that the region of eddy formation is shifting

poleward with time. The zonal winds show an annular mode-like structure, with enhanced westerlies at  $\sim 50^\circ$  latitude and anomalous easterlies at  $\sim 30^\circ$  latitude; the “node” of this pattern moves poleward with time, representing a shift in the latitudinal position of the mid-latitude jet. At this level there are also anomalous westerlies at  $\sim 15^\circ$  latitude that form around day 80, potentially associated with the Coriolis force acting on a weakened equatorward branch of the Hadley cell circulation. The eddy momentum flux response at 850 hPa is weak.

Slices of the response as a function of time and pressure are shown in Figure 4.7.

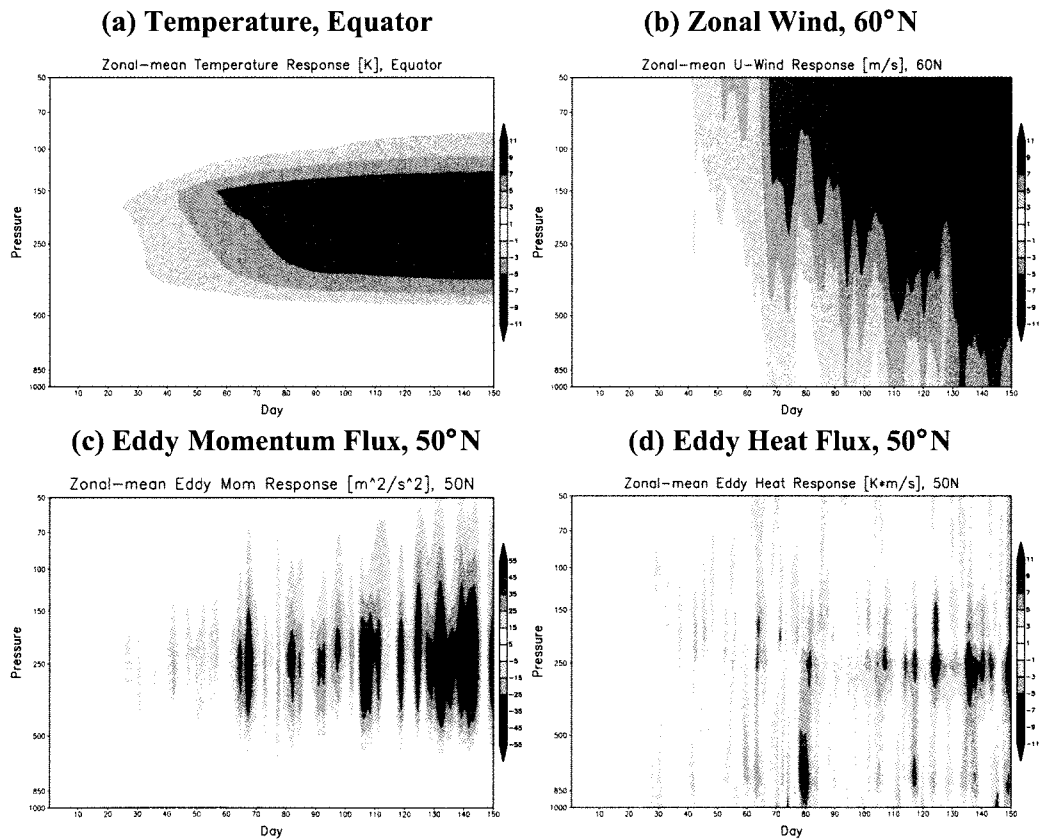


**Figure 4.7.** Time versus pressure contour plots of the response (ensemble forced run minus ensemble control run) for the (a) temperature [K] at the equator; (b) zonal wind [m/s] at  $60^\circ N$ ; (c) eddy momentum flux [ $m^2/s^2$ ] at  $50^\circ N$ ; and (d) eddy heat flux [ $K \cdot m/s$ ] at  $50^\circ N$ .

The strongest temperature response (Fig. 4.7a) remains below the tropical tropopause (~100 hPa) but some heating does occur in the tropical lower stratosphere after ~day 50. The peak heating occurs ~150 hPa even though the forcing is centered at 300 hPa. The zonal wind response at 60°N (Fig. 4.7b) shows the downward propagation of westerly wind anomalies from upper levels to the surface; at 40°N (not shown here), the upper level westerlies are underlain by anomalous easterlies in the troposphere. At 60°N, the fastest downward propagation of westerlies appears to occur following the strongest increases in eddy momentum flux, such as ~day 68, 110, and 130.

Both the poleward eddy momentum fluxes (Fig. 4.7c) and the eddy heat fluxes (Fig. 4.7d) at 50°N increase the most at ~250 hPa. The poleward eddy heat fluxes at 50°N also increase over time at the surface and have higher frequency variability. Changes in the surface eddy heat fluxes tend to slightly lead changes in upper level eddy heat fluxes, and are usually the same sign, as we might expect from a vertically propagating wave (see Fig. 4.17). At least part of the enhancement of the poleward eddy heat flux at ~250 hPa appears independent from changes at the surface; for example, around day 70-80, there are reduced poleward eddy heat fluxes of nearly the same magnitude below and above 250 hPa, but neutral to weakly enhanced eddy heat fluxes at 250 hPa.

#### **4.4 Cooling in the Polar Stratosphere**

The thermal forcing imposed in the second transient experiment is the polar stratospheric cooling described in Table 3.1. As documented in Figure 3.4a, in the

steady-state experiment we observed a poleward shift of the jet and enhanced stratospheric wave driving indicative of a stronger Brewer-Dobson circulation. In the transient experiment, polar temperatures in the lower stratosphere where the forcing is applied decrease by  $\sim 8\text{K}$  in  $\sim 100$  days (Fig. 4.8a). The polar temperatures show much greater high-frequency variability than the temperatures in the tropics (Fig. 4.5a) due to substantial dynamic variability in the polar regions. The zonal winds at  $60^\circ\text{N}$  and 100 hPa increase almost immediately after the forcing is turned on, while the winds at the surface take until  $\sim$ day 30 before they start becoming more westerly (Fig. 4.8b). The time series for the eddy momentum and eddy heat fluxes are not shown here as the

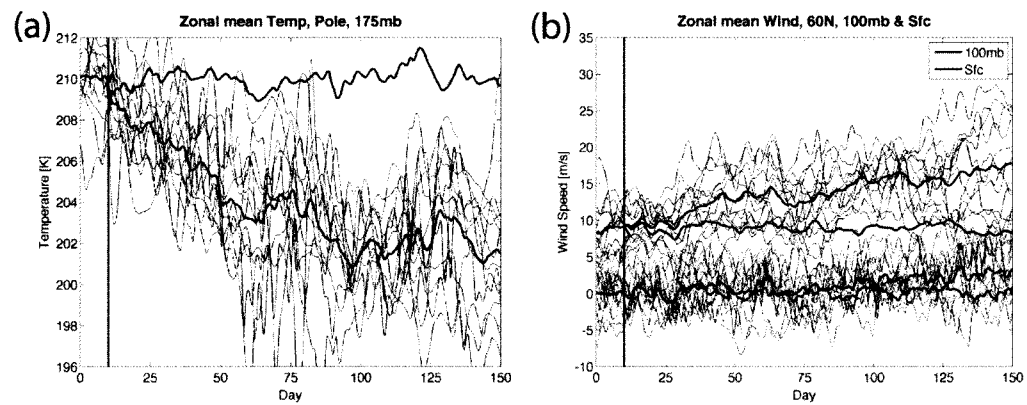


**Figure 4.8.** Time series from the polar cooling transient simulation. 12 individual forced runs shown in thin lines, ensemble-mean run shown in heavy line for both the control and the forced run (the control run stays relatively flat over time). (a) Zonal-mean temperature [K] at the pole and 175 hPa. (b) Zonal-mean zonal wind [m/s] at  $60^\circ\text{N}$  and 100 hPa (blue) and the surface (red).

changes are weaker than in the tropical heating run and are difficult to discern relative to the high natural variability in the time series.

Latitudinal slices of the response to the polar stratospheric cooling are shown in Figure 4.9. For the rest of this chapter we show only the hemisphere where the forcing is

applied. The temperature changes (left panels, black contours) are strongest polewards of  $80^{\circ}\text{N}$  at 100 hPa, and extend to  $\sim 45^{\circ}\text{N}$ . Strong increases in the poleward eddy heat flux

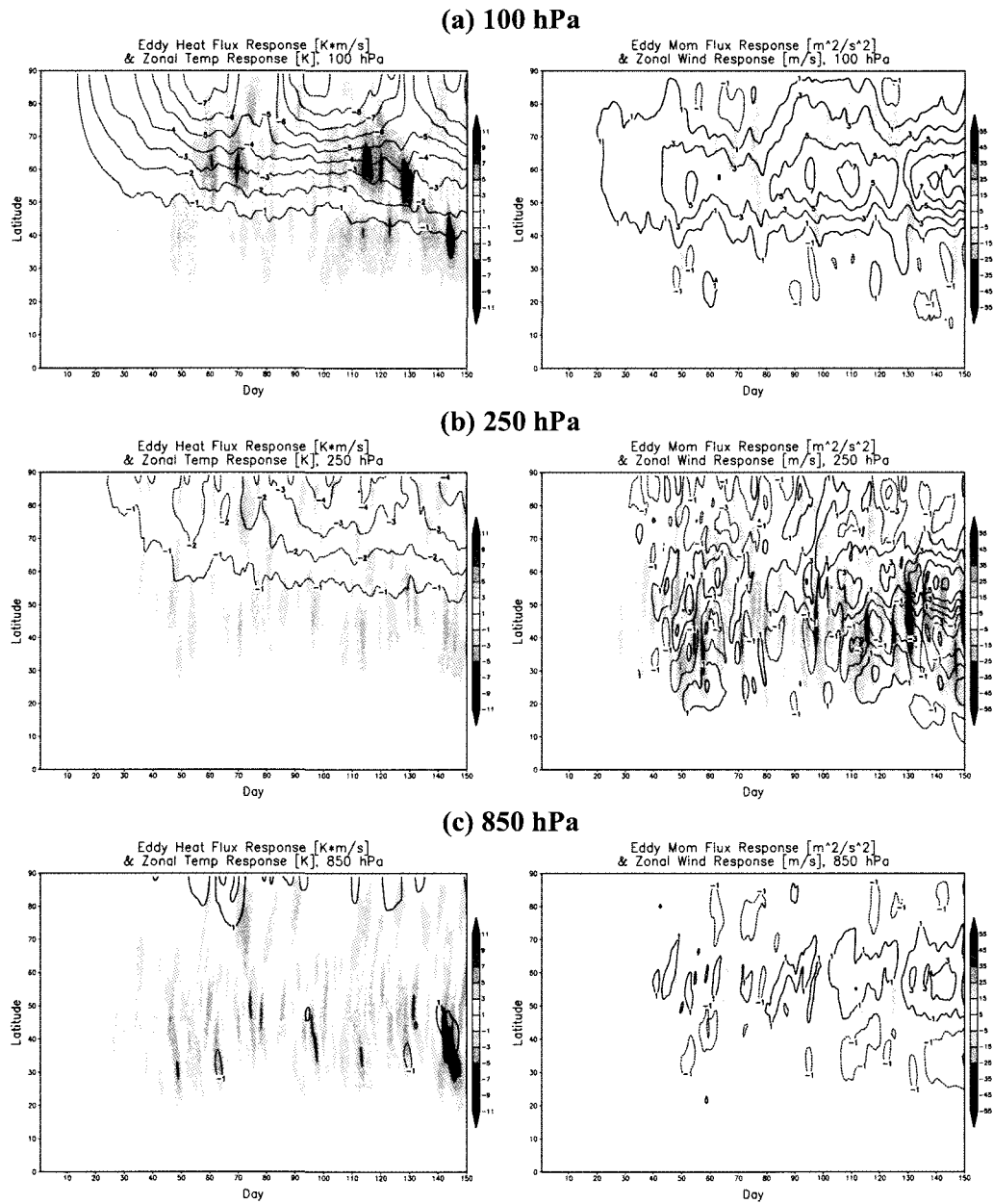


**Figure 4.9.** Time versus latitude contour plots of the response (ensemble forced run minus ensemble control run) for the (left panels) eddy heat flux (shading,  $[\text{K}\cdot\text{m}/\text{s}]$ ) and temperature (contours,  $[\text{K}]$ ); and (right panels) eddy momentum flux (shading,  $[\text{m}^2/\text{s}^2]$ ) and zonal wind (contours,  $[\text{m}/\text{s}]$ ). 3 different pressure levels are shown: (a) 100 hPa, (b) 250 hPa, and (c) 850 hPa.

(left panels, shading), suggestive of enhanced stratospheric wave drag, occur at 100 hPa from 50-70°N. As we expect, the temperature tends to increase (against the forced cooling) following periods of increased poleward eddy heat flux. The eddy heat flux is damped equatorward of 50°N at 100 hPa. At lower levels (Fig. 4.9c), variability in the eddy heat flux response is apparent, but the response does not seem to trend strongly in one direction. The lower-level eddy heat flux response also appears “bow-shaped”, suggesting that changes in the eddy heat fluxes occur first ~40-50°N, where the baroclinicity is the greatest, and then same-signed anomalies follow at both lower and higher latitudes (this is also apparent in Fig. 4.6c). This pattern is likely because the eddy heat fluxes act against the temperature gradient at the surface by transporting heat polewards, but as they transport heat polewards they create new regions of strong baroclinicity both south and north of the original region of strongest baroclinicity.

The zonal winds at upper levels (Fig. 4.9a, right panel, black contours) increase where the strongest increases of meridional temperature gradient occur (~60°N) as required by thermal wind. At lower and mid-levels (Fig. 4.9b,c), the zonal wind changes project onto the annular mode pattern, with enhanced westerlies at ~60°N and anomalous easterlies at ~40°N. Consistent with these circulation changes being eddy-driven, this pattern appears strongest following large changes in the eddy momentum fluxes (right panels, shading). Changes in the eddy momentum fluxes are large at 250 hPa (where the climatological eddy momentum fluxes are the greatest) and fairly small at 850 and 100 hPa.

Pressure versus time “slices” of the response (Figure 4.10) give more clues as to the order of events. The cooling at the pole (Fig. 4.10a) is centered ~125 hPa and does

not generally descend much further past the polar tropopause at  $\sim 225$  hPa. Occasionally the sinking motion that initially accompanies a forcing by a cold anomaly leads to adiabatic warming in the polar troposphere. The enhanced westerlies at  $60^\circ\text{N}$  (Fig.

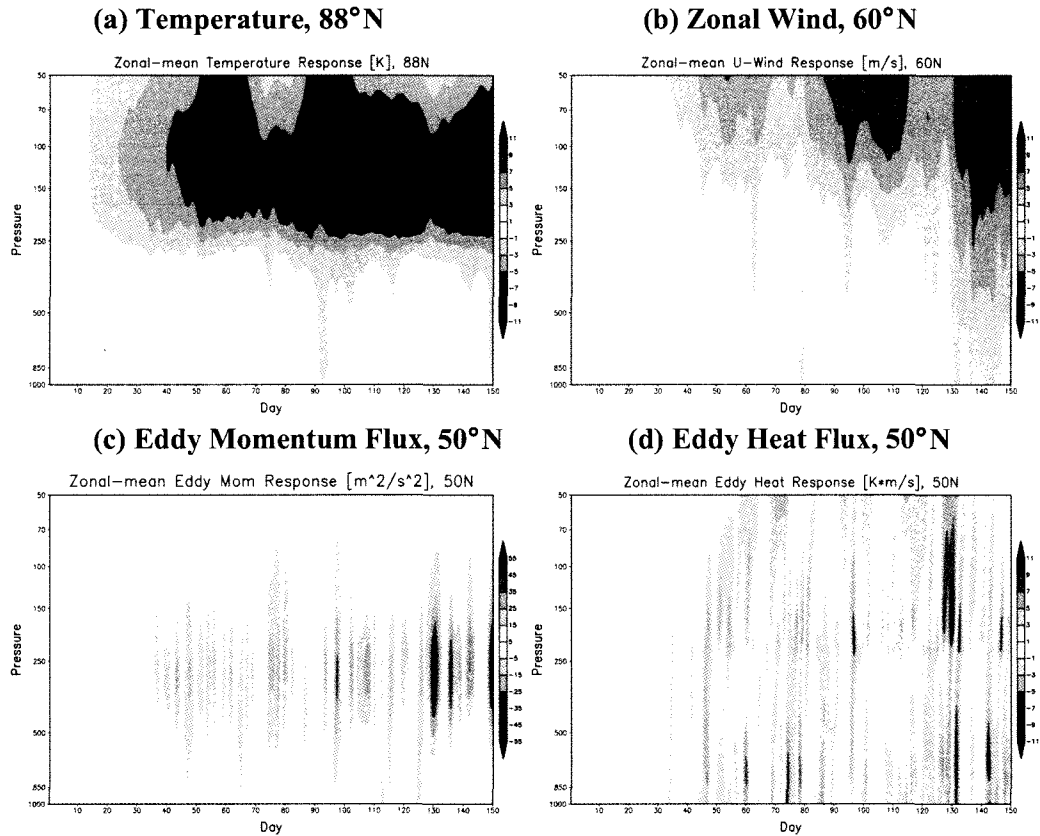


**Figure 4.10.** Time versus pressure contour plots of the response (ensemble forced run minus ensemble control run) for the (a) temperature [K] at  $88^\circ\text{N}$ ; (b) zonal wind [m/s] at  $60^\circ\text{N}$ ; (c) eddy momentum flux [ $\text{m}^2/\text{s}^2$ ] at  $50^\circ\text{N}$ ; and (d) eddy heat flux [ $\text{K}\cdot\text{m}/\text{s}$ ] at  $50^\circ\text{N}$ .

4.10b) propagate downward, and generally descend the fastest and farthest right after large increases in eddy momentum or eddy heat flux. An example of this rapid descension occurs  $\sim$ day 130. In this case, the eddy heat fluxes at the surface appear to increase first, followed by strong upper level increases in the eddy heat flux, increases in eddy momentum flux, and a rapid descension of westerly anomalies from 100 hPa to the

surface within days. The polar cooling is also reduced at this time, presumably due to the enhanced wave breaking which drives a stronger residual circulation, and thus strong sinking and adiabatic warming.

#### **4.5 Shallow Cooling in the Polar Stratosphere- Two Cases**

We next examine the two shallow polar stratospheric cooling cases that yielded such dramatically different tropospheric circulation responses in the steady-state experiments (Fig. 3.5a & b). To summarize, the shallow cooling centered at 200 hPa led to a poleward shift in the mid-latitude jet while the cooling centered only 25 hPa higher at 175 hPa led to an equatorward shift in the jet. These circulation changes were quite robust. Both experiments showed little change in the eddy heat fluxes but robust and opposite-signed changes in the eddy momentum fluxes. Here we compare the responses to these two forcings in the transient simulations.

Figure 4.11 shows the time series of the polar temperature at 175 hPa and the zonal mean winds at 60°N and the surface/100 hPa for the forcing centered at 200 hPa (Fig. 4.11a) and at 175 hPa (Fig. 4.11b). We will refer to these forcings as the low and high forcings, respectively. The temperature response (left panel) is similar in both cases, with cooling on the order of ~7K after 75 days. This amplitude is consistent with the steady-state experiments. However, the zonal winds for both thermal forcings (right panel) show increases at 60°N, rather than increases for low forcing and decreases for the high forcing as observed in the steady-state experiments. The wind changes for the high forcing (row b) do seem weaker than for the low forcing (row a), particularly before ~day

80, but nonetheless the winds increase over time in both scenarios. It's possible that with longer runs or more transient simulations, we would see the circulation differences observed in the steady-state experiments.

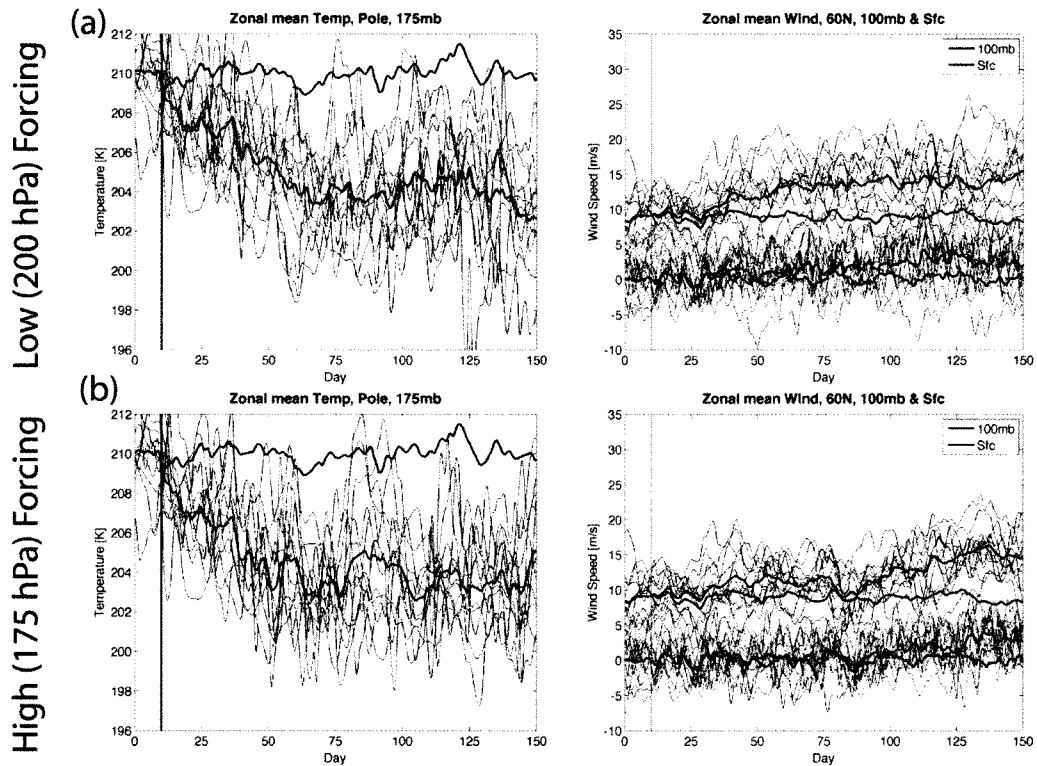


**Figure 4.11.** Time series from the polar cooling transient simulation. 12 individual forced runs shown in thin lines, ensemble-mean run shown in heavy line for both the control and the forced run (the control run stays relatively flat over time). (left panels) Zonal-mean temperature [K] at the pole and 175 hPa. (right panels) Zonal-mean zonal wind [m/s] at 60°N and 100 hPa (blue) and the surface (red). (a) is for forcing at 200 hPa, (b) is for forcing at 175 hPa.

Since the temperature and eddy heat flux changes are similar in both cases, we only examine the zonal wind and eddy momentum fluxes more carefully. Figure 4.12 shows the latitudinal slices of these fields at 3 different levels for both forcings. We can see that at every level, the circulation changes driven by the low forcing (left panels) are

stronger and more robust than the circulation changes driven by the high forcing (right panels). The main circulation changes for the high forcing occur  $\sim$ day 130, when strong

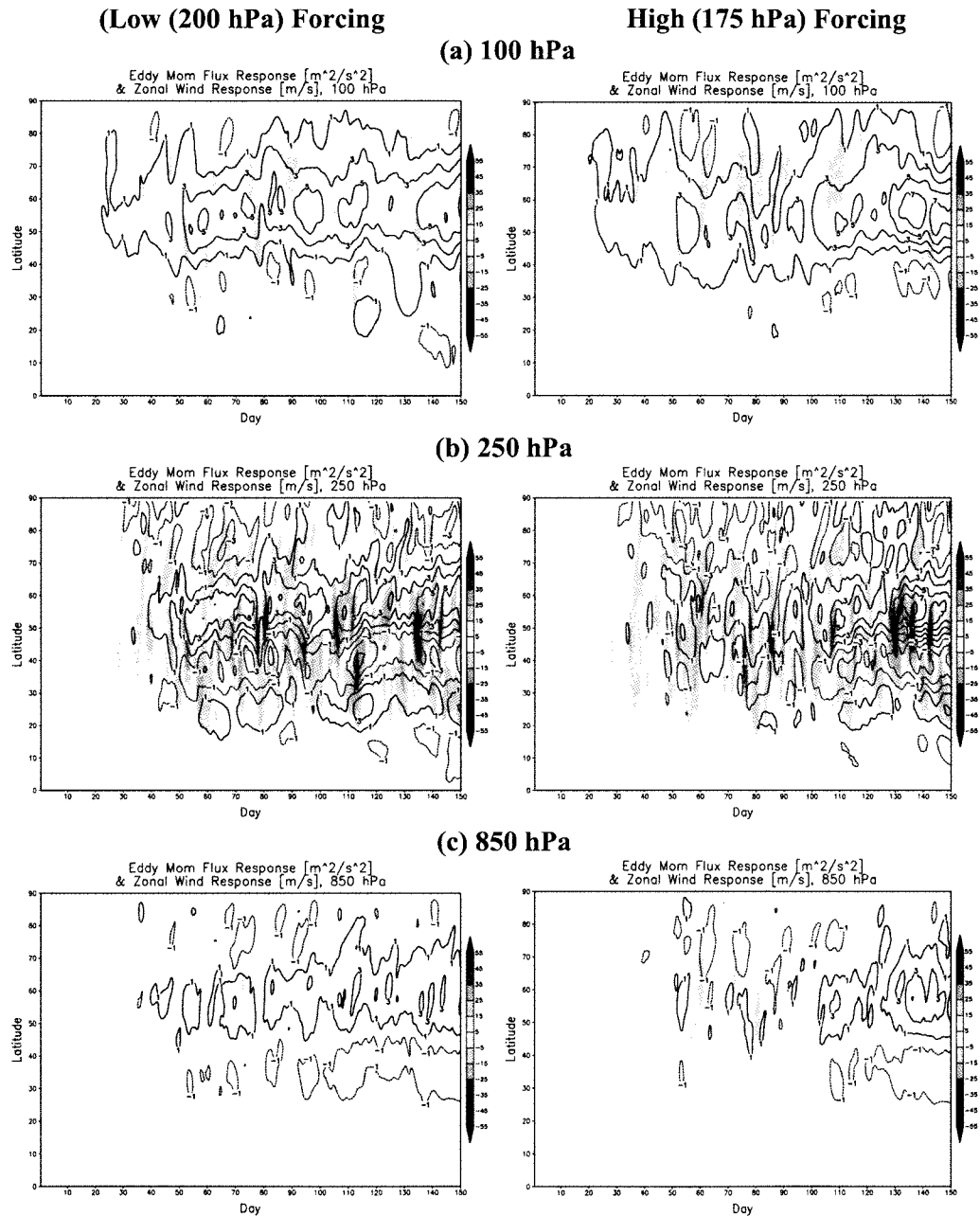


**Figure 4.12.** Time versus latitude contour plots of the response (ensemble forced run minus ensemble control run) for the eddy momentum flux (shading,  $[m^2/s^2]$ ) and zonal wind (contours,  $[m/s]$ ) for (left panels) the forcing at 200 hPa and (right panels) the forcing at 175 hPa. 3 different pressure levels are shown: (a) 100 hPa, (b) 250 hPa, and (c) 850 hPa.

increases in eddy momentum flux at  $\sim 50^\circ\text{N}$  drive a poleward shift in the jet at 250 hPa and 850 hPa. However, the initial response to the high forcing is a general decline in the eddy momentum flux, at least through  $\sim$ day 90. Conversely, increases in the eddy momentum flux and a poleward shift of the jet occur in the low forcing case much earlier,  $\sim$ day 50.

A time versus pressure plot of the polar temperature response (contours) and zonal wind response at  $60^\circ\text{N}$  (shading) is shown in Figure 4.13 for each case. Here the contour levels of the zonal wind response have been adjusted so that small changes occurring near the beginning of the run can be seen. As depicted schematically in Figure 4.2, in both cases we see easterlies below the region of cooling right after the cooling is turned on (before day 20), with the region of easterlies shifting upwards in the high

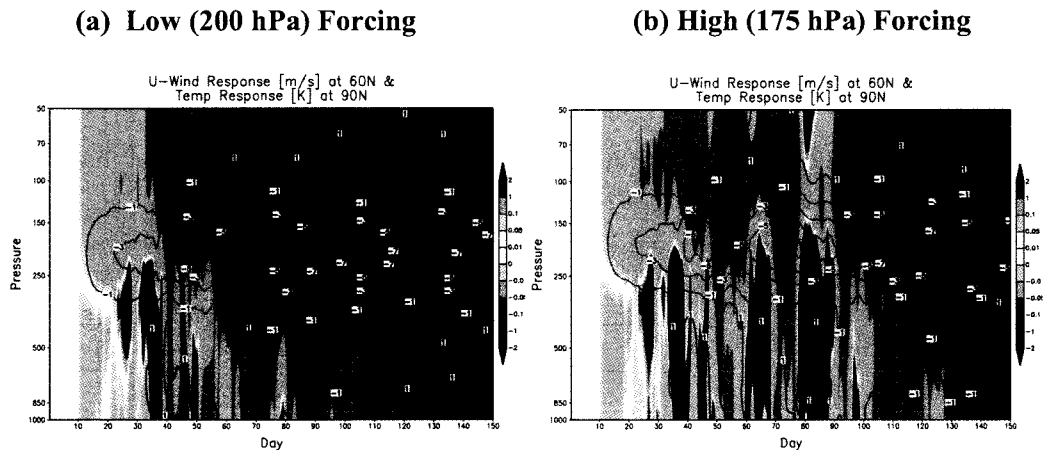


**Figure 4.13.** Time versus pressure contour plots of the response (ensemble forced run minus ensemble control run) of the temperature [K] at  $88^\circ\text{N}$  (contours) and the zonal wind [m/s] at  $60^\circ\text{N}$  (shading). Note: the shaded contour levels are non-linear.

forcing case (note: we show the changes at  $60^\circ\text{N}$  because these wind changes are more likely to project onto the climatological eddy momentum fluxes; but the region of

easterlies below the cooling exists at all latitudes from 60-90°N). However, the region of easterlies extends to the surface and does not just lie in the shallow layer beneath the cooling, likely due to overshooting by the sinking motion. Nonetheless, the vertical shift in where the winds change sign from the low forcing case to the high forcing case right after the forcing begins may contribute to the sign of the subsequent tropospheric circulation changes, as discussed in section 4.1. We can also see that the tropospheric winds at 60°N become westerly early on in the low forcing case, but remain mostly easterly through ~day 90 in the high forcing case.

#### 4.6 Warming at the Polar Surface

The final transient experiment examines the changes that occur when a polar surface heating, as described in Table 3.1 and Figure 3.6, is imposed. The time series of

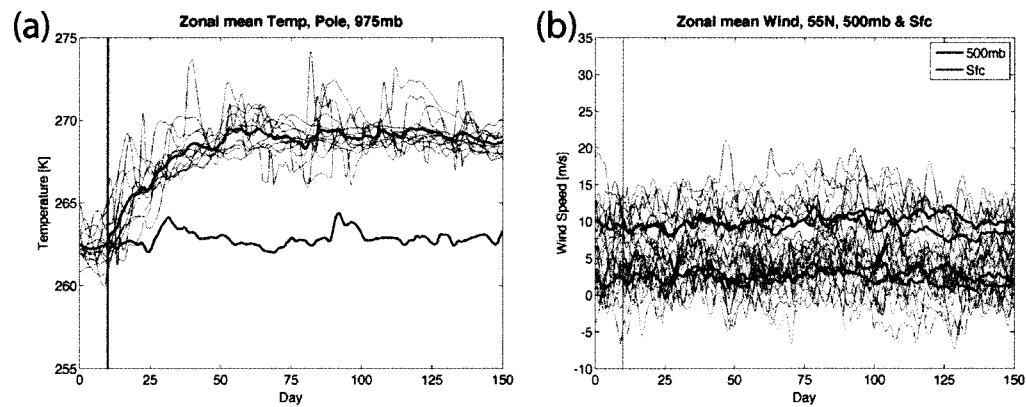


**Figure 4.14.** Time series from the polar surface warming transient simulation. 12 individual forced runs shown in thin lines, ensemble-mean run shown in heavy line for both the control and the forced run (the control run stays relatively flat over time). (a) Zonal-mean temperature [K] at the pole and 975 hPa. (b) Zonal-mean zonal wind [m/s] at 55°N and 500 hPa (blue) and the surface (red).

the polar temperature at 975 hPa and the zonal wind at 55°N and the surface/500 hPa (where the greatest changes occurred in the steady-state experiments) are shown in Figure 4.14. The temperature increases  $\sim 6\text{K}$  over 50 days and then comes to a new equilibrium. The zonal winds at 55°N show fairly small decreases, indicative of a weak equatorward shift in the location of the mid-latitude jet. In contrast to previous forcings which drove circulation changes in the upper levels of the atmosphere first, in this experiment the surface winds change just slightly before the winds aloft.

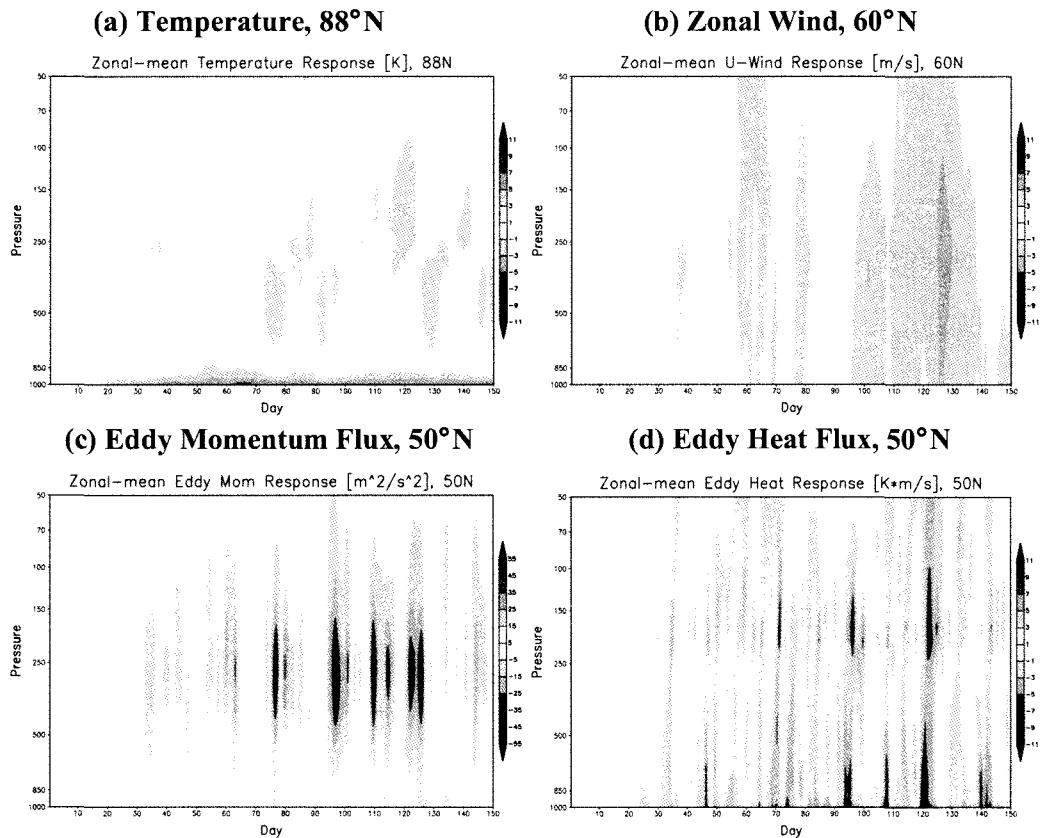


**Figure 4.15.** Time versus pressure contour plots of the response (ensemble forced run minus ensemble control run) for the (a) temperature [K] at 88°N; (b) zonal wind [m/s] at 60°N; (c) eddy momentum flux [m<sup>2</sup>/s<sup>2</sup>] at 50°N; and (d) eddy heat flux [K\*m/s] at 50°N.

Figure 4.15 shows the polar temperature, zonal wind at 60°N, and eddy heat and momentum fluxes at 50°N as a function of time and pressure. The polar temperature changes are strongest right at the surface and generally do not extend above 800 hPa (Fig. 4.15a). The zonal winds at 60°N start to decrease around day 60 (as the zonal winds at 40°N start to increase; not shown), and the weaker winds extend throughout the atmosphere at this latitude (Fig. 4.15b). The eddy momentum and eddy heat fluxes generally decrease after the forcing is turned on (Fig. 4.15c,d). The eddy heat flux response at the surface leads the eddy heat flux response aloft. The substantial amplitude of the negative eddy heat flux response at the surface, particularly right before the largest decreases in the zonal wind, suggest that the reduction in eddy heat flux (and thus the reduction in vertically propagating waves) due to the weakened surface meridional temperature gradient is a key mechanism in the surface warming experiment. The hemispherically-averaged eddy heat flux at 100 hPa is also weakly reduced (not shown), suggesting a small reduction in the stratospheric Brewer-Dobson circulation.

#### **4.7 Testing the Mechanisms**

The two major theories we will test regarding the tropospheric circulation changes in response to the tropical tropospheric heating are: (1) changes in eddy phase speeds [Chen and Held 2007; Chen et al. 2007]; and (2) changes in static stability [Frierson 2008; Lu et al., 2008]. For theory (1), we examine whether the following physical changes occur in this order: 1) an enhanced meridional temperature gradient at upper levels induces westerly flow in the vicinity of the wave fluxes in the upper troposphere;

2) the enhanced westerly flow increases the eastward phase speeds of the wave fluxes; 3) the increased phase speeds shift the latitude of maximum wave breaking poleward in the subtropics; 4) the anomalously poleward wave breaking drives thermally damped meridional circulation anomalies that enhance the lower tropospheric baroclinicity in middle latitudes; and 5) the enhanced lower tropospheric baroclinicity draws the region of largest wave generation and hence heat fluxes poleward.

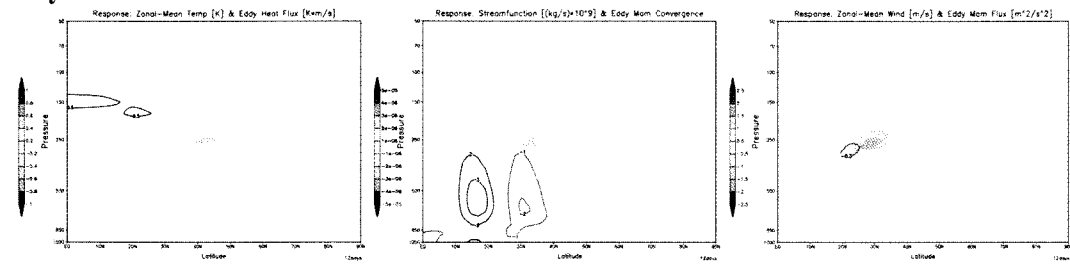
Figure 4.16 documents the 2-day averaged response to the tropical heating run (switched on at day 10) as functions of pressure and latitude. In the tropical heating run, an enhanced meridional temperature gradient and an enhanced westerly flow in the upper troposphere occur nearly simultaneously once the heating is turned on (top two rows of panels, left and right figures; the contour levels chosen here don't reflect the immediate wind changes). We can't calculate the eddy phase speed spectra for the transient simulations (the length of the record is too short to resolve slower-propagating waves). However, if the faster eastward phase speeds shift the latitude of wave breaking poleward in the subtropics, then changes in the subtropical eddy momentum flux divergence should occur before changes in the mid-latitude tropospheric eddy momentum flux convergence and the mid-latitude surface zonal wind. The middle panels of Fig. 4.16 show that the subtropical eddy momentum flux divergence (blue shading) changes almost immediately after the heating is applied on day 10, with the mid-latitude eddy momentum flux convergence (red shading) following a couple of days later (a small region of eddy momentum convergence occurs just equatorward of the region of divergence as well). Also, the lower-level mid-latitude wind (Fig. 4.16, right, contours) increases only after an increase in the upper-level mid-latitude eddy momentum convergence, ~day 20.

### Temp & Eddy Heat

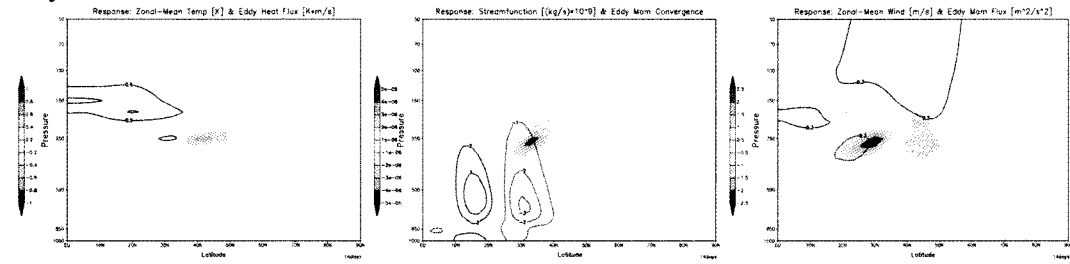
### Streamfunction & Eddy Mom Convergence

### Wind & Eddy Mom

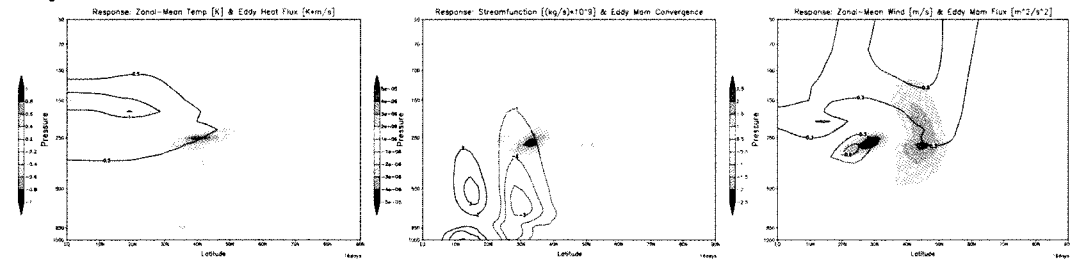
#### Day 12-13



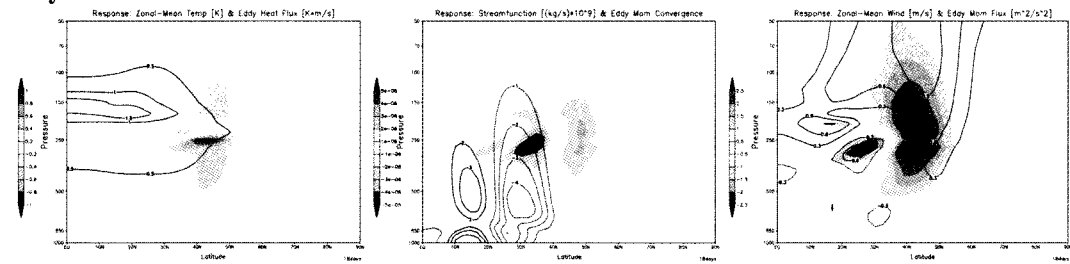
#### Day 14-15



#### Day 16-17



#### Day 18-19



#### Day 20-21

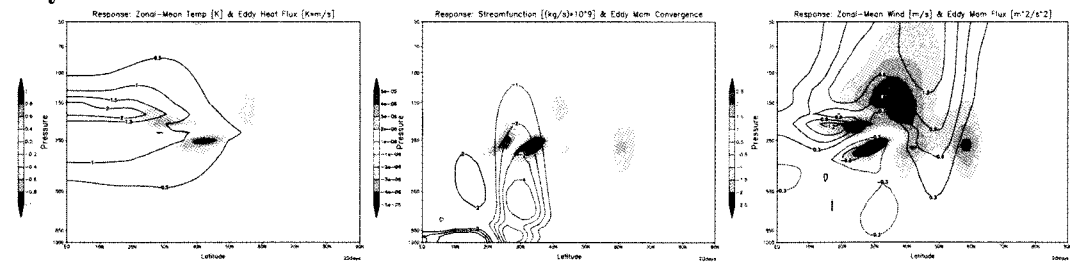


**Figure 4.16** (cont'd from previous page) Pressure versus latitude response averaged over 2-day time periods for: (left) Zonal-mean temperature [K, contours] and eddy heat flux [ $\text{K}\cdot\text{m/s}$ , shading] (middle) Streamfunction [ $(\text{kg/s})\cdot 10^9$ , contours] and eddy momentum flux convergence (shading). Dashed contours represent clockwise circulations. (right) Zonal-mean zonal wind [ $\text{m/s}$ , contours] and eddy momentum flux [ $\text{m}^2/\text{s}^2$ , shading].

---

The region of subtropical eddy momentum flux divergence that forms right after the heating begins then generates an anomalous meridional circulation cell (middle panels, contours) which represents anomalous poleward flow  $\sim 250$  hPa and anomalous equatorward flow near the surface; this circulation will act to reduce the subtropical low-level baroclinicity. Although the mid-latitude eddy momentum flux convergence that grows stronger from days 14-19 doesn't appear to be associated with a substantial anomalous circulation here (the changes are smaller than our chosen contour interval), later time-averages suggest that eventually its associated anomalous meridional circulation cell is comparable in magnitude to its subtropical counterpart, enhancing mid-latitude low-level baroclinicity.

So far these changes are consistent with theory (1), but if we look at other fields, the picture becomes more complex. Fig. 4.16 (left, shading) shows the changes in the eddy heat fluxes. A region of enhanced eddy heat flux in the mid-latitude troposphere appears immediately after the temperatures start to change in the tropics. It's possible this eddy flux increase below 250 hPa is associated with the enhanced mid-latitude baroclinicity discussed in the previous paragraph, but there is no corresponding reduction in eddy heat flux in the subtropics (although a reduction does occur some time later- see Fig. 4.18). The region of largest increase in eddy heat fluxes does correspond to the region of largest increase in the mid-latitude eddy momentum flux (Fig. 4.16, right,

shading). Lag correlations (Figure 4.17(a) and (b)) suggest that changes in the low-level mid-latitude eddy heat fluxes lead changes in both the upper-level eddy heat fluxes and the eddy momentum fluxes. Changes in the low-level mid-latitude eddy heat fluxes lead upper-level heat fluxes by  $\sim 1$  day and lead eddy momentum fluxes by  $\sim 1.5$  days. But why the changes in the low-level eddy heat fluxes occur in the first place is unclear.

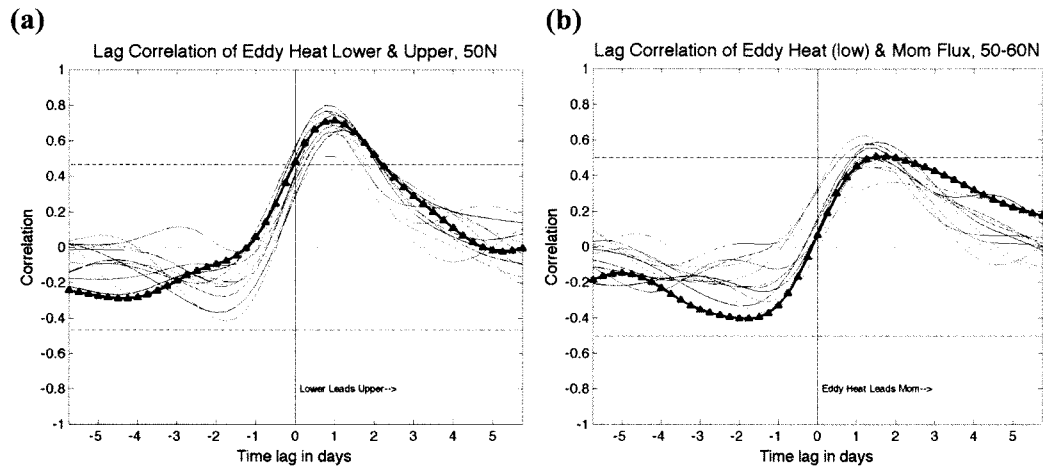


**Figure 4.17.** (a) Lag correlation of the (detrended) eddy heat flux response below 250 hPa to the eddy heat flux response above 250 hPa at 50°N. (b) Lag correlation of the eddy heat flux response below 250 hPa to the total column eddy momentum flux response from 50-60°N. Individual simulations are shown in colored lines; ensemble mean is the black line. Dashed horizontal lines represent 95% significance levels based on a 2-tailed  $t$ -test.

For theory (2), we assess whether the following things occur in this order: 1) static stability increases in both the tropics and extratropics, followed by 2) a reduction in baroclinic growth rates on the equatorward side of the jet; 3) a poleward shift of the latitude of baroclinic instability onset (i.e. the edge of the Hadley cell); and finally, 4) a poleward shift in the eddy formation region and subsequent eddy propagation. Figure 4.18 shows the time series of the mid-tropospheric vertical temperature gradient response

( $dT/dz$ ) from 20-40°N (magenta); the 850 hPa eddy heat flux response from 20-40°N (green); the change in latitudinal extent of the Hadley cell circulation (black), as measured by the location at the surface where easterlies become westerlies; and the change in latitude of maximum surface westerlies (red). Note that we use the vertical temperature gradient as a proxy for the static stability, and that the latitudinal extent of the Hadley cell and latitude of maximum surface westerlies look like step-functions due to discrete 2.25° latitude bands. The latitudinal change in maximum surface westerlies represents the mid-latitude jet shift, where positive values represent a poleward shift.

We certainly see increased static stability as shown by decreasing  $dT/dz$ . There are substantial increases in the static stability from the equator to ~50°N; almost no change occurs poleward of 50°N (not shown). We also see a reduction in baroclinic

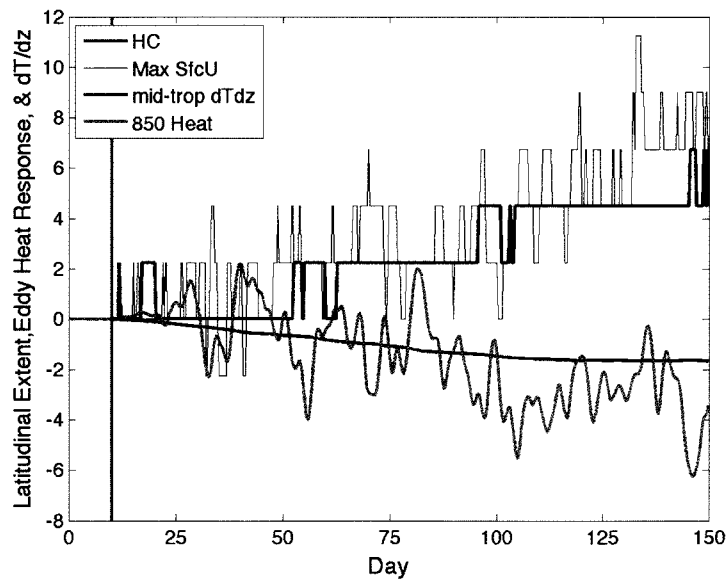


**Figure 4.18.** Time series of mid-tropospheric (300-500 hPa) vertical temperature gradient response ( $dT/dz$ ) from 20-40°N (magenta), the 850 hPa eddy heat flux response from 20-40°N (green), the change in latitudinal extent of the Hadley cell circulation (black), and the change in latitudinal location of the maximum surface westerly (red).

growth on the equatorward side of the jet (after ~day 50), as shown by the decrease in the subtropical eddy heat flux response; and an increase in the latitudinal extent of the Hadley cell circulation. The shifts in the mid-latitude jet location, while more variable than the shift in the Hadley cell extent, occur at the same time or slightly before the shifts in the Hadley cell extent.

The increase (decrease) in static stability ( $dT/dz$ ) occurs congruently with the reduction in subtropical eddy heat fluxes. However, it is unclear from this analysis whether the change in static stability leads the change in the eddy heat fluxes or vice versa. The increase in Hadley cell extent generally occurs after substantial reductions in the eddy heat fluxes, but with such a small sample size it's hard to prove the significance of this relationship. One interesting observation is that the subtropical eddy heat fluxes are significantly anti-correlated to the latitudinal location of maximum surface westerlies (not unexpectedly, the mid-latitude eddy momentum flux convergence response at 250 hPa is significantly correlated to these surface wind changes as well). So clearly the change in the subtropical eddy heat fluxes is an important factor in the shifts of the mid-latitude jet. Overall, the analyses suggest that the change in the subtropical eddy heat fluxes near the surface results from the changes in wave breaking at upper levels (theory #1) rather than from changes in static stability (theory #2).

With regards to changes in stratospheric circulation changes, we examine the following two theories: (1) changes in eddy generation [Butchart and Scaife 2001; Rind et al. 2001; Eichelberger and Hartmann 2005] and (2) changes in stratospheric background flow and eddy propagation [Garcia and Randel 2008; Sigmond and Scinocca 2009]. As discussed with regards to Fig. 4.5, the initial weakening of the Brewer-Dobson

circulation in our tropical heating run likely occurs ~day 30-50, as the tropical upper tropospheric temperature change starts to flatten out. This weakened stratospheric circulation then likely drives a positive feedback, enhancing the initial tropical heating and weakening the stratospheric circulation further. Here we use changes in both the lower-stratospheric polar temperatures and the 100 hPa hemispherically-averaged eddy heat fluxes as proxies for the strength of the Brewer-Dobson circulation.

Figure 4.19a shows the time series of lower-stratospheric polar temperatures (red) and the 100 hPa hemispherically-averaged eddy heat fluxes (black), along with the subtropical (green) and mid-latitude (light blue) eddy heat fluxes at 850 hPa, representative of changes in eddy generation near the surface. The polar lower-stratospheric temperature response (red) declines from day 30-50, then returns to zero ~day 60, then starts to decrease once again, in agreement with our theorized changes in the Brewer-Dobson circulation. The hemispherically-averaged eddy heat fluxes at 100 hPa (black) show weak decreases over time; even though the hemispherically-averaged eddy heat fluxes at 850 hPa show no trend (not shown). However, the lower-level eddy heat fluxes steadily increase in the mid-latitudes (light blue) but decrease in the subtropics (green). Intriguingly, the low-level subtropical eddy heat fluxes are positively correlated to both the upper hemispheric eddy heat fluxes and the polar lower-stratospheric temperatures (with a lead of ~2 days); while the low-level mid-latitude heat fluxes have much weaker correlations to both fields. This result suggest again that (1) the subtropical eddy heat flux response is strongly associated not only with changes in the tropospheric circulation as discussed above, but also with changes in the stratospheric circulation; and (2) that theory #1 has some validity as changes in eddy generation near

the surface, particularly in the subtropics, seem to be associated with changes in the stratosphere.

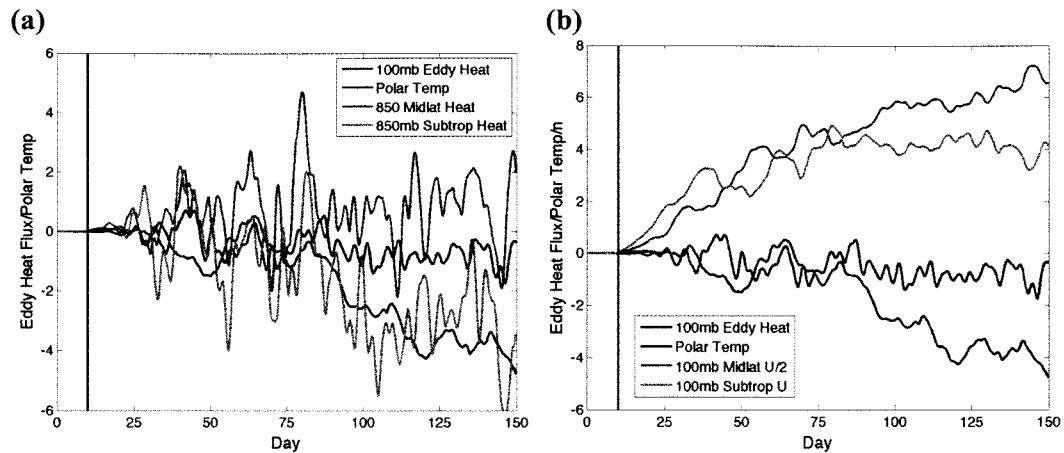


**Figure 4.19.** Time series of the lower-stratospheric (100 hPa) polar ( $88^{\circ}\text{N}$ ) temperature response (red) and the 100 hPa hemispherically-averaged (and cosine-weighted) eddy heat flux response (black). In (a), also the 850 hPa subtropical ( $20\text{-}40^{\circ}\text{N}$ ) eddy heat flux response (green) and the 850 hPa mid-latitude ( $40\text{-}60^{\circ}\text{N}$ ) eddy heat flux response (light blue), divided by 2. In (b), also the 100 hPa subtropical U-wind response (green) and 100 hPa mid-latitude U-wind response (light blue), divided by 2.

However, this theory still does not explain why, when the polar temperatures decrease from day 30-50, the low-level eddy heat fluxes in both the subtropics and the mid-latitudes are increasing- which by the eddy generation argument alone, would drive an enhanced Brewer-Dobson circulation and polar lower-stratospheric warming. Likely, the ability of eddies to propagate at upper-levels plays an important role. Figure 4.19b shows the response of the subtropical and mid-latitude zonal winds at 100 hPa. The winds become more westerly in both regions at upper-levels, but on shorter time scales the subtropical zonal winds have variations that are anti-correlated with variations in the mid-latitude winds- presumably due to the divergence of eddy momentum out of the subtropics and into the mid-latitudes. These high-frequency variations are also correlated

with variations in our proxy time series for the Brewer-Dobson circulation, suggesting that the upper-level zonal mean background flow may be important.

Why- if winds at upper levels are increased at all latitudes- do we see a reduced wave flux in the subtropics and enhanced wave flux at mid-latitudes, with the reduction in the subtropics dominating the hemispheric average? Our theory is as follows. Keep in mind that the hemispherically-averaged changes in eddy heat flux near the surface are essentially zero, so changes in eddy generation can't account entirely for this upper level difference. The background zonal flow itself isn't what's important, but rather the quantity  $\bar{u} - c$ , which we can use as a general estimate for wave propagation; the index of refraction is inversely proportional to this quantity (we note that the index of refraction also depends upon the meridional gradient of potential vorticity, the zonal wavenumber, and the buoyancy frequency, all of which we do not examine here). If  $\bar{u} - c < 0$ , waves cannot propagate.

In the control run, eddy phase speeds are ~5-10 m/s (Fig. 4.1); this is close to the background flow in the subtropics and much slower than the background flow in the mid-latitudes. Thus waves tend to propagate through upper levels of the mid-latitudes and break in the subtropics. In the heating run, eddy phase speeds increase to ~10-15 m/s (a change of 5-10 m/s; Fig. 4.1). Although the background flow is also increasing in the subtropics, we can see from Fig. 4.19b that the maximum changes are only ~4 m/s. This means that in general the phase speeds  $c$  are almost always larger than the background flow, and most waves are prevented from propagating into the subtropical region- thus the subtropical eddy heat fluxes at upper levels are reduced. In the mid-latitudes, the zonal wind changes are substantially stronger (~12-15 m/s) than the simultaneous

increases in the eddy phase speeds ( $\sim 5\text{-}10$  m/s changes) at those latitudes. Hence, the difference in  $\bar{u} - c$  becomes more positive over time. As a result, the index of refraction becomes smaller in the mid-latitudes; and waves tend to propagate away from regions of low index of refraction. Essentially, although more waves are being generated at the mid-latitude surface and propagate upward in the heating experiment, above  $\sim 250$  hPa the background flow becomes so fast that wave propagation at upper levels is limited by a reduction in the index of refraction.

In summary, the analyses suggest that the tropical upper tropospheric heating drives changes as follows.

(1) The enhanced upper level temperature gradient nearly instantaneously drives faster westerly winds in the stratosphere.

(2) Eddy phase speeds become more eastward, and thus break further polewards in the subtropics.

(3) The region of subtropical eddy momentum flux divergence at  $\sim 250$  hPa moves polewards and drives an anomalous meridional circulation that reduces baroclinicity at the subtropical surface. Less than a day or so later, the region of upper level mid-latitude eddy momentum flux convergence also shifts polewards and drives an anomalous meridional circulation that enhances baroclinicity at the mid-latitude surface, moving the mid-latitude jet polewards.

(4a) The reduced baroclinicity in the subtropics drives a decrease in tropospheric eddy heat fluxes at those latitudes. Similarly, the enhanced baroclinicity in middle latitudes drives an increase in eddy heat fluxes at those latitudes.

(4b) At around the same time in the stratosphere, fewer waves are propagating into the stratosphere in the subtropics and more waves are propagating in the stratosphere at mid-latitudes; however, due to the strong wind changes in the mid-latitude stratosphere, some of the mid-latitude waves are blocked, and hence the decreased wave driving in the subtropics overwhelms the increased wave driving in middle latitudes. The decrease in hemispherically averaged wave driving causes the Brewer-Dobson circulation to weaken.

(5) The weakened Brewer-Dobson drives cooling in the polar stratosphere and enhances the original heating in the tropical troposphere.

## **CHAPTER 5: SUPPLEMENTAL CHAPTER ON LOWER STRATOSPHERIC TEMPERATURES AND OZONE**

The majority of the research in this dissertation examines the simulated atmospheric circulation response to climate change. We are also interested in better understanding the *observed* changes in the atmospheric circulation. Trends in lower-stratospheric temperatures have recently been thought to indicate poleward shifts in the tropospheric jets [Fu et al. 2006]. Both lower-stratospheric temperatures and ozone should reflect variability and trends in the stratospheric Brewer-Dobson circulation, which has historically been difficult to measure [Thompson and Solomon 2009]. In this chapter, we examine the variability, trends, and relationships of observed stratospheric temperatures and ozone to see what information they contain regarding past changes in the atmospheric circulation.

### **5.1 Observed Trends in Lower-Stratospheric Temperatures**

Previous analysis of satellite-based temperature measurements from the Microwave Sounding Unit (MSU) suggests that over the last few decades, stronger temperature changes have occurred in the extratropics relative to the tropics [Fu et al. 2006]. In particular, between  $\sim 20^{\circ}$ - $45^{\circ}$  latitude, the lower stratosphere has cooled and the troposphere has warmed relative to other latitudes (e.g., Figure 5.2). Greenhouse gas

forcing is unlikely to cause these patterns of temperature trends through radiative effects alone; in the lower stratosphere, the cooling effects of increased greenhouse gases are weak (with the strongest cooling occurring at 40-50 kilometers), and in the troposphere, most models predict stronger warming in the tropics than in the mid-latitudes [World Meteorological Organization (WMO) 2003]. Ozone depletion could certainly have some influence on the observed trends in the lower stratosphere, as total column ozone loss has been observed in the mid-latitudes of both hemispheres since 1980. However, while models forced with the observed ozone trends can simulate the general spatial structure of the lower stratospheric temperature trends, the magnitudes of the mid-latitude trends are considerably weaker than observed, even if greenhouse gases are also included [WMO 2003]. Stratospheric water vapor changes probably have some effect on temperatures, but relatively little is known about their temporal and spatial variations.

Clearly, the reason for these spatial patterns in the temperature trends is unclear, but Fu et al. [2006] postulate that these mid-latitude temperature trends indicate a poleward shift in the subtropical jets and a widening of the Hadley circulation. We seek to further examine the spatial patterns in the lower stratospheric temperature trends, using both satellite data and radiosondes.

We focus on two datasets of lower-stratospheric temperatures. The first is the satellite-based Microwave Sounding Unit (MSU). The MSU measures brightness temperatures over four channels, which correspond to the average temperature of the atmosphere averaged over each channel's weighting function [Figure 5.1a; e.g., Mears and Wentz 2008]. In our study we focus on channel 4 (or TLS), which represents a weighted sum of atmospheric temperatures between ~300 hPa to ~10 hPa, with a

maximum weighting near 90 hPa. The global-mean time series of MSU4 temperatures (Figure 5.1b) shows an overall cooling associated largely with ozone depletion (and to a much weaker extent, with increasing greenhouse gases), plus stronger step-like cooling,

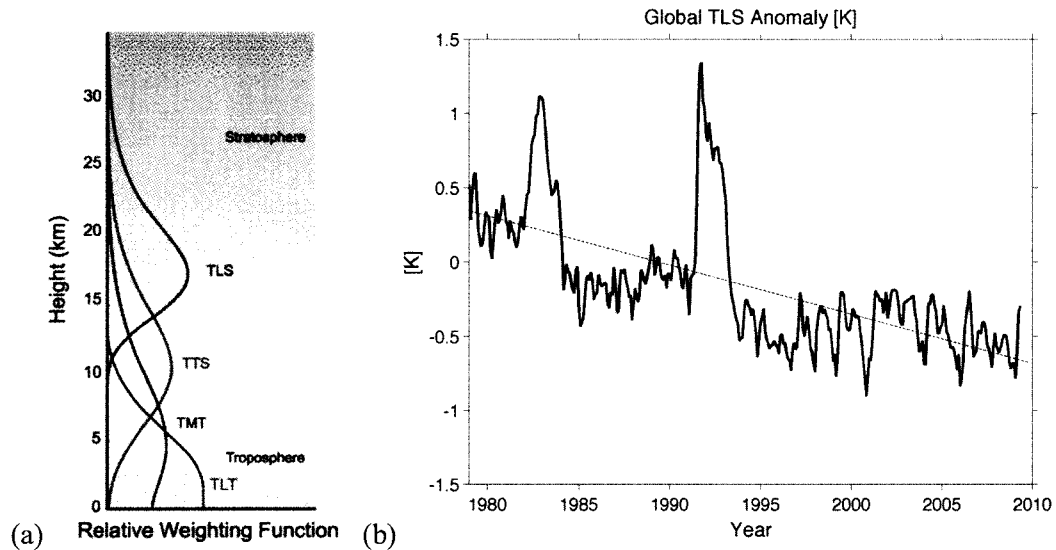


**Figure 5.1.** (a) The MSU weighting functions for the 4 MSU channels. From [http://www.ssmi.com/msu/msu\\_data\\_description.html](http://www.ssmi.com/msu/msu_data_description.html). (b) Global-mean MSU4/TLS temperature time series [K], from 1979-2009.

with the largest temperature decreases occurring immediately after the large warmings associated with the El Chichon and Mount Pinatubo eruptions [Ramaswamy et al. 2006; Thompson and Solomon 2009]. Volcanic aerosols can have competing radiative and chemical impacts (through acceleration of ozone depletion) on stratospheric temperatures [e.g., Solomon et al. 1996; Robock 2000]. The linear trend of the global-mean MSU4 temperature time series is  $-0.33$  K/decade for 1979 to mid-2009, but since 1995 the trend has been nearly zero, largely due to increases in global-mean ozone in the last 15 years [Thompson and Solomon, 2009].

Spatial patterns of the MSU4 temperature trends for 1979-2009 indicate a maximum cooling trend in the extratropical lower-stratosphere relative to the cooling trend in the tropical lower-stratosphere over the last few decades [Figure 5.2; e.g., Fu et al. 2006]. The extratropical cooling peaks near 40° latitude in the NH and near 30° latitude in the SH. This pattern is robust for a variety of different time periods and also after removing the three years following both El Chichon and Mt. Pinatubo, although it is less robust for the second half of the record (Fig. 5.2 bottom)

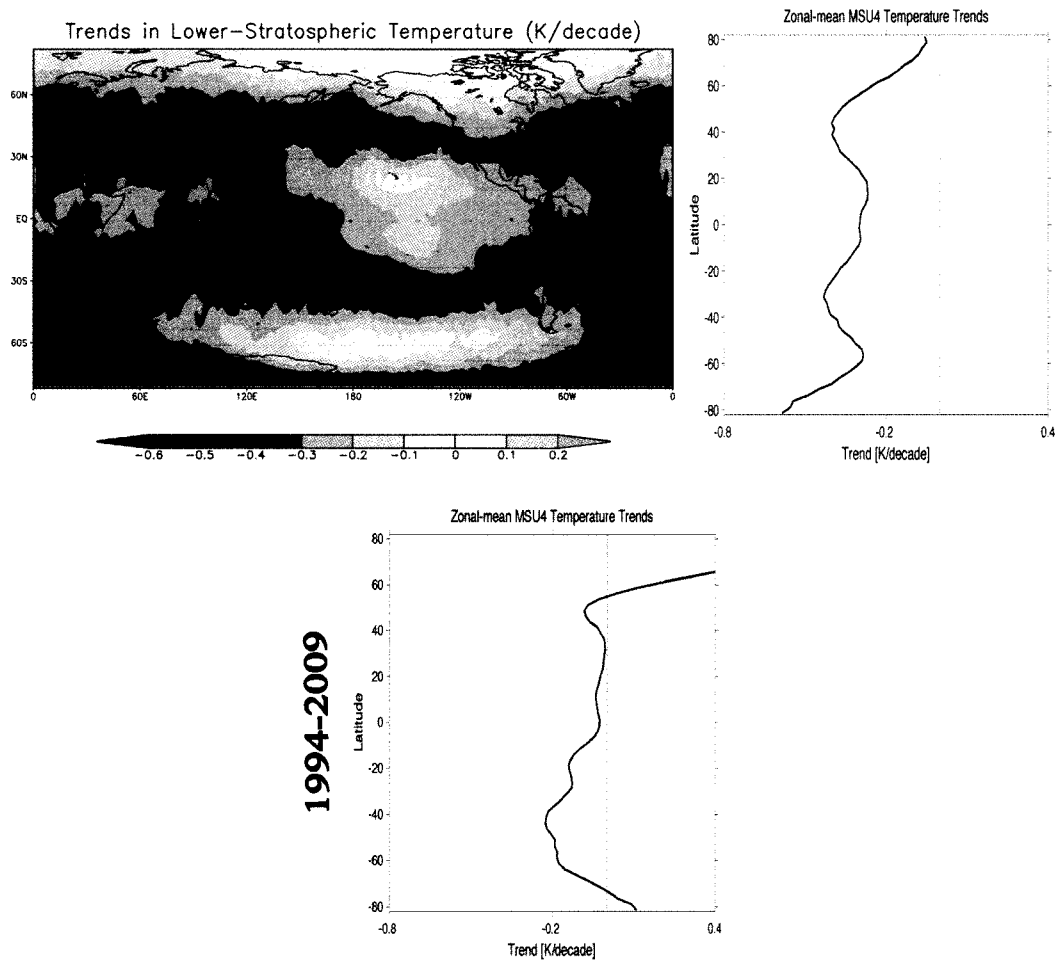


**Figure 5.2.** (left) MSU4 linear temperature trends, 1979-2009 [K/decade]. (right) Zonal-mean MSU4 temperature trends [K/decade]. (bottom) same as (right) but for 1994-2009.

In Figure 5.3, we investigate the seasonality of these trends. We find that the NH extratropical cooling maximum occurs mostly in the boreal winter months of January, February, and March (JFM). The SH extratropical cooling maximum occurs year-round at shifting latitudes, with strongest amplitudes near 40° latitude in January but closer to 30° latitude the rest of the year (strong cooling also occurs polewards of 60° latitude in the SH from October through January, largely associated with ozone depletion over this time period; e.g., Randel and Cobb 1994). Overall, the bimodal cooling structure is most apparent in NH winter (JFM), with the peak mid-latitude trends in both hemispheres significant at the 95% level. We also note the strong warming trend at NH polar latitudes that occurs in January/February, perhaps driven dynamically by an enhanced Brewer-Dobson circulation over this time period [Hu and Tung 2002; Randel et al. 2006; Thompson and Solomon 2009], though these trends are not significant at the 95% level.

We are interested in understanding what causes this spatial trend pattern of

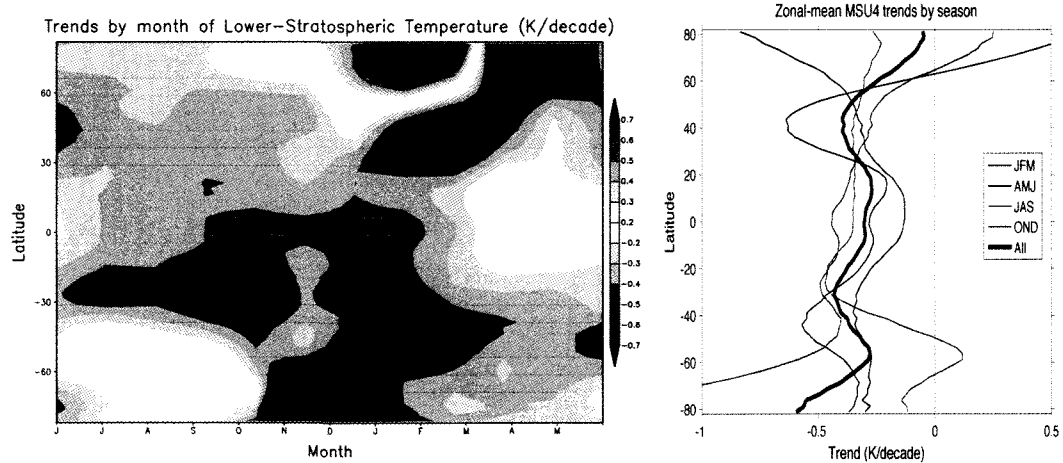


**Figure 5.3.** (left) MSU4 temperature trends from 1979-2009 as a function of month and latitude [K/decade]. (right) Zonal-mean MSU4 temperature trends by seasonal average [K/decade].

extratropical cooling maxima relative to tropical cooling. Is this pattern also seen in radiosonde observations? Can it be explained by shifts in the subtropical or mid-latitude jet location (as suggested by Fu et al. 2006)? Or is it perhaps an artifact created by the slope of the tropopause and the weighting function that the MSU employs?

To begin to answer this question, we first introduce the second dataset of lower-stratospheric temperatures, the Radiosonde Atmospheric Temperature Products for Assessing Climate [RATPAC; see Free et al. 2005]. Measurements are provided from 85 stations around the world, for 13 pressure levels from the surface to 30 hPa. While these data are useful because they provide independent measurements of upper-air temperatures, they also have more limited potential due to changes in instruments and practices at the different radiosonde stations, which create many inhomogeneities in the data records. They also lack the spatial coverage of satellite-measurements. RATPAC attempts to reduce the inhomogeneities in the radiosonde data and to create large-scale regional mean time series that can be used in trend analysis [Free et al. 2005], but some problems with the radiosonde dataset still exist, particularly in the tropics where some stations in the already-limited dataset seem to exhibit a systematic cooling bias relative to satellite measurements [Randel and Wu 2006].

The radiosonde measurements show significant cooling in the tropical lower stratosphere, in contrast to the MSU4 data, which shows enhanced cooling in the extratropical stratosphere relative to the tropical stratosphere [Thompson and Solomon 2005]. However, because of the radiosonde measurement issues, particularly in the tropics, there has been some debate about the amplitude of these trends [Randel and Wu 2006]. Recent analysis accounting for these discrepancies suggests that the tropical

stratosphere is cooling at nearly the same rate as the extratropical stratosphere in radiosonde data [Randel et al. 2009]; although the stratospheric cooling trends at 70 hPa as measured by the radiosondes are generally stronger than those measured by the MSU4, even without the inclusion of problematic radiosonde stations (Figure 5.4). One

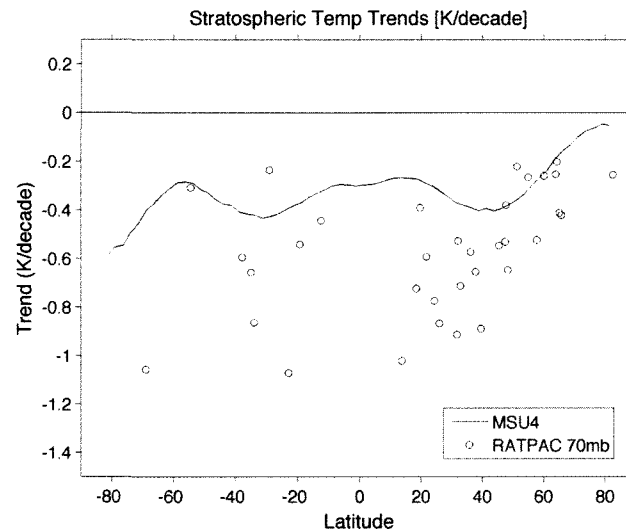


**Figure 5.4.** Lower-stratospheric zonal-mean temperature trends for 1979-2009 from (solid line) MSU4 [K/decade] and (circles) 70 hPa temperature trends [K/decade] from selected RATPAC stations from Randel and Wu [2006]. Only those stations with no missing data between 250-50 hPa are included here, and trends are calculated only for stations with >75% data over the record (34 out of the original 47 stations).

possibility is that the MSU4 shows weaker cooling in the tropical stratosphere due to the sloping tropopause height with latitude and the weighting function that the MSU4 data employs.

We next investigate in detail the effect of the weighting function on the MSU4 trends. Because the lower-stratospheric temperature trends from MSU are a reflection of a weighted sum of atmospheric temperatures between ~300 hPa to ~10 hPa, and because the tropopause slopes from a peak height of ~100 hPa in the tropics to ~300 hPa in the

poles, the weighting function includes a substantial fraction of the upper troposphere in the tropics. Therefore, we expect MSU lower-stratospheric cooling trends in the tropics to be reduced by the inclusion of a warming troposphere in the weighted average. In the following analysis, we quantify the expected reduction in MSU retrievals of tropical lower-stratospheric cooling trends and explore the effect of the weighting function when applied to RATPAC radiosonde retrievals.

In Fu et al. [2004], it was argued that upper tropospheric temperature anomalies do *not* have a big impact on MSU4 trends. Figure 5.5 shows the expected MSU4 measurement of temperature anomaly assuming a given stratospheric temperature anomaly (y-axis) and a tropospheric anomaly (x-axis). Figure 5.5a is the example shown in Fu et al. [2004], and it depicts the changes in MSU4 for a typical standard atmospheric temperature profile with a tropopause height of 200 hPa (which would be typical polewards of the subtropics). In this case, if the actual stratospheric trend were -0.5 K/decade (y-axis), the trend in MSU4 (contours) would be essentially the same as the real stratospheric value (-0.5 K/decade) no matter whether the troposphere were warming or cooling. However, in reality the tropical tropopause height is ~100 hPa. If we repeat the Fu et al. analysis using a tropical temperature profile with a 100 hPa tropopause, we find that the tropospheric trends start to influence MSU4 (Figure 5.5b). In this case, if the actual stratospheric trend were -0.5 K/decade (y-axis) but the tropospheric trend were +0.15 K/decade (x-axis), the MSU4 trend (contours) would be ~ -0.3 K/decade. Note that even if the troposphere is cooling, as long as the magnitude of the tropospheric cooling is less than the stratospheric cooling, the MSU4 trend is less than the true stratospheric cooling magnitude.

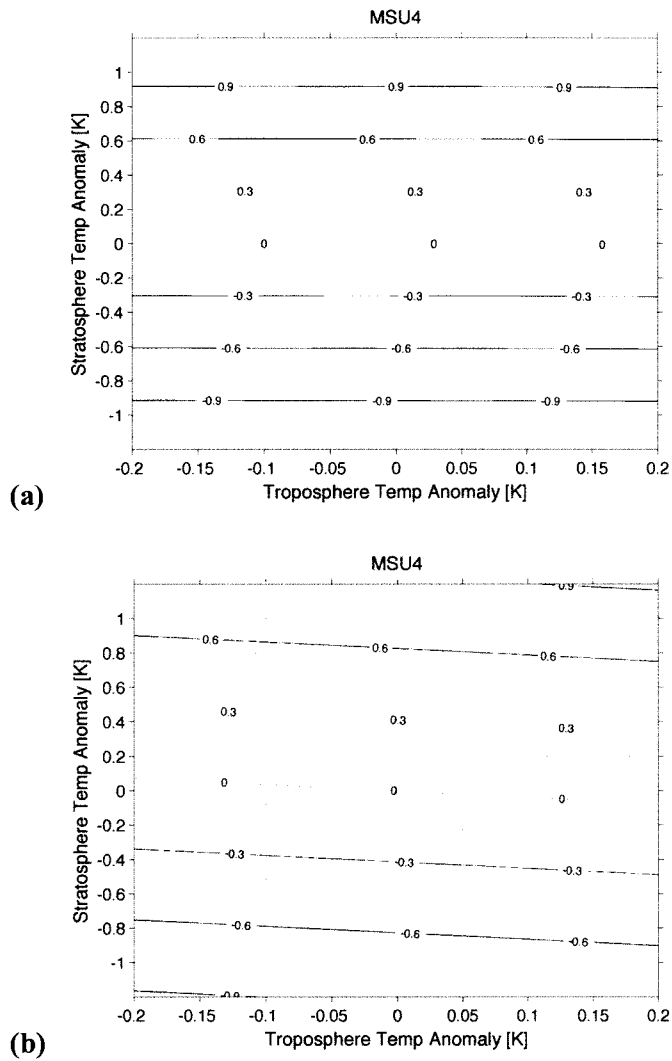


**Figure 5.5.** Response of MSU4 temperatures to changes in tropospheric and stratospheric temperatures assuming (a) a standard atmospheric temperature profile with a tropopause height of 200 hPa (as in Fu et al. [2004], Figure 1) and (b) a tropical atmospheric temperature profile with a tropopause height of 100 hPa.

Clearly the weighting function effect could have a big impact on tropical MSU4 trends ( $\sim 0.2$  K/decade). We now experiment with whether this artificial reduction in tropical stratospheric trends can be replicated if applied to radiosonde data. In Figure 5.4, we showed the RATPAC temperature trends at a specific level in the stratosphere (70

hPa). We now compare those results to radiosonde trends in which the MSU4 weighting function has been applied [Figure 5.6, triangles]. We can see that applying the weighting function to the radiosonde data has a significant impact on the resulting trends. As we might expect, temperature trends at almost all latitudes are weaker after applying the weighting function and averaging vertically compared to cooling trends at 70 hPa, where the cooling is likely the strongest. An interesting result, however, is that the trends are

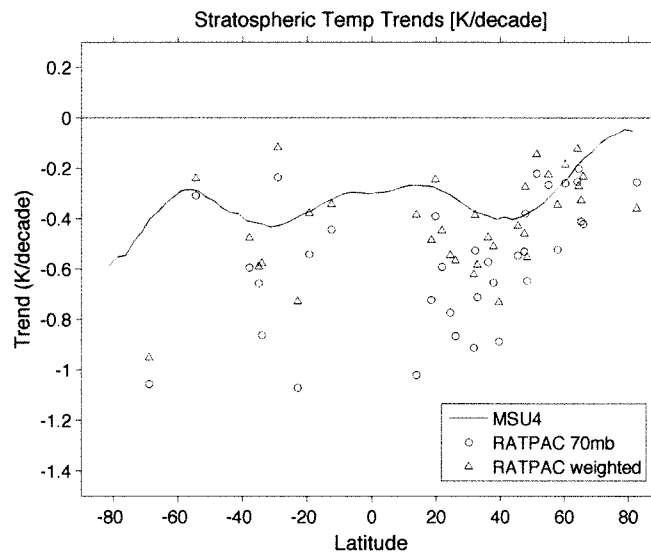


**Figure 5.6.** Lower-stratospheric zonal-mean temperature trends for 1979-2009 from (solid line) MSU4 [K/decade], (circles) 70 hPa temperature trends [K/decade] from selected RATPAC stations from Randel and Wu [2009], and (triangles) temperature trends [K/decade] from the same RATPAC stations with MSU4 weighting applied. Only those stations with no missing data between 250-50 hPa are included here, and trends are calculated only for stations with >75% data over the record (34 out of the original 47 stations).

more greatly reduced at tropical and subtropical stations than at extratropical stations, which may suggest that the inclusion of the upper tropospheric temperature changes at

those latitudes where the tropopause height is higher causes an additional reduction in the tropical stratospheric temperature trends.

This result is further illuminated by looking at the RATPAC-B regional data, created by performing large-scale arithmetic averaging on all the individual stations. The station data include radiosonde measurements that are bias-adjusted and produced by Lanzante, Klein, Seidel [2003] (“LKS”) from 1958-1997 and unadjusted data from the Integrated Global Radiosonde Archive (IGRA) after 1997 (thus inhomogeneities may still be present in the data after 1997). Figure 5.7 shows the regionally-averaged RATPAC-B

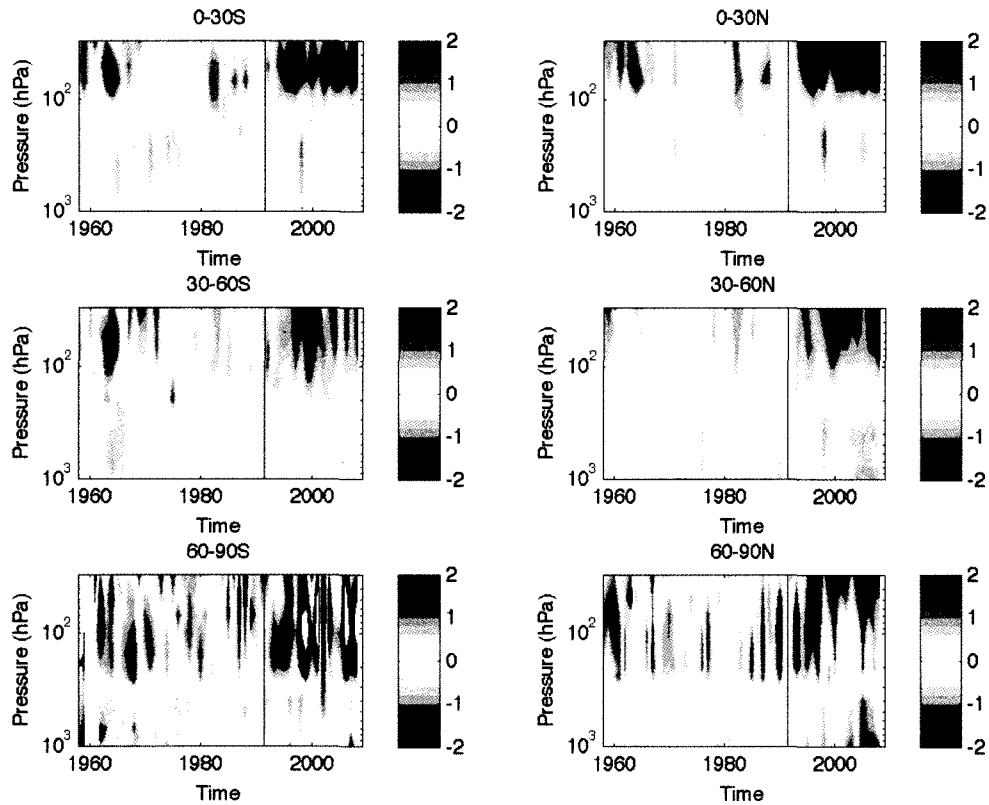


**Figure 5.7.** Annual-mean temperature anomalies [K] from the RATPAC-B regionally-averaged dataset for 1958-2009. The SH latitude bands comprise the left panels while the NH latitude bands comprise the right panels. The black vertical line in 1991 marks the Mt. Pinatubo eruption.

temperature anomaly time series from 1958-2009 as a function of pressure. Notable observations from this figure are (1) the troposphere is warming and the stratosphere is cooling in all latitude bands as expected from greenhouse gas forcing; (2) the tropopause height in each latitude band can be approximated by where the temperature anomalies change sign with height; (3) as expected, the tropopause height is  $\sim 100$  hPa in the tropical regions and closer to 250 hPa in the polar regions, although there is interannual variability in tropopause height; (4) certain events are visible, such as the sudden stratospheric warming of the SH polar region in 2002, the large tropospheric warming associated with the El Niño-Southern Oscillation event in 1998, and the strong Arctic surface warming that has been observed over the last decade. The strong cooling at all latitude bands seems to mostly occur right after the Pinatubo eruption (marked by the black vertical line in 1991). According to this observational dataset, the tropical upper troposphere has warmed but not as much as the NH extratropical and polar regions. In addition, the tropical stratosphere appears to be cooling more strongly than the extratropics, although the regional averages here include data from tropical stations found to have systematic cooling biases.

In Figure 5.8 we compare the temperature time series at 150 hPa to the time series at 70 hPa for each region, which shows that the vertical gradient in the trends across  $\sim 100$  hPa is largest in the tropics (equatorward of 30 degrees latitude). The trend at 150 hPa in the tropical regions is nearly zero, while the trend at 70 hPa is  $\sim -0.5$  K/decade. Also, the interannual variability of the time series at 150 hPa and 70 hPa agrees the least in the tropics and the most at the poles. Thus, a vertical average of the layers from 250 hPa to

30 hPa such as MSU4 employs may not be a very accurate representation of the variability and trends in the tropical stratosphere.

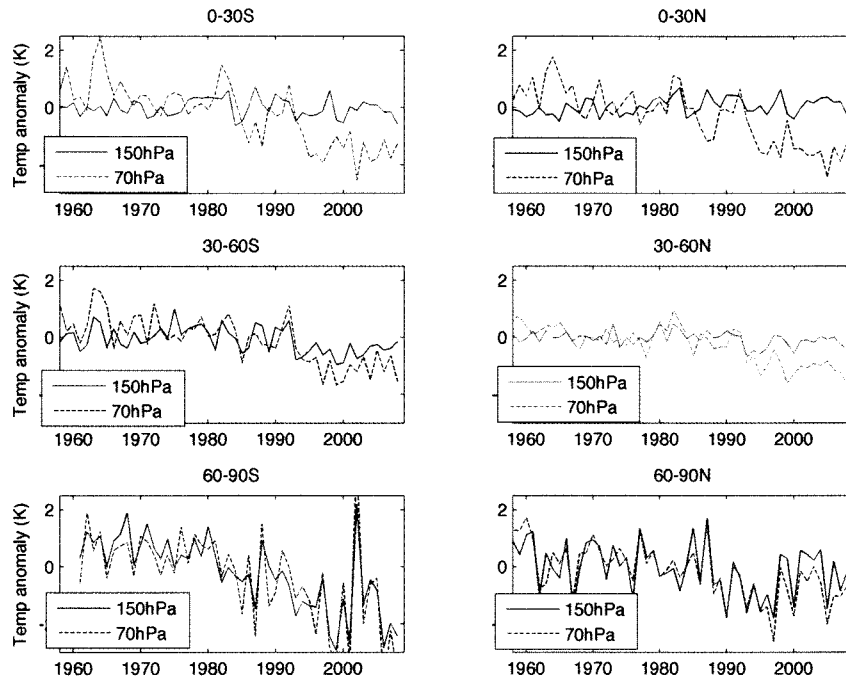


**Figure 5.8.** Annual-mean temperature anomaly time series [K] from the RATPAC-B regionally-averaged dataset for 1958-2009 at 150 hPa (solid line) and 70 hPa (dashed line). The SH latitude bands comprise the left panels while the NH latitude bands comprise the right panels.

In conclusion, the effect of the MSU4 weighting function on the sloping tropopause is a substantial reduction ( $\sim 0.2$  K/decade) of the stratospheric cooling trends in the tropics and subtropics, with little influence on extratropical and polar trends. In addition, the MSU4 time series in the tropics may not accurately represent the interannual variability of the tropical stratosphere. However, it is difficult to conclude from this study that the MSU weighting function effect causes the bimodal spatial pattern of the stratospheric cooling shown in Figure 5.3, although there is a hint of the pattern in the

radiosonde data after the MSU weighting is applied in Figure 5.6. While it is possible that the reduction in trends at the tropics is greater than the reduction of trends in the subtropics, which creates a tropical cooling minimum in the MSU4 data, it is not conclusive from evidence shown here that the cooling maxima near 30-40° degrees latitude in each hemisphere is also associated with this effect. The significance and robustness of the spatial pattern, particularly in NH winter, suggests that this pattern could indeed reflect changes in the atmospheric circulation. Does it reflect changes in the stratospheric or tropospheric circulation? We next look at vertical profiles and total column ozone to try to understand other mechanisms for this bimodal cooling pattern in the stratospheric temperature trends.

## **5.2 Observed Trends in Vertical Profiles of Ozone**

For our analysis we had access to a new global dataset of vertical profiles of ozone, the Binary Database of Profiles [BDBP; Hassler et al. 2008]. These profiles are unique because they include original, rather than derived monthly mean, quality controlled measurements from both satellites (HALOE, POAM II and III, and SAGE I and II) and ground-based ozonesondes. There is higher natural variability in these measurements, as opposed to previous vertical profile datasets that are generated by multiple regression models [e.g., Randel and Wu 2007, hereafter RW]. In addition, this dataset includes measurements from 136 ozonesonde stations around the world, while past datasets have used ozonesonde records only minimally. The advantages of using the ozonesondes include: the availability of data since the early 1960s to 2006 (much longer

than satellite records); generally small and quantifiable measurement uncertainties; and coverage in both the stratosphere and the troposphere (the available satellites have only measured ozone at levels greater than 10 kilometers). Basic quality-control has been performed on both satellite and ozonesonde data; however, this version of the BDBP does not take into account inhomogeneities between the different data sources, so that systematic differences between the data sources are likely [Hassler et al. 2008].

We combine the raw data within  $5^\circ$  latitude bins, reject values greater than  $\pm 2\sigma$  at each level as a crude way to discard extreme values, and then calculate monthly means of the data. At least 3 values for a given latitude band and altitude must be available to create the monthly mean, and the data are weighted by the error of the measurement, so that measurements with higher error are weighted less. Monthly mean ozone anomalies are created by removing the seasonal cycle. We focus on the time period 1979-2005 for better data coverage as well as the ability to compare with RW results.

Figure 5.9a shows the time series of BDBP ozone anomalies, in units of Dobson Units (DU) per kilometer, at the equator ( $0-5^\circ\text{N}$ ) as a function of pressure. The Quasi-Biennial Oscillation (QBO) with a period of approximately 28 months is apparent as descending positive and negative ozone anomalies, where positive anomalies occur when the tropical lower stratospheric zonal winds are westerly and negative anomalies occur when the zonal winds are easterly [Baldwin et al. 2001]. If we compare the BDBP ozone anomalies with the RW ozone anomalies (Fig. 5.9b), which are continuous due to the multiple regression model used, we can see that the BDBP ozone is quantitatively similar to the smoothed RW dataset but has much more natural variability. BDBP measurements

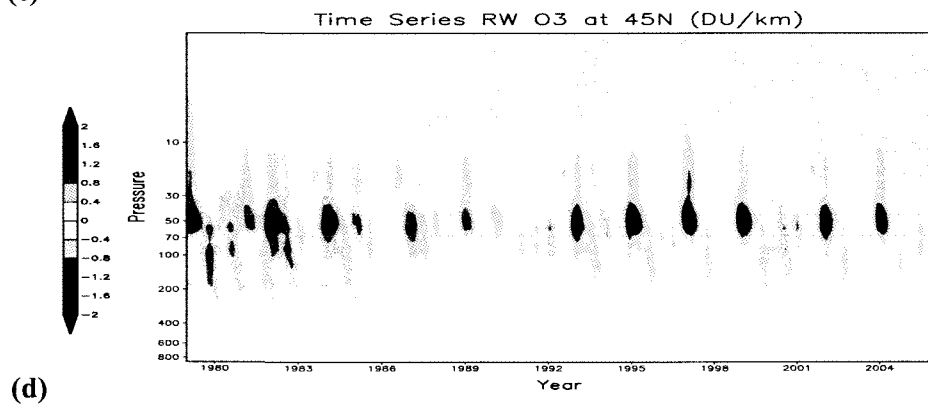
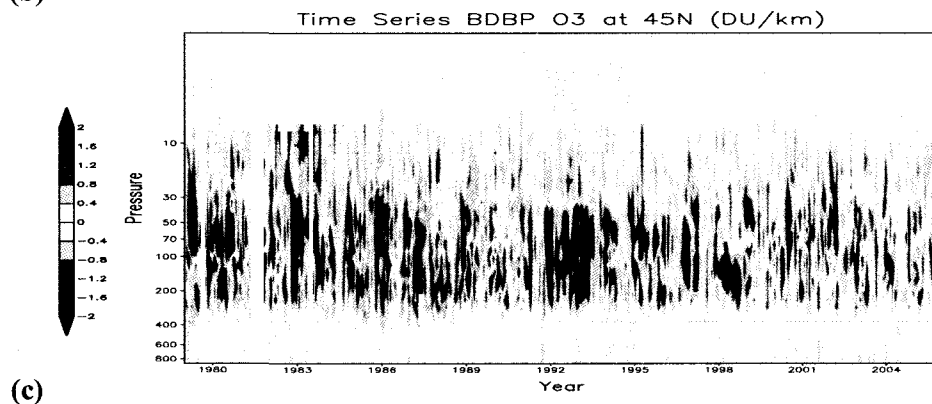
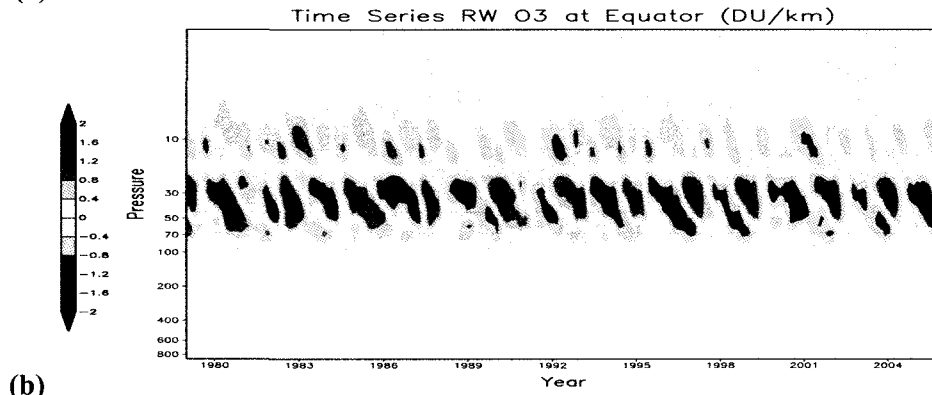
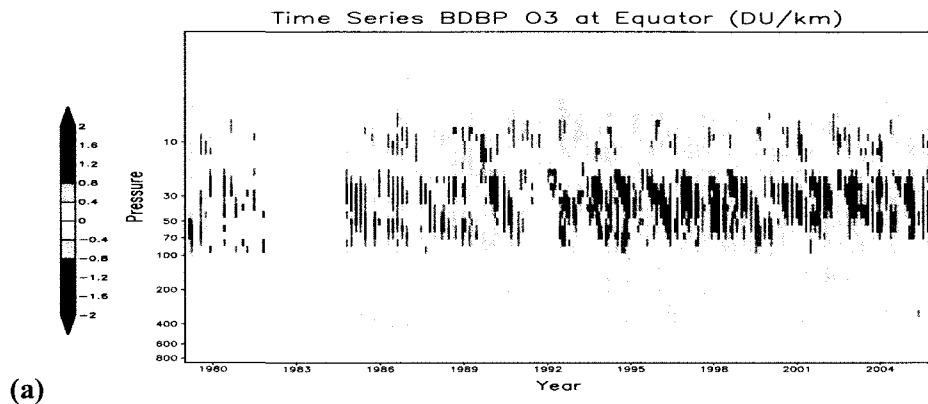


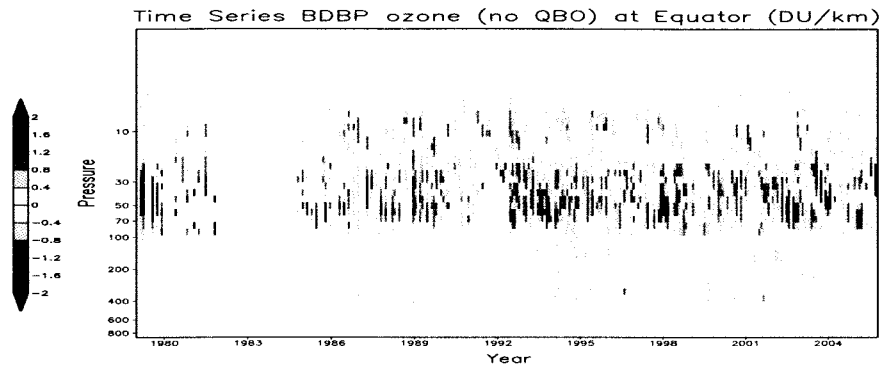
**Figure 5.9** (previous page). Time series of ozone anomalies as a function of pressure [DU/km] for (a) BDBP ozone from 0-5°N, (b) RW ozone from 0-5°N, (c) BDBP ozone from 45-50°N, and (d) RW ozone from 45-50°N. Pixelation in (a) is due to difficulty in shading with missing data.

below ~100 hPa may be questionable prior to 1998, as the data from 1985-1998 is from SAGE II only. After 1998, two ozonesonde stations also contribute at this location.

The higher natural variability captured in the BDBP ozone dataset is much more evident in the mid-latitudes, where more ozonesonde data is available (Fig. 5.9c).

Whereas most of the interannual variability in the RW dataset at 45-50°N is from the extratropical QBO signal, the BDBP has much higher frequency variability as well as changes in ozone in response to the volcanic eruptions of El Chichon and Mt. Pinatubo. Volcanic aerosols cause major ozone losses in the mid-latitudes because heterogeneous chemical reactions can occur on the sulfate particles [Hofmann and Solomon 1989].

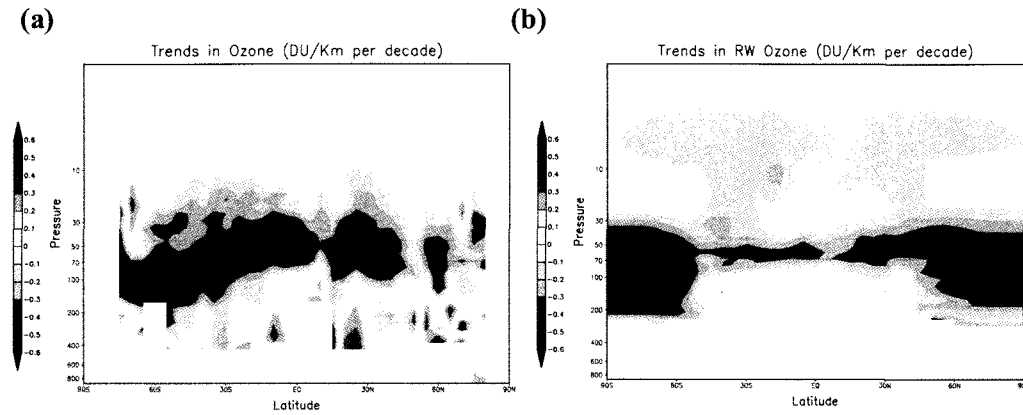
The QBO signal can be removed either by simple regression onto an equatorial wind index defined by zonal mean winds at 30 or 50 hPa, or by using Singular Value Decomposition (SVD) analysis on the covariance matrix between equatorial winds (70-10 hPa) from NCEP/NCAR reanalysis and the ozone data [Randel and Wu 1996]. We use the latter method here because we can get ozone-QBO regression patterns as functions of latitude and pressure and thus effectively remove the QBO signal everywhere. Figure 5.10 shows the BDBP ozone anomaly time series at the equator with the QBO signal removed (some residual signal appears to remain here). Without the QBO signal, a long-term decrease in equatorial ozone is apparent, although the earliest data from 1979-1981 is from SAGE I alone and may be less reliable.



**Figure 5.10.** Time series of BDBP ozone anomalies as a function of pressure [DU/km] for 0-5°N, with the QBO signal removed. Pixelation is due to difficulty in shading with missing data.

We can also see this long-term decrease in the equatorial BDBP ozone anomalies by calculating the linear trends (Fig. 5.11a). Only grid spaces with >40% available data from 1979- 2005 are included in the trend analysis (note that this means we lose trend information poleward of 80° latitude). According to this data, ozone has been decreasing at nearly every latitude in the lower stratosphere, including in the tropics. This result is in contrast to the RW ozone dataset (Fig. 5.11b), which shows strong ozone losses over both poles but weaker decreases in the subtropics and tropics. The considerable discrepancies between the two datasets may be due to (1) a greater amount of data sources in the BDBP dataset; (2) inhomogeneities between the various data sources in BDBP; or (3) the regression model used in the RW dataset that fills in missing data and smooths out high frequency variability.

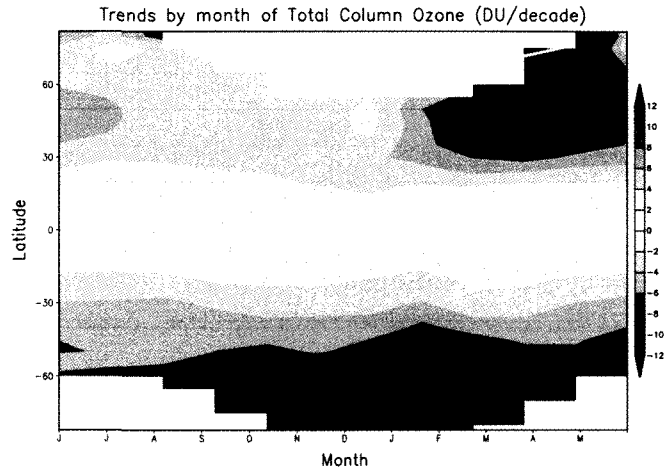
To complicate matters further, measurements of “total column” ozone from the Total Ozone Mapping Spectrometer (TOMS) over this time period show near zero trends in the tropics year-round (Fig. 5.12). The neutral trends in the total column ozone data



**Figure 5.11.** Linear ozone trends [DU/km per decade] from 1979-2005 for (a) BDBP ozone and (b) RW ozone. Seasonal cycle and QBO signal have been removed.

could suggest that either (a) there are strong enough increases in tropical tropospheric ozone to cancel the decreases in tropical stratospheric ozone when vertically integrated over the entire column or (b) the tropical stratospheric trends are overestimated due to uncertainties in the SAGE I and II measurements, on which the tropical trends in both RW and BDBP are largely based [Randel and Wu 2007]. The BDBP does show increases in upper tropospheric ozone, in agreement with a previous study based on aircraft measurements [Bortz et al. 2006]; but the accuracy of these trends requires further study, as other studies find no significant trends in tropical tropospheric ozone [Ziemke et al. 2005]. It is a definite possibility that the uncertainties in SAGE I and II measurements lead to overestimated tropical stratospheric trends, although the fact that BDBP shows stronger cooling than RW with the addition of ozonesonde and HALOE data may suggest this is not the case.

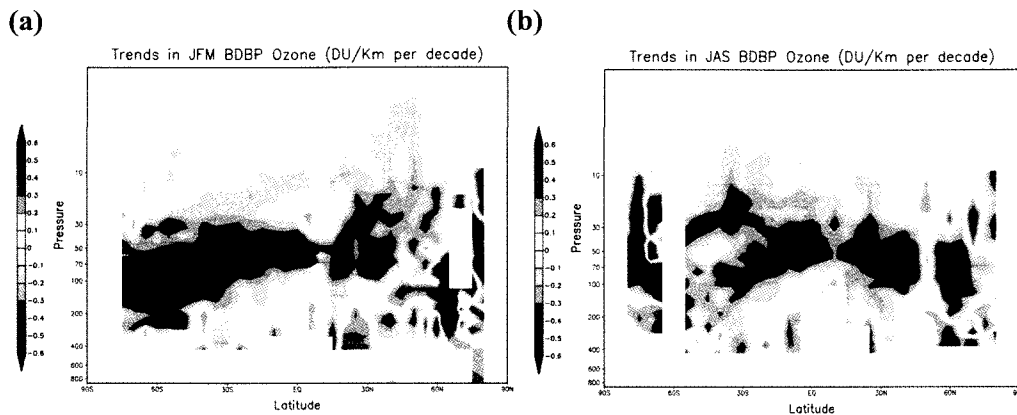
Determining whether ozone is indeed decreasing in the tropics is important because of the potential radiative impacts on the tropical stratosphere, as well as the upper troposphere [Forster et al. 2007]; and because tropical ozone loss may imply



**Figure 5.12.** Linear ozone trends [DU per decade] from 1979-2005 for TOMS total column ozone as a function of latitude and month. Seasonal cycle and QBO signal have been removed.

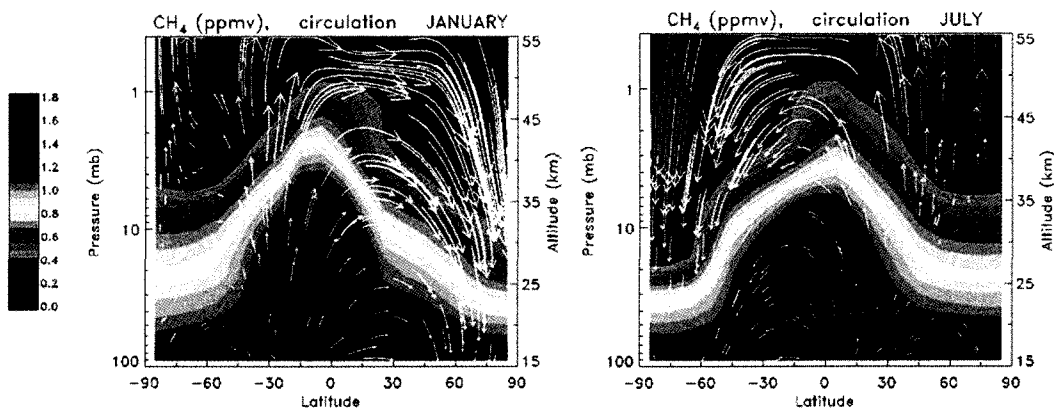
changes in stratospheric dynamics, as chemical ozone depletion is unlikely in the lower tropical stratosphere due to low levels of reactive halogen gases [WMO 2003]. For example, ozone decreases in the tropical stratosphere could be caused by increased tropical upwelling by an enhanced Brewer-Dobson circulation. The Brewer-Dobson circulation is strongest at those times of year when planetary waves can propagate into and break in the stratosphere, namely during the winter in each hemisphere, when stratospheric zonal winds are westerly. If the Brewer-Dobson circulation has been increasing over the last several decades, we might expect to see tropical ozone decreases and extratropical ozone increases during the winter months of each hemisphere. We explore the possibility that stratospheric circulation changes are driving the tropical ozone losses by looking at the seasonality of the trends.

Figure 5.13 shows the BDBP ozone trends (as in Fig. 5.11) but for boreal winter months (January, February, March) and austral winter months (July, August, September). In NH winter (Fig. 5.13a), strong decreases in ozone occur in the tropics and SH



**Figure 5.13.** Linear BDBP ozone trends [DU/km per decade] from 1979-2005 for (a) boreal winter months (JFM) (b) austral winter months (JAS). Seasonal cycle and QBO signal have been removed.

subtropics and mid-latitudes, while increases in ozone are seen at  $\sim 60^\circ\text{N}$ . Studies of long-lived tracers in the stratosphere (e.g., methane) suggest that in the NH winter, upward mass transport from the Brewer-Dobson circulation as far south as  $30^\circ\text{S}$  to  $\sim 10^\circ\text{N}$ , while strong downward transport occurs poleward of  $50^\circ\text{N}$  (refer to schematic in Figure 5.14). Thus at least qualitatively, the JFM ozone trends appear to agree with an



**Figure 5.14.** Zonally-averaged methane concentrations (ppmv) in shaded contours, and a schematic of the inferred Brewer-Dobson circulation (arrows) for (left) January and (right) July. Figure from *Stratospheric Ozone: An Electronic Textbook*, NASA GSFC.

enhancement of the NH wintertime Brewer-Dobson circulation. The SH wintertime ozone trends (Fig. 5.13b) also seem to suggest a trend towards a stronger Brewer-Dobson circulation, with large decreases in ozone occurring in the NH subtropics and increases near 50-70°S. These patterns appear to be fairly robust for different time periods (e.g., after 1985 and if data through 2007 is included).

We can more closely examine the ozone trends by looking at the seasonality at certain latitudes. Figure 5.15 shows the BDBP ozone trends as a function of pressure and month at 65°N, the equator, and 35°S, as well as the corresponding time series at the specified locations. At the equator (Fig. 5.15a), decreases in ozone are seen year-round in the shallow layer from ~70-30 hPa, with a slightly stronger decrease in December and January. In the NH at 65°N (Fig. 5.15b), a strong increase in ozone is seen from November through March, with decreases the rest of the year. During those same months, a strong decrease in ozone is observed at 35°S (Fig. 5.15c), which at this location and time of the year seems unlikely to be associated with chemical ozone depletion. The corresponding JFM time series at 70 hPa show the increase in ozone at 65°N and the decrease at 35°S (note: the trends are robust to removal of points prior to 1985). It is likely that a significant part of the positive trend at 65°N is due to the ozone loss that occurred following the Mt. Pinatubo eruption in the early-1990s, after which the majority of data is available to calculate the trend. However, even after removal of points from 1992-1994 (and even through 1997), a positive trend is present. It is possible that this trend, combined with the concurrent ozone loss at 35°S, is indicative of an enhanced Brewer-Dobson circulation in the NH winter (and thus an increase in wave driving). Similarly, increases in ozone at 65°S and decreases in ozone at 35°N during austral

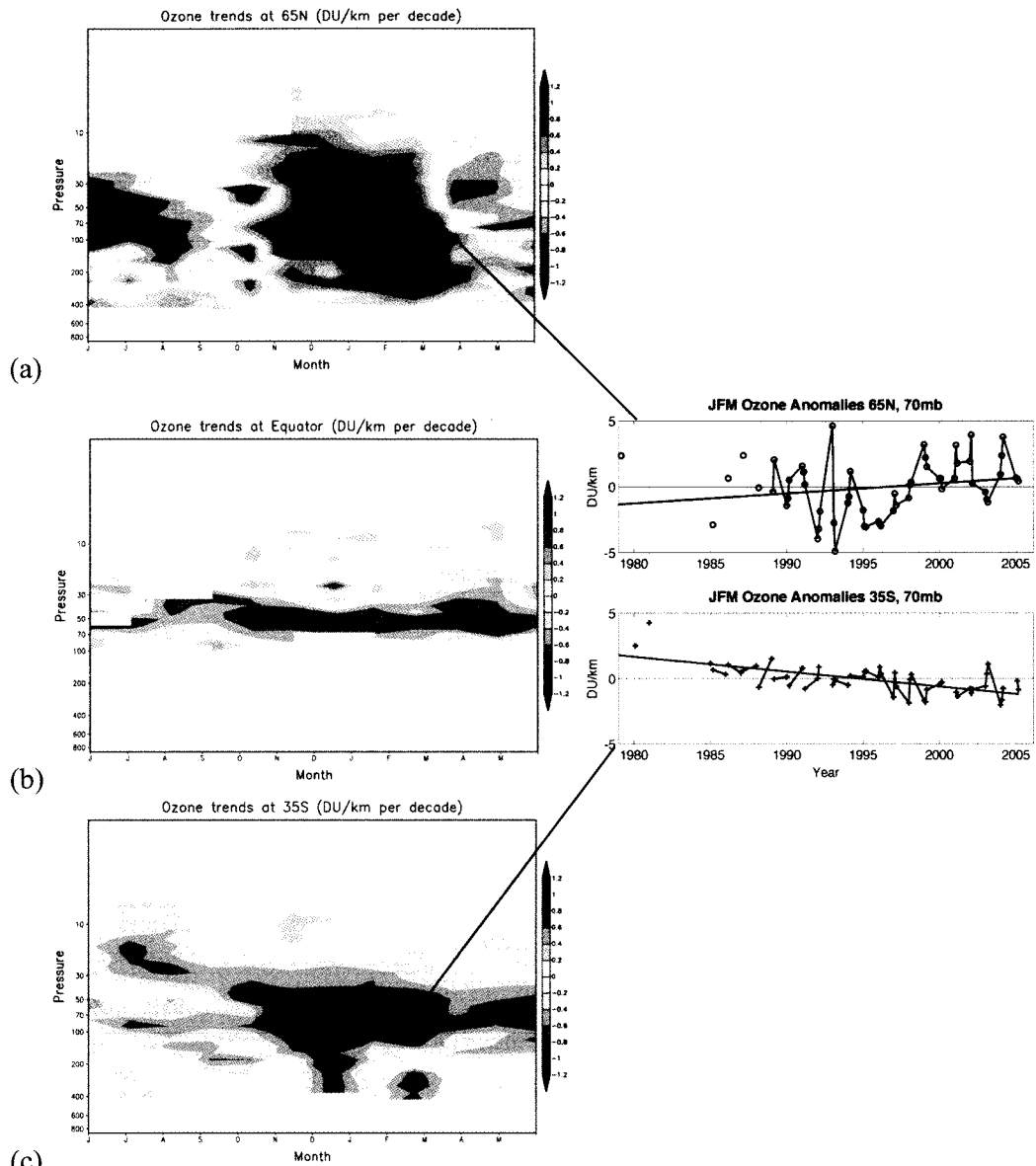


**Figure 5.15.** BDBP linear ozone trends [DU/km per decade] from 1979-2005 as a function of pressure and month at (a) 65°N, (b) the equator, and (c) 35°S. Only grid spaces with >40% available data are included. Right panel shows time series of JFM ozone anomalies at 70 hPa and 65°N (red) or 35°S (blue) as indicated by black boxes in (a) and (c).

winter might suggest an enhancement of the Brewer-Dobson circulation in the SH, although these trends seem less robust. While this result requires further study and

significance testing, if valid it suggests that this vertical profile ozone dataset provides useful insight into dynamical changes in the stratosphere, which can be difficult to measure.

How does this relate to the spatial patterns in the MSU4 stratospheric temperature trends? In January and February, there is strong warming poleward of 65°N and as well as strong cooling near 35°S (Figure 5.3) that matches the changes in ozone described here, which may suggest that part of the spatial pattern in temperature trends could be associated with changes in the Brewer-Dobson circulation. Changes in the Brewer-Dobson circulation would change temperatures both dynamically, through adiabatic lifting and compression, and radiatively, by removing ozone in some locations and depositing it in others. However, this theory does not explain the particularly strong cooling observed near 40°N in the boreal winter, nor the subtropical increases in tropospheric temperature underlying the decreases in stratospheric temperature [Fu et al. 2006], and thus seems unlikely to be the major cause of the bimodal cooling pattern observed in Figure 5.2. Nonetheless, because lower-stratospheric temperatures and ozone may provide information about the stratospheric circulation, we examine the relationships between these two fields in the next section.

### **5.3 Observed Relationships between MSU4 and Ozone**

In this section we briefly examine the relationships between MSU4 and the BDBP vertical ozone profiles on month-to-month timescales. The seasonal cycle, linear trend, and the QBO signal are removed from both datasets. In addition, the 3 years after El Chichon and Mt. Pinatubo are removed from MSU4, since volcanic aerosols have

opposing influences on ozone and temperature. We first look at the correlation between the MSU4 and the vertical ozone profiles (Fig. 5.16). As we might expect, correlations

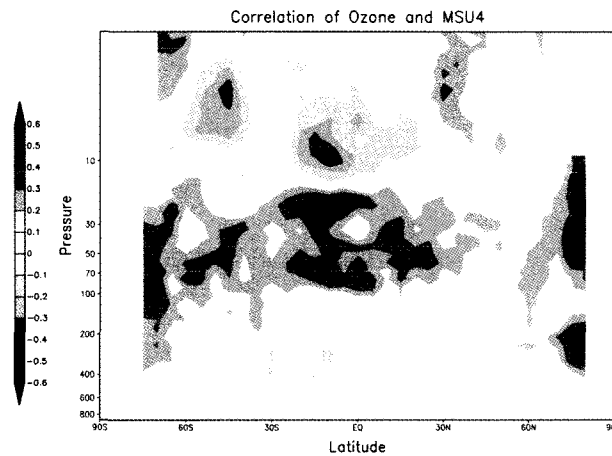


**Figure 5.16.** The correlation between BDBP monthly mean ozone anomalies and MSU4 lower-stratospheric temperature anomalies. Data coverage at each grid point must be at least 40% for correlation to be calculated.

are positive everywhere in the lower stratosphere, because (1) radiatively, the temperature should decrease/increase as ozone decreases/increases and (2) dynamical changes such as rising/sinking motion will cause both temperature to cool/warm adiabatically and ozone to decrease/increase. However, we can also look at the relationship of ozone at each grid cell with just tropical MSU4. The tropical MSU4 time series is created by cosine weighting and then averaging the MSU4 data from 30°S-30°N.

In Figure 5.17a, the ozone anomalies are regressed onto the standardized tropical MSU4 time series. In this case, we see a more interesting relationship- the lower-stratospheric ozone anomalies are positively correlated with tropical MSU4 in the tropical region but negatively correlated with tropical MSU4 polewards of  $\sim 30^\circ$  latitude in each hemisphere. In other words, as the temperature increases (decreases) in the tropical lower stratosphere, tropical ozone also increases (decreases) but extratropical

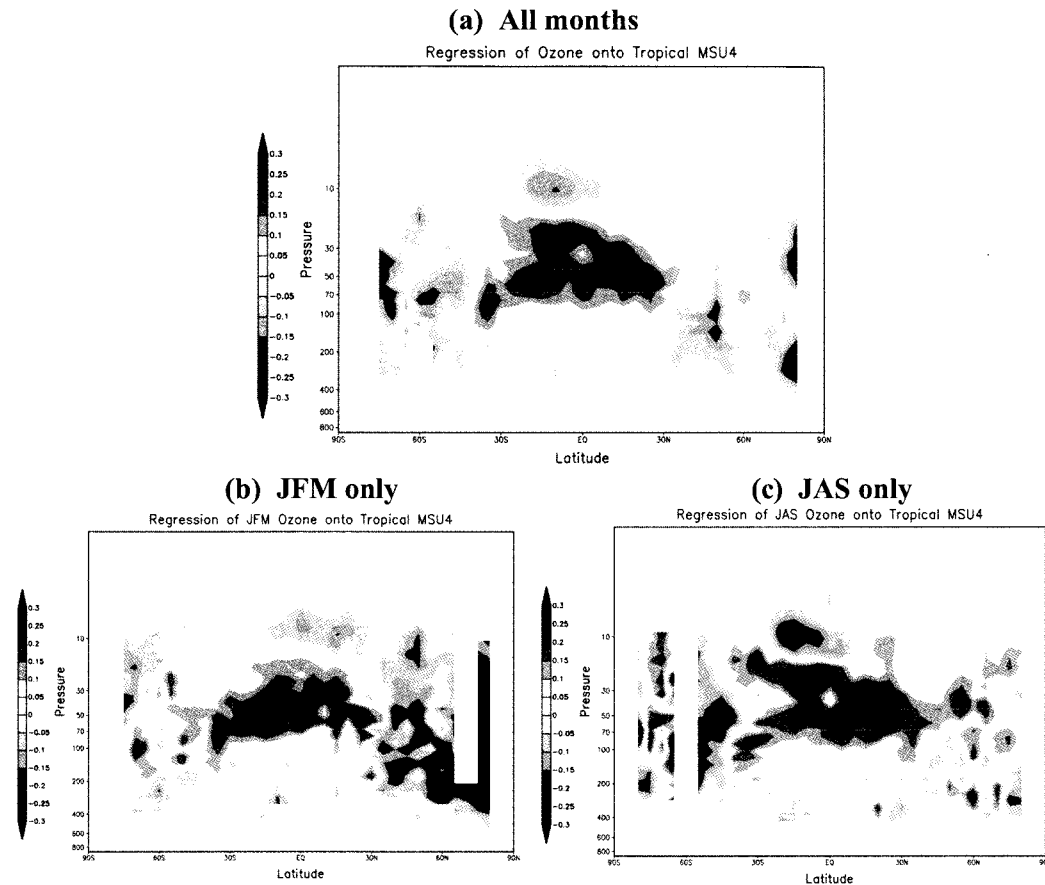


**Figure 5.17.** The regression of BDBP monthly mean ozone anomalies onto standardized MSU4 lower-stratospheric temperature anomalies [DU/km per standard deviation of the MSU4] for (a) all months, (b) JFM, and (c) JAS. Data coverage at each grid point must be at least 35% for correlation to be calculated.

ozone decreases (increases). This pattern is likely due to the Brewer-Dobson circulation. Further evidence is observed in Fig. 5.17b & c, which divides the response in boreal winter and austral winter, respectively. During NH winter months (Fig. 5.17b), ozone anomalies from  $\sim 40^{\circ}\text{S}$  to  $30^{\circ}\text{N}$  are positively correlated with tropical MSU4, while ozone anomalies poleward of  $30^{\circ}\text{N}$  are negatively correlated. This result is in agreement with variability driven by the NH Brewer-Dobson circulation, as the rising branch would cause decreased tropical temperatures as well as anomalously lower ozone (a positive

correlation) and the sinking branch would cause anomalously higher ozone (a negative correlation with tropical MSU4). The opposite relationship is observed for SH winter months (Fig 5.17c). Although these relationships describe variations on month-to-month timescales, they look somewhat similar to the changes observed in the long-term ozone trends in Figure 5.13 (the shading is opposite since one plot shows correlations and the other shows long-term trends, but the meaning is consistent). Thus the patterns in Figure 5.17 may provide further evidence that the trends in Figure 5.13 represent (at least to some extent) long-term changes in the Brewer-Dobson circulation; namely, an increase in this circulation over the last couple of decades. Other studies have found an enhancement of the Brewer-Dobson circulation using reanalysis data of eddy heat fluxes [Hu and Tung 2002] and chemical data to infer changes in tropical upwelling [Randel et al. 2006]. Thompson and Solomon [2009] find a similar result by looking at the relationship between trends in MSU4 and TOMS total column ozone. But this analysis may be the first to use vertical ozone profiles to look at changes in the residual mean stratospheric circulation.

#### **5.4 Summary and Future Work**

In this chapter we have reviewed our initial analysis of the spatial patterns in the MSU4 lower-stratospheric temperature trends, the trends in the new BDBP vertical ozone profile dataset, and the relationships between the MSU4 and the BDBP ozone data, in order to learn more about past changes in the atmospheric circulation. We describe the key findings in this section.

(1) The MSU4 weighting function, in combination with a sloping tropopause with latitude, certainly reduces the MSU4 trends in the tropics. Potentially, trends could be 0.2 K/decade less than trends measured at specific levels in the stratosphere by radiosondes. While this discrepancy is important to account for, as colder tropical trends could imply changes in stratospheric circulation or chemistry, it seems unlikely that the weighting function is responsible for the bimodal cooling pattern seen in the MSU4 zonal-mean trends. The Fu et al. [2006] theory regarding this pattern as a result of poleward shifting tropospheric jets remains the prominent candidate.

(2) The raw BDBP ozone profile data show stronger ozone loss over the tropics and subtropics during the last few decades than the RW ozone data created by a multiple linear regression model. Knowing whether this result is false due to inhomogeneities in the BDBP data sources, or true due to the higher natural variability and greater data sources in the BDBP, requires further analysis. In addition, the BDBP shows increases in tropical upper tropospheric ozone, perhaps corroborating the theory that the TOMS total column ozone trends are near zero because increasing ozone in the upper troposphere cancels out decreasing ozone in the tropical stratosphere in the vertical average. However, these tropospheric trends require much more significance testing and error analysis.

(3) The pattern of the BDBP ozone trends as well as their seasonality may suggest an enhancement of the Brewer-Dobson circulation from 1979-2005, and thus an increase in stratospheric wave driving, particularly in the NH. In addition, month-to-month variability between ozone anomalies and temperature in the lower-stratosphere appears to

be dominated by the Brewer-Dobson circulation (after the QBO and volcanic signal is removed), and the pattern is reminiscent of the long-term ozone trends.

Much work remains to be done on this analysis, particularly in regards to the BDBP ozone. More time needs to be spent ascertaining that inhomogeneities between data sources are not spuriously creating trends in the data. It would be interesting to break the trend analysis into components by source-type- ozonesondes, HALOE, SAGE, and POAM- and see whether trends in certain locations are dominated entirely by one source. The error of each source also needs to be accounted for in a more rigorous manner, and significance testing needs to be performed. Further investigation into the upper tropospheric ozone trends would be interesting. More detailed analysis could be done to better understand the BDBP ozone, such as analyzing the variance or the dominant pattern of variability in the data (similar to the Randel and Cobb [1994] analysis using TOMS total column ozone, but using vertical profile data instead). Finally, it would be interesting to explore the spatial patterns in ozone following volcanic eruptions, as ozonesonde data is available following the eruptions of Pinatubo and El Chichon whereas SAGE satellite measurements are not (so RW ozone data, for example, cannot be used to look at changes following eruptions).

## CHAPTER 6: CONCLUSIONS

### 6.1 Summary of Key Findings

The atmospheric circulation has changed over the last few decades and is expected to change in the future, due to variations in temperature gradients caused by both radiative (e.g., ozone and greenhouse gases) and physical (e.g., ice-albedo feedbacks, enhanced latent heat release by water vapor condensation) effects. In the troposphere, both simulated and observed circulation changes include a poleward shift of the storm tracks and an expansion of the Hadley cell circulation. In the stratosphere, the Brewer-Dobson circulation will likely be affected. Ultimately, these circulation changes could have significant impacts on surface climate. How these changes occur is thus an important topic in research today.

The broad goal of this thesis is to use an idealized GCM to better understand how and why the circulation changes in response to thermal forcings associated with anthropogenic emissions. We designed three forcings that mimic expected anthropogenically-driven temperature changes: a warming in the tropical upper troposphere, a cooling in the polar stratosphere, and a warming at the polar surface. We examined both the equilibrated steady-state response (Chapter 3) and the transient evolving response (Chapter 4) of the circulation to these forcings.

In the steady-state runs, the key findings include:

1) Warming in the tropical troposphere drives a poleward shift of the storm tracks and an expansion of the Hadley cell circulation, which suggests heating in the tropical troposphere plays a fundamental role in the tropospheric circulation changes found in IPCC-class climate simulations. Warming of the tropical troposphere also causes a weakening of the stratospheric Brewer-Dobson circulation, in the opposite sense of the changes in the stratospheric overturning circulation found in most previous climate change experiments.

2) Cooling in the polar stratosphere also shifts the storm tracks poleward, as noted in previous studies. But the response of the tropospheric circulation is sensitive to the level of the forcing: if the forcing is centered near the polar tropopause, the mid-latitude jet shifts poleward; if the forcing is centered just 25 hPa higher, the mid-latitude jet shifts equatorward; when the cooling is lifted another 25 hPa, the tropospheric response is negligible.

3) Warming at the polar surface shifts the storm tracks equatorward. The tropospheric circulation response to polar surface warming is thus in the opposite sense of the response to tropical tropospheric heating. Expected hemispheric asymmetries in polar warming may therefore cause hemispheric asymmetries in the tropospheric circulation response to anthropogenic forcing.

4) The combined response to all three thermal forcings does not equal the sum of the responses to the individual forcings. Thus the response of the GCM to a given thermal forcing is a function of the other thermal forcings applied to the model.

Using the transient simulations, we document the changes that occur when the thermal forcings are turned on. Key findings include:

1) Warming the tropical troposphere appears to drive a positive feedback whereby the initial warming weakens the Brewer-Dobson circulation, which reinforces the heating in the tropical upper troposphere/lower stratosphere. The upper-tropospheric/lower-stratospheric winds respond immediately to changes in the upper-level temperature gradient, and are collocated with changes in eddy momentum flux, suggesting the eddies are responding to, rather than driving, winds in the stratosphere. In contrast, the convergence/divergence of the eddy momentum flux drives the zonal-wind variations (i.e., the shift in the mid-latitude jet) in the troposphere. A large enhancement of mid-latitude eddy heat fluxes occurs at the level ( $\sim 250$  hPa) where the meridional temperature gradient strengthens the most. But nonetheless the hemispherically-averaged wave drag is reduced, not enhanced, in the stratosphere.

2) Cooling in the polar stratosphere also drives a large enhancement of eddy heat fluxes where the meridional temperature gradient strengthens the most, but since this level occurs in the stratosphere ( $\sim 100$  hPa), the hemispherically-averaged stratospheric wave drag is enhanced, driving a stronger Brewer-Dobson circulation. The changes in the tropospheric wind field are preceded by changes in the surface eddy heat fluxes, the tropospheric eddy momentum fluxes and the upper-level eddy heat fluxes.

3) Raising/lowering the shallow cooling in the polar stratosphere does not have as clear an effect in the transient scenarios as it does in the steady-state experiments, although some key differences are still apparent. The tropospheric eddy momentum fluxes tends to increase initially in the lower (200 hPa) cooling case, but decrease initially

in the higher (175 hPa) cooling case. Over a longer time period, we may have seen the opposite-signed tropospheric circulation response found in the steady-state run.

4) Warming at the polar surface drives changes at the surface before changes at upper-levels, largely due to reductions in the mid-latitude eddy heat flux in response to a reduced surface meridional temperature gradient. Ultimately this drives an equatorward shift of the mid-latitude jet.

We examine major theories regarding both tropospheric and stratospheric circulation changes, and then test them using the tropical tropospheric heating run. For the tropospheric circulation changes, two main categories of theories exist: those in which the atmospheric circulation response is driven predominantly by changes in the meridional temperature gradient, and those in which the response is driven predominantly by changes in the vertical temperature gradient. The theory by Chen and Held [2007], which falls in the former category, is the most consistent with our results.

They hypothesize that when the upper level meridional temperature gradient is increased, then 1) enhanced westerly zonal flow in the vicinity of the tropopause/lower stratosphere increases eastward eddy phase speeds there; 2) the enhanced eastward eddy phase speeds are associated with a poleward shift in the latitude of maximum wave breaking - and thus easterly momentum deposition - in the subtropics; 3) the poleward shift in the easterly momentum deposition in the subtropical upper troposphere increases lower tropospheric baroclinicity in the middle latitudes via an anomalous thermally damped meridional circulation cell, shifting baroclinic wave generation poleward; and 4) the resulting baroclinic wave fluxes reinforce a) the original poleward shift in the easterly

momentum deposition in the subtropical upper troposphere and b) the westerly momentum deposition that maintains the new location of the mid-latitude jet.

In our tropical tropospheric heating experiment, we note a robust increase in the eastward eddy phase speeds in the steady-state run. In the transient run, the subtropical tropospheric eddy momentum flux divergence lead changes in the mid-latitude eddy heat and momentum fluxes as well as changes in the surface winds, also in support of the Chen and Held [2007] theory. Changes in tropospheric static stability occur but do not seem strongly related to changes in the tropospheric eddies.

Regarding the stratospheric overturning circulation changes, the two main categories of mechanistic theories are that the circulation response is either predominantly driven by changes in eddy generation at tropospheric levels, or by changes in eddy propagation at stratospheric levels. For the tropical tropospheric heating experiment, the evidence provided here suggests that both are relevant to the stratospheric circulation response. The subtropical eddy heat fluxes near the surface, representative of changes in the eddy generation, are well-correlated to our proxy time series for the Brewer-Dobson circulation, suggesting subtropical eddy generation plays an important role in stratospheric circulation changes. However, changes in eddy propagation, as measured by the change in the stratospheric background flow relative to the change in eddy phase speed, likely explain why the greatly enhanced vertical wave propagation in the tropospheric mid-latitudes is not reflected in the stratosphere: in the mid-latitudes, the stratospheric background flow increases more than the eddy phase speeds, so that the index of refraction gets smaller and waves propagate away from this region. The result is that stratospheric wave drag is reduced in the subtropics due to a

reduction in subtropical eddy generation, but is only weakly increased in the mid-latitudes due to a reduction in mid-latitude eddy propagation. Over the entire hemisphere, the reduction in subtropical stratospheric wave drag is greater than the weak increases in mid-latitude stratospheric wave drag, and the Brewer-Dobson circulation is weakened.

In Chapter 5, we look at observations of vertical profiles of ozone and lower-stratospheric temperatures in order to better understand observed changes in the tropospheric and stratospheric circulations. We find:

(1) The MSU4 weighting function has an impact on observed trends in MSU4 lower-stratospheric tropical temperatures that should be accounted for when using this data.

(2) The spatial pattern of lower-stratospheric temperature trends is robust (particularly in boreal winter). The weighting function can't account for the spatial structure of these temperature trends. We simulate similar spatial patterns using our idealized GCM in response to tropical tropospheric heating, suggesting that this bimodal cooling pattern could be indicative of poleward shifts in the subtropical/mid-latitude tropospheric jets as suggested by Fu et al. [2006].

(3) Trends in vertical profiles of ozone suggest an increase in the Brewer-Dobson circulation over the past few decades, in agreement with several previous studies. This observed change is in the opposite-sense to the idealized GCM stratospheric overturning circulation change forced by tropical tropospheric warming but in the same sense as the overturning circulation change forced by polar stratospheric cooling. This observation may then imply that the effects of a cooling polar stratosphere (known to have occurred

over the last few decades due to ozone depletion at least in the SH) have outweighed the effects of a warming troposphere over the last few decades.

## **6.2 Remaining Questions and Future Work**

The idealized GCM is a useful tool for breaking down the response of the atmospheric circulation to a given forcing. The results in this thesis provide new insight into the processes that drive large-scale changes in both tropospheric and stratospheric circulations. But many questions remain unanswered. The major questions include:

1) To what extent does the state of the tropospheric/stratospheric background flow impact the response of the circulation? We use equinoctial conditions in this study, which simplifies our analysis because of the hemispheric symmetry of the background flow, but certainly the stronger polar stratospheric vortex and enhanced surface baroclinicity in winter could have a significant effect on the circulation response to an imposed thermal forcing. As we see in the transient simulations, the propagation of waves can be strongly impacted by the state of the stratospheric zonal-mean flow. Simulations are currently in progress to assess the circulation response to the same forcings under solstitial conditions.

2) The circulation response to an El Nino event is in the opposite sense (i.e., an equatorward shift of the storm tracks) to the changes we have found for our tropical tropospheric heating experiment, despite the fact that both involve heating of the deep tropics [L'Heureux and Thompson 2006; Lu et al. 2008]. Narrowing the heating (Fig. 3.1c) weakens the response but does not change the direction. Imposing a wavenumber 2

thermal forcing at 300 hPa in the tropics to simulate the temperature response to an El Nino event also does little to change the circulation response (not shown). It is unclear why the idealized GCM does not capture the El Nino extratropical circulation response, but this question is certainly worthy of further investigation. Lu et al. [2008] suggests that an El Nino event drives stronger increases in subtropical upper-tropospheric/lower-stratospheric zonal winds, which ultimately draws the critical latitude, and thus eddy wave breaking, equatorward. As we saw in our eddy phase speed analysis (Fig. 4.1), the subtropical upper-level zonal-mean zonal winds in our tropical heating experiment do not show significant increases, which perhaps accounts for the different response.

3) Are the mechanisms that we attribute to the circulation response for the tropical tropospheric heating run the same mechanisms responsible for the circulation response in the stratospheric polar cooling run? The increased westerly winds in the stratosphere occur further poleward in the polar stratospheric cooling run than in the tropical tropospheric warming run, and this shift in where the background flow changes the most could explain why we see a different stratospheric circulation response in the two experiments. Can we better understand the sensitivity of the tropospheric circulation to the level of stratospheric forcing at the poles? Both these questions are currently under investigation using analysis similar to that performed in Chapter 4.7.

## REFERENCES

- Arblaster, J. and G. Meehl, 2006: Contributions of external forcings to southern annular mode trends. *J. Climate*, 19, 2896-2905.
- Ambaum, M.H.P., B.J. Hoskins, and D.B. Stephenson, 2001: Arctic Oscillation or North Atlantic Oscillation?, *J. Climate*, 14, 3495-3507.
- Baldwin, M.P., and coauthors, 2001: The Quasi-Biennial Oscillation, *Reviews of Geophysics*, 39, 179-229.
- Baldwin, M. P., and T. J. Dunkerton, 2001: Stratospheric harbingers of anomalous weather regimes, *Science*, 294, 581–584.
- Bortz, S.E., M.J. Prather, J.P. Cammas, V. Thouret, and H. Smit, 2006: Ozone, water vapor, and temperature in the upper tropical troposphere: variations over a decade of MOZAIC measurements, *J. Geophys. Res.*, 111, D05305, doi:10.1029/2005JD006512.
- Brandefelt, J. and E. Kallen, 2004: The response of the Southern Hemisphere atmospheric circulation to an enhanced greenhouse gas forcing. *J. Climate*, 17, 4425-4442.
- Bretherton, C., M. Widmann, V. Dymnikov, J. Wallace, and I. Blade, 1999: The effective number of spatial degrees of freedom of a time-varying field. *J. Climate*, 12, 1990-2009.
- Butchart, N. and A. Scaife, 2001: Removal of chlorofluorocarbons by increased mass exchange between the stratosphere and troposphere in a changing climate. *Nature*, 410, 799-802.
- Cai, W., P. Whetton, and D. Karoly, 2003: The response of the Antarctic Oscillation to increasing and stabilized atmospheric CO<sub>2</sub>. *J. Climate*, 16, 1525-1538.
- Chan, C. J. and R. A. Plumb, 2009: The response to stratospheric forcing and its dependence on the state of the troposphere, *J. Climate*, 66, 2107-2115.
- Charney, J.G. and P.G. Drazin, 1961: Propagation of planetary-scale disturbances from the lower into the upper atmosphere, *J. Geophys. Res.*, 66 (1), 83-109.

- Chen, G. and I.M. Held, 2007: Phase speed spectra and the recent poleward shift of Southern Hemisphere surface westerlies. *Geophys. Res. Lett.*, 34, L21805, doi:10.1029/2007GL031200.
- Chen, G., I.M. Held, W.A. Robinson, 2007: Sensitivity of the latitude of the surface westerlies to surface friction. *J. Atmos. Sci.*, 64, 2899-2915.
- Christiansen, B., 2005: Downward propagation and statistical forecast of the near-surface weather, *J. Geophys. Res.*, 110, D14104, doi:10.1029/2004JD005431.
- Cohen, J. and D. Entekhabi, 1998: Eurasian snow cover variability and Northern Hemisphere climate predictability, *Geophys. Res. Lett.*, 26 (3), 345-348.
- Deser, C., R. Tomas, M. Alexander, and D. Lawrence, 2009: The seasonal atmospheric response to projected Arctic Sea ice loss in the late 21st Century, *J. Climate*, submitted.
- Eichelberger, S.J. and J.R. Holton, 2002: A mechanistic model of the northern annular mode. *J. Geophys. Res.*, 107(19), 4388, doi:10.1029/2001JD001092.
- Eichelberger, S.J. and D.L. Hartmann, 2005: Changes in the strength of the Brewer-Dobson circulation in a simple AGCM, *Geophys. Res. Lett.*, 32, L15807, doi:10.1029/2005GL022924.
- Forster, P.M., G. Bodeker, R. Schofield, S. Solomon, and D.W.J. Thompson, 2007: Effects of ozone cooling in the tropical lower stratosphere and upper troposphere, *Geophys. Res. Lett.*, 34, L23813, doi:10.1029/2007GL031994.
- Free, M., D.J. Seidel, J.K. Angell, J. Lanzante, I. Durre, and T.C. Peterson, 2005: Radiosonde Atmospheric Temperature Products for Assessing Climate (RATPAC): a new data set of large-area anomaly time series, *J. Geophys. Res.*, 110, D22101, doi:10.1029/2005JD006169.
- Frierson, D.M.W., 2006: Robust increases in midlatitude static stability in simulations of global warming, *Geophys. Res. Lett.*, 33, L24816, doi:10.1029/2006GL027504.
- Frierson, D., J. Lu, and G. Chen, 2007: Width of the Hadley cell in simple and comprehensive general circulation models, *Geophys. Res. Lett.*, 34, L18804, doi:10.1029/2007GL031115.
- Frierson, D.M.W., 2008: Midlatitude static stability in simple and comprehensive general circulation models, *J. Atmos. Sci.*, 65, 1049-1062.
- Fu, Q., C.M. Johanson, S.G. Warren, and D.J. Seidel, 2004: Contribution of stratospheric cooling to satellite-inferred tropospheric temperature trends, *Nature*, 429, 55-58.

- Fu, Q., C.M. Johanson, J.M. Wallace, and T. Reichler, 2006: Enhanced mid-latitude tropospheric warming in satellite measurements, *Science*, 312, 1179.
- Fu, Q., S. Solomon, and P. Lin, 2009: On the seasonal dependence of tropical lower-stratospheric temperature trends, *Atmos. Chem, Phys.*, submitted.
- Fyfe, J., G. Boer, and G. Flato, 1999: The Arctic and Antarctic oscillations and their projected changes under global warming, *Geophys. Res. Lett.*, 26, 1601-1604.
- Garcia, R.R., and W.J. Randel, 2008: Acceleration of the Brewer-Dobson circulation due to increases in greenhouse gases. *J. Atmos. Sci.*, 65, 2731-2739.
- Gerber, E. and G. Vallis, 2007: Eddy-zonal flow interactions and the persistence of the zonal index, *J. Atmos. Sci.*, 64, 3296-3311.
- Gerber, E., S. Voronin, and L. Polvani, 2008: Testing the annular mode autocorrelation time scale in simple atmospheric general circulation models, *Mon. Wea. Rev.*, 136, 1523-1536.
- Gerber, E. and L. Polvani, 2009: Stratosphere-troposphere coupling in a relatively simple AGCM: The Importance of Stratospheric Variability, *J. Climate*, 22, 1920-1933.
- Gillett, N.P., G. C. Hegerl, M.R. Allen, and P. A. Stott, 2000: Implications of observed changes in the Northern Hemisphere circulation for the detection of anthropogenic climate change. *Geophys. Res. Lett.*, 27, 993-996, 2000.
- Gillett, N.P., M. R. Allen, and K.D. Williams, 2002: The role of stratospheric resolution in simulating the Arctic Oscillation response to greenhouse gases. *Geophys. Res. Lett.* 29, 1500-1503.
- Gillett, N.P., M. R. Allen, and K.D. Williams, 2003: Modeling the atmospheric response to doubled CO<sub>2</sub> and depleted stratospheric ozone using a stratosphere-resolving coupled GCM. *Q.J.R. Meteorol. Soc.*, 129(589), 947-966.
- Gillett, N.P., and D.W.J. Thompson, 2003: Simulation of Recent Southern Hemisphere Climate Change. *Science*, 302(5643), 273-275, 10.1126/science.1087440.
- Gillett, N.P., T.D. Kell, and P.D. Jones, 2006: Regional climate impacts of the Southern Annular Mode, *Geophys. Res. Lett.*, 33, L23704, doi:10.1029/2006GL027721.
- Haigh, J., M. Blackburn, and R. Day, 2005: The response of tropospheric circulation to perturbations in lower-stratospheric temperature, *J. Climate*, 18, 3672-3685.
- Hartmann, D., 1994: *Global Physical Climatology*. Academic Press, San Diego, New York, Boston, London, Sydney, Tokyo, and Toronto.

- Hartmann, D. and F. Lo, 1998: Wave-driven zonal flow vacillation in the Southern Hemisphere. *J. Atmos. Sci.*, 55, 1303-1315.
- Hassler, B., G.E. Bodeker, M. Dameris, 2008: Technical Note: A new global database of trace gases and aerosols from multiple sources of high vertical resolution measurements. Pre-print.
- Hayashi, Y., 1971: A generalized method of resolving disturbances into progressive and retrogressive waves by space Fourier and time cross-spectral analyses, *J. Meteor. Soc. Japan*, 49, 125-128.
- Hegerl, G.C., F. W. Zwiers, P. Braconnot, N.P. Gillett, Y. Luo, J.A. Marengo Orsini, N. Nicholls, J.E. Penner and P.A. Stott, 2007: Understanding and Attributing Climate Change. In: *Climate Change 2007: The Physical Science Basis. Contribution of Working Group I to the Fourth Assessment Report of the Intergovernmental Panel on Climate Change* [Solomon, S., D. Qin, M. Manning, Z. Chen, M. Marquis, K.B. Averyt, M. Tignor and H.L. Miller (eds.)]. Cambridge University Press, Cambridge, United Kingdom and New York, NY, USA
- Heikes, R. P., and D. A. Randall, 1995: Numerical integration of the shallow water equations on a twisted icosahedral grid. Part I: Basic design and results of tests. *Mon. Wea. Rev.*, 123, 1862-1880.
- Held, I.M. and M.J. Suarez, 1994: A proposal for the intercomparison of the dynamical cores of atmospheric general circulation models. *BAMS*, 75(10), 1825-1830.
- Higgins, R.W., A. Leetmaa, and V.E. Kousky, 2002: Relationships between climate variability and winter temperature extremes in the United States, *J. Climate*, 15 (13), 1555-1572.
- Hofmann, D.J. and S. Solomon, 1989: Ozone destruction through heterogeneous chemistry following the eruption of El Chichon, *J. Geophys. Res.*, 94, 5029-5041.
- Hu, Y. and K.K. Tung, 2002: Interannual and decadal variations of planetary wave activity, stratospheric cooling, and Northern Hemisphere Annular Mode, *J. Climate*, 15, 1659-1673.
- Hu, Y., and Q. Fu, 2007: Observed poleward expansion of the Hadley circulation since 1979. *Atmospheric Chemistry and Physics*, 7, 5229-5236.
- Hudson, R.D., M.F. Andrade, M.B. Follette, and A.D. Frolov, 2006: The total ozone field separated into meteorological regimes- Part II: Northern Hemisphere mid-latitude total ozone trends, *Atmos. Chem. Phys.*, 6, 5183-5191.
- Hurrell, J. W., 1995: Decadal trends in the North Atlantic Oscillation region temperatures and precipitation. *Science*, 269, 676-679.

Hurrell, J.W., 1996: Influence of variations in the extratropical wintertime teleconnections on Northern Hemisphere temperatures. *Geophys. Res. Lett.*, 23, 665-668.

Intergovernmental Panel on Climate Change (IPCC) Fourth Assessment Report (AR4).

Johanson, C.M., and Q. Fu, 2009: Hadley cell widening: model simulations versus observations, *J. Climate*, 22, 2713-2725.

Kindem, I., and B. Christiansen, 2001: Tropospheric Response to Stratospheric Ozone Loss, *Geophysical Res. Let.*, 28, 1547-1550.

Kodama, C. and T. Iwasaki, 2009: Influence of the SST rise on baroclinic instability wave activity under an aquaplanet condition, *J. Atmos. Sci.*, 66, 2272-2287.

Konor, C. and A. Arakawa, 1997: Design of an atmospheric model based on a generalized vertical coordinate. *Mon. Wea. Rev.*, 125, 1649-1673.

Kraucunas, I. and D.L. Hartmann, 2005: Equatorial superrotation and the factors controlling the zonal-mean zonal winds in the tropical upper troposphere, *J. Atmos. Sci.*, 62, 371-389.

Kushner, P., I. Held, and T. Delworth, 2001: Southern Hemisphere atmospheric circulation response to global warming, *J. Climate*, 14, 2238-2249.

Kushner, P. and L. Polvani, 2004: Stratosphere-troposphere coupling in a relatively simple AGCM: The role of eddies, *J. Climate*, 17(3), 629-639.

L'Heureux, M.L. and D.W.J. Thompson, 2006: Observed relationships between the El Nino- Southern Oscillation and the extratropical zonal-mean circulation, *J. Climate*, 19, 276-287.

Li, F., J. Austin, and J. Wilson, 2008: The strength of the Brewer-Dobson circulation in a changing climate: Coupled chemistry-climate model simulations, *J. Climate*, 21, 40-57.

Liu, J., J.A. Curry, Y. Dai, and R. Horton, 2007: Causes of the northern high-latitude land surface winter climate change, *Geophys. Res. Lett.*, 34 (14), L14702.

Lorenz, D.J., and D.L. Hartmann, 2001: Eddy-Zonal Flow Feedback in the Southern Hemisphere, *J. Atmos. Sci.*, 58, 3312-3327.

Lorenz, D.J. and D.L. Hartmann, 2003: Eddy-Zonal Flow Feedback in the Northern Hemisphere Winter, *J. Climate*, 16 (8), 1212-1227.

- Lorenz, D.J. and E.T. DeWeaver, 2007: Tropopause height and zonal wind response to global warming in the IPCC scenario integrations, *J. Geophys. Res.*, 112, D10119, doi:10.1029/2006JD008087.
- Lu, J., R.J. Greatbatch, and K.A. Peterson, 2004: Trend in Northern Hemisphere winter atmospheric circulation during the last half of the Twentieth Century, *J. Climate*, 17 (19), 3745.
- Lu, J., G. A. Vecchi, and T. Reichler, 2007: Expansion of the Hadley cell under global warming, *Geophys. Res. Lett.*, 34, L06805, doi:10.1029/2006GL028443.
- Lu, J., G. Chen, and D. Frierson, 2008: Response of the Zonal Mean Atmospheric Circulation to El Nino versus Global Warming. *J. Climate*, 21, 5835-5851.
- Marshall, J., Y. Kushner, D. Battisti, P. Chang, A. Czaja, et al., 2001: North Atlantic climate variability: Phenomena, impacts, and mechanisms, *International Journal of Climatology*, 21, 1863-1898.
- Marshall, G.J., A. Orr, N.P.M. van Lipzig, and J.C. King, 2006: The impact of a changing Southern Hemisphere Annular Mode on Antarctic Peninsula summer temperatures, *J. Climate*, 19 (20), 5388.
- Mears, C.A. and F.J. Wentz, 2008: Construction of the RSS V3.2 lower-tropospheric temperature dataset from the MSU and AMSU Microwave sounders, *J. Atmos. Oceanic Technol.*, 26, 1493-1509.
- Miller, R.L., G.A. Schmidt and D.T. Shindell, 2006: Forced annular variations in the 20th century Intergovernmental Panel on Climate Change Fourth Assessment Report models. *J. Geophys. Res.*, 111, D18101, doi:10.1029/2005JD026030263.
- Ostermeier, G.M. and J.M. Wallace, 2003: Trends in the North Atlantic Oscillation/Northern Hemisphere Annular Mode during the Twentieth-Century, *J. Climate*, 16, 336-341.
- Overland, J. E., and M. Wang, 2005: The Arctic climate paradox: The recent decrease of the Arctic Oscillation, *Geophys. Res. Lett.*, 32, L06701, doi:10.1029/2004GL021752.
- Polvani, L.M. and P.J. Kushner, 2002: Tropospheric response to stratospheric perturbations in a relatively simple general circulation model, *Geophys. Res. Lett.*, 29, doi: 10.129/2001GL014284.
- Quadrelli, R., V. Pavan, and F. Molteni, 2001: Wintertime variability of Mediterranean precipitation and its links with large-scale circulation anomalies. *Climate Dynamics*, 17, 457-466.

- Ramaswamy, V., M. Schwarzkopf, W.J. Randel, B.D. Santer, B.J. Soden and G.L. Stenchikov, 2006: Anthropogenic and natural influences in the evolution of lower stratospheric cooling. *Science*, 311, 1138-1141.
- Randel, W.J. and I.M. Held, 1991: Phase speed spectra of transient eddy fluxes and critical layer absorption, *J. Atmos. Sci.*, 48 (5), 688-697.
- Randel, W.J. and F. Wu, 1999: Cooling of the Arctic and Antarctic polar stratospheres due to ozone depletion, *J. Climate*, 12, 1467-1479.
- Randel, W.J. and J.B. Cobb, 1994: Coherent variations of monthly mean total ozone and lower stratospheric temperature, 99 (D3), 5433-5447.
- Randel, W.J. and F. Wu, 2006: Biases in stratospheric and tropospheric temperature trends derived from historical radiosonde data, *J. Climate*, 19, 2094-2104.
- Randel, W.J., F. Wu, G. Nedoluha, H. Vomel, and P. Forster, 2006: Decreases in stratospheric water vapor since 2001: Links to changes in the tropical tropopause and the Brewer-Dobson circulation, *J. Geophys. Res.*, 111, D12312, doi:10.1029/2005JD006744.
- Randel, W.J. and F. Wu, 2007: A stratospheric ozone profile data set for 1979-2005: variability, trends, and comparisons with column ozone data, *J. Geophys. Res.*, 112, D06313, doi:10.1029/2006JD007339.
- Randel, W.J. and coauthors, 2009: An update of observed stratospheric temperature trends, *J. Geophys. Res.*, 114, D02107, doi:10.1029/2008JD01042.
- Renwick, J.A., 2002: Southern hemisphere circulation and relations with sea ice and sea surface temperature. *J. Climate*, 15, 3058-3068.
- Rind, D., D. Shindell, P. Lonergan, and N.K. Balachandran, 1998: Climate change and the middle atmosphere. Part III: The doubled CO<sub>2</sub> climate revisited, *J. Climate*, 11, 876-894.
- Rind, D., J. Lerner, and C. McLinden, 2001: Changes of tracer distribution in the doubled CO<sub>2</sub> climate, *J. Geophys. Res.*, 106 (D22), 2806128080.
- Ring, M.J., and R.A. Plumb, 2007: Forced annular mode patterns in a simple atmospheric general circulation model. *J. Atmos. Sci.*, 64, 3611-3626.
- Ring, M. and R. Plumb, 2008: The response of a simplified GCM to axisymmetric forcings: applicability of the Fluctuation-Dissipation theorem, *J. Atmos. Sci.*, 65, 3880-3898.

- Ringler, T. D., R. P. Heikes, and D. A. Randall, 2000: Modeling the atmospheric general circulation using a spherical geodesic grid: A new class of dynamical cores. *Mon. Wea. Rev.*, 128, 2471-2490.
- Robinson, W., 1994: Eddy feedbacks on the zonal index and eddy zonal flow interactions induced by zonal flow transience. *J. Atmos. Sci.*, 51, 2553-2562.
- Robinson, W., 1996: Does eddy feedback sustain variability in the zonal index? *J. Atmos. Sci.*, 53, 3556-3569.
- Robinson, W. A., 2000: A baroclinic mechanism for the eddy feedback on the zonal index. *J. Atmos. Sci.*, 57, 415-422.
- Robinson, W.A., 2006: On the self-maintenance of midlatitude jets, *J. Atmos. Sci.*, 63, 2109-2122.
- Robock, A., 2000: Volcanic eruptions and climate, *Reviews of Geophysics*, 38 (2), 191-219.
- Scaife, A.A., J.R. Knight, G.K. Vallis, and C.K. Folland, 2005: A stratospheric influence on the winter NAO and North Atlantic surface climate, *Geophys. Res. Lett.*, 32, L18715, doi:10.1029/2005GL023226.
- Schneider, D.P., E.J. Steig, and J.C. Comiso, 2004: Recent climate variability in Antarctica from satellite-derived temperature data. *J. Climate*, 17, 1569-1583.
- Seidel, D. J., and W. Randel, 2007: Recent widening of the tropical belt: Evidence from tropopause observations. *J. Geophys. Res.* 112, D20113.
- Seidel, D.J., Q. Fu, W.J. Randel, T.J. Reichler, 2008: Widening of the tropical belt in a changing climate. *Nature Geoscience*, 1, 21-24.
- Sexton, D.M.H., 2001: The effect of stratospheric ozone depletion on the phase of the Antarctic Oscillation. *Geophys. Res. Lett.*, 28, 3697-3700.
- Shindell, D., R. Miller, G. Schmidt, and L. Pandolfo, 1999: Simulation of recent northern winter climate trends by greenhouse-gas forcing. *Nature*, 399, 452-455.
- Shindell, D.T., G.A. Schmidt, R.L. Miller, and D. Rind 2001. Northern Hemisphere winter climate response to greenhouse gas, ozone, solar, and volcanic forcing. *J. Geophys. Res.* 106, 7193-7210.
- Shindell, D. and G. Schmidt, 2004: Southern Hemisphere climate response to ozone changes and greenhouse gas increases. *Geophys. Res. Lett.*, 31, L18209, doi:10.1029/2004GL020724.

- Sigmond, M., P.J. Kushner, and J.F. Scinocca, 2007: Discriminating robust and non-robust atmospheric circulation responses to global warming. *J. Geophys. Res.*, 112, D20121, doi:10.1029/2006JD008270.
- Sigmond, M. and J.F. Scinocca, 2009: The influence of the basic state on the Northern Hemisphere circulation response to climate change, submitted.
- Simpson, I. R., M. Blackburn, and J. D. Haigh, 2009: The role of eddies in driving the tropospheric response to stratospheric heating perturbations, *J. Atmos. Sci.*, 66, 1347-1365.
- Solomon, S., R.W. Portmann, R.R. Garcia, L.W. Thomason, L.R. Poole, and M.P. McCormick, 1996: The role of aerosol variations in anthropogenic ozone depletion at northern midlatitudes, 101 (D3), 6713-6727.
- Son, S. and S. Lee, 2005: The response of westerly jets to thermal driving in a primitive equation model, *J. Atmos. Sci.*, 62, 3741-3757.
- Son, S. and S. Lee, 2006: Preferred modes of variability and their relationship with climate change. *J. Climate*, 19, 2063-2075.
- Son, S., L. Polvani, D. Waugh, H. Akiyoshi, R. Garcia, D. Kinnison, S. Pawson, E. Rozanov, T. Shepherd, and K. Shibata, 2008: The impact of stratospheric ozone recovery on the Southern Hemisphere westerly jet. *Science*, 320, 1486-1489.
- Terray, L., and C. Cassou, 2000: Modes of low-frequency climate variability and their relationships with land precipitation and surface temperature: application to the Northern Hemisphere winter climate. *Stochastic Environmental Research and Risk Assessment*, 14, 339-369.
- Thompson, D. and J. Wallace, 2000: Annular modes in the extratropical circulation. Part I: Month-to-month variability. *J. Climate*, 13, 1000-1016.
- Thompson, D. W. J., J. M. Wallace, and G. C. Hegerl, 2000: Annular modes in the extratropical circulation. Part II: Trends. *J. Climate*, 13, 1018-1036.
- Thompson, D. W. J., and J. M. Wallace, 2001: Regional climate impacts of the Northern Hemisphere annular mode. *Science*, 293, 85-89.
- Thompson, D. W. J., and S. Solomon, 2002: Interpretation of recent Southern Hemisphere climate change. *Science*, 296, 895-899.
- Thompson, D. W. J., and S. Solomon, 2005: Recent stratospheric climate trends: Global structure and tropospheric linkages, *J. Climate*, 18, 4785-4795.
- Thompson, D. W. J., J. C. Furtado, and T. G. Shepherd, 2006: On the tropospheric

response to anomalous stratospheric wave drag and radiative heating, *J. Atmos. Sci.*, 63 (10), 2616-2629, doi:10.1175/JAS3771.1.

Thompson, D. W. J., and S. Solomon, 2009: Understanding recent stratospheric climate change, *J. Climate*, 22, 1934-1943.

World Meteorological Organization, 2003: Scientific assessment of ozone depletion: 2002, *Global Ozone Res. and Monit. Proj., Rep. 47*, Geneva.

Xu, K.M., and K.A. Emanuel, 1989: Is the tropical atmosphere conditionally unstable?, *Mon. Weather Rev.*, 117, 1471-1479.

Yin, J.H., 2005: A consistent poleward shift of the storm tracks in simulations of 21<sup>st</sup> century climate. *Geophys. Res. Lett.*, 32, L18701, doi:10.1029/2005GL023684.

Yu, J. and D. Hartmann, 1993: Zonal flow vacillation and eddy forcing in a simple GCM of the atmosphere. *J. Atmos. Sci.*, 50, 3244-3259.

Ziemke, J.R., S. Chandra, and P.K. Bhartia, 2005: A 25-year data record of atmospheric ozone in the Pacific from Total Ozone Mapping Spectrometer (TOMS) cloud slicing: implications for ozone trends in the stratosphere and troposphere, *J. Geophys. Res.*, 110, D15105, doi:10.1029/2004JD005687.